TIME-TEMPERATURE CURING RELATIONSHIP OF AN ADHESIVE BINDER WITH RICE STRAW

A Thesis

presented to

the Faculty of California Polytechnic State University,

San Luis Obispo

In Partial Fulfillment

Of the Requirements for the Degree

Master of Science in Engineering, with Specialization in Materials Engineering

by

Kevin Ka-wan Ng

February 2010

COMMITTEE MEMBERSHIP

TITLE:	TIME-TEMPERATURE CURING RELATIONSHIP OF AN ADHESIVE BINDER WITH RICE STRAW
AUTHOR:	KEVIN KA-WAN NG
DATE SUBMITTED:	FEBRUARY 2010
COMMITTEE CHAIR:	DR. LINDA VANASUPA, PROFESSOR
COMMITTEE MEMBER:	DR. BLAIR LONDON, PROFESSOR
COMMITTEE MEMBER:	DR. PHILIP COSTANZO, ASSISTANT PROFESSOR

ABSTRACT

Time-temperature curing relationship of an adhesive binder with rice straw

Kevin Ka-Wan Ng

Rice straw is a global and proliferate agricultural waste whose production grossly outstrips viable uses. Current disposal methods are not sustainable, and more convenient methods – such as incineration – exude poor environmental stewardship. Although the direct use of straw bales in building construction presents a practical and sustainable alternative, engineering challenges associated with using it prevent its wide adoption. The Stak Block – a composite formed from compressed rice straw and a heat-cured adhesive – may overcome challenges associated with straw bale building. However, the times and temperatures needed to cure the binder with straw are not well understood. Therefore, the goal of this thesis was to study straw cubes (in lieu of the full-scale Stak Block) to discern a time-temperature relationship.

A finite element (FE) model of the Stak Block was created to simulate the heating process. The results of this study indicated that the adhesive may actually cure at temperatures less than 100°C. This data influenced the times and temperatures that binder-treated straw cubes were baked at for the first of several iterations. A chemical dye was used to discern if cubes had cured or not. In addition, mechanical testing was used to inspect cubes for curing and to support the results obtained from using a chemical dye. Results from cubes inspected with the chemical dye method were then used to develop an inverse relationship between time and temperature needed to cure the cubes – with the lowest observed cure temperature to be 65°C for 2 hours and the fastest cure time of 30 minutes at 150 and 125°C. Following the iterative experiments, an FE model of the cube was created and fitted to the results of the iterative experiments. Values for thermal conductivity (k = 0.1 W/m-K)and specific heat (C_p = 2000 J/kg-K) used to fit the FE cube model were applied appropriately to the Stak Block FE model in order to estimate curing times at different temperatures.

ACKNOWLEDGEMENTS

This work would not have been possible without the material donations of the nascent, yet innovative, Oryzatech Inc. I am especially grateful for the advice and insight from the company's founders: Jay Ruskey and Ben Korman. I would also like to thank my thesis advisor, Dr. Linda Vanasupa, for seeing such a rich research opportunity, finding funds, and providing guidance. I am indebted to statistics professor Dr. Karen McGaughey for developing an experimental plan that met very tough requirements and providing statistical advice. I am also very thankful for Dr. Phil Costanzo's advice on the adhesive, as well as Dr. Blair London's recommendations on the mechanical testing. In addition, much credit goes to my family, relatives, and close friends who encouraged and supported me throughout this work.

TABLE OF CONTENTS

Page

LIST OF TABLES

LIST OF FIGURES

CHAPTER 1: INTRODUCTION

Currently, there is a strong worldwide focus on global climate change and its associated challenges. As scientists further understand the Earth's weather systems, more of them are convinced that human activity is the culprit for the rise in global temperatures over the last few centuries – a scenario that could prove to be costly and cause undue hardship for a majority of the Earth's human population. These findings are summarized in the Intergovernmental Panel on Climate Change's (IPCC) 2007 Fourth Assessment Report.

Climate experts still do not know if humans can reverse this process, but the general consensus – as expressed in the IPCC's Fourth Assessment Report – is that humans must alter their activities to mitigate climate change and avoid realizing a catastrophic scenario. This task seems insurmountable, but we have a present opportunity that we are not far from realizing: the development of rice straw as a mainstream building material.

Rice Straw: An Agricultural Residue

The term "rice straw" refers to the stalk of the rice plant – a part that is considered the least useful once the crop is harvested. In fact, only about 13,000 short tons of the 562,500 usable short tons of rice straw (i.e., <3%) produced by California in 1997 had successfully found a use (e.g., compost, animal feed) – a situation that left growers few options to dispose of it (Hrynchuk, 1998). This may seem like a minor environmental challenge, but it is worth noting that California constitutes less than 1% of global rice production (2.15 million of 477.7 million short tons of rice harvested globally in 2008 according to the National Agricultural Statistics Service online database). Rice producing countries around the world face the same problem collectively on a much grander scale.

A straightforward and globally practiced method to dispose of unneeded straw is to burn it right in the fields or as a fuel. Unsurprisingly, this adds carbon dioxide to the atmosphere and easily defeats efforts to mitigate climate change. The other obvious alternative would be to incorporate straw back into the soil as compost, but rice growers object to this practice because "they believe it is costly, may be conducive to increased incidence of crop diseases, and causes logistics problems with field management" (Hrynchuk, 1998).

Although there are currently a few uses for rice straw in California, so far they have not created enough demand to match the rate of production. The main uses include soil erosion control, animal bedding, and animal feed (Hrynchuk, 1998). Even if current uses could be developed enough to match straw production, it would not be prudent to assume this scenario could also be realized globally. Therefore, developing more technologies that

enable people to use rice straw in other ways, such as to manufacture industrial chemicals, make paper, or construct buildings are imperative to address this issue.

Use in Building Construction

Straw use in building construction has a long and time-tested history. It was typically not used alone but often combined with other materials into a composite, with the earliest example going as far back as the Biblical times of Moses when it was mixed with clay and baked into adobe bricks. Although proven and viable, combining straw into mud/clay composites may not be sufficient enough to solve the straw waste problem; it calls into question how much straw would realistically be used among a host of other logistical challenges.

In order to use as much straw as possible, it seems only natural to simply tap into the rectangular shape of the bale that straw is bundled into, as shown in Figure 1. On more than one occasion it has been suggested that bales be stacked into walls and a roof installed on top. This goal is not too far-fetched – several structures have been built with straw bales (derived from other types of grain) as the load-bearing material or as infill for insulation.

Figure 1. Shape of straw bale. Dimensions are approximately 18" x 14" x 35-40".

The first straw bale building was likely a one-room schoolhouse constructed near Bayard, Nebraska in either 1886 or 1887. During this early period of straw bale building, approximately 20 to 60 straw bale structures were erected, including houses and even a church (Bill, et al., 1994). All of these structures employed some sort of plaster or coating on both the interior and exterior straw walls for protection and increased structural strength. A

number of examples remain standing to this day with the walls intact, although variation in stewardship has permitted some to deteriorate faster than others. However, in each case, the straw's resistance to decay, insects, and fire still demonstrate its potential.

Up until 1936 the straw bales also served as the structural support for the roof. But in that year a two-story mansion with timber posts and beams for the structural support was built, except the voids between posts were filled with straw bales, essentially relegating straw to insulation (Bill, et al., 1994). This method has become popular among straw bale builders in the present day, but is not entirely superior to using straw structurally; it still requires a significant amount of timber for structural framing.

Despite the abundance of inexpensive straw and its time-tested historical successes, there are challenges that prevent its entrance to mainstream building and even in niche markets. The straw's behavior as a building material is not well understood, and this makes it difficult to design measures to handle any weaknesses it harbors. Appropriately, the same approval processes intended to protect consumers from unsafe buildings often prevent straw from being widely adopted as a structural building material.

Challenges in Straw Bale Building

Consistent Mechanical Properties

Among the first engineering challenges to using straw bales is determining their mechanical properties: yield strength and modulus of elasticity. Succinctly, yield strength refers to the maximum load (applied over a unit of area) which a material can handle before it permanently deforms: it will not return to its original shape and size after the load is removed. The modulus of elasticity refers to how stiff the material is: very stiff materials are more difficult to stretch or compress compared to less stiff materials. Knowledge of these two parameters is necessary for engineers to reasonably estimate the maximum safe load the bales can handle and how much the wall will compress under load. Unfortunately, the methods used to make straw bales do not produce units that perform consistently enough to design with these properties in mind. This is indicated by the summary data of two independent tests in Table 1.

Table 1. Comparison of Straw Bale Properties from Independent Tests. (Steinicke, 2005)

	Maximum Compressive Strength (psi)	Modulus of Elasticity (psi)
Bou-Ali Master's Thesis, wheat straw bales, University of Arizona, 1993	70 - 84	60 - 260
Ship Harbor Project Test, wheat/barely/oat straw bales, 1993	6 - 10	18 - 26

More importantly, not only were the mechanical properties inconsistent within the same study, but there was also great variation between the studies' results.

Less Suitable Mechanical Properties

The straw bale by itself is by no means as stiff or strong as other building materials, as shown in Table 2. For this very reason many modern enthusiasts are deterred from using it. Thicker walls can be used to compensate for a low stiffness and yield strength, but this sharply reduces the amount of usable space.

Table 2. Comparison of Mechanical Properties.

	Modulus of Elasticity (10^6 psi)	Yield Strength (10^3 psi)
Structural Steel (ASTM-A36)[a]	29	36
Timber (Red Fir, *Abies Magnifica*)[b]	1.81	6
Concrete (Structural Lightweight)[b]	3.05	4.06
Adobe Walls[c]	0.08 to 0.120	Not Tested
Unplastered Straw Bale Wall[c]	0.000015	.006 - 0.084[d]

[a]From database matweb.com. (MatWeb, 2010)
Same values also given in Beer & Johnston. (Beer, et al., 2006)
[b]From database CES EduPack 2009. (Granata Design Limited, 2009)
[c]From Steinecke. (Steinicke, 2005)
[d]Estimated using Bou-Ali's and Ship Harbor data cited by Steinecke.(Steinicke, 2005)

Creep

Straw bale builders have universally observed that straw bale structures seem to settle and get "shorter" as time passes since installation. This phenomenon, known as creep, happens to all materials to some degree and needs to be considered when designing structures. Creep testing done by the Ecological Building Network showed that straw bale walls will creep up to 1.2% of the wall height under a relatively small stress (1.46 psi, 404 lb_f/linear foot of wall) (King, 2006). More interestingly a straw bale wall loaded at 1.9 lb_f/in^2 continued to creep throughout the entire experiment – beyond 10 weeks. Although the experiment authors did not comment on how repeatable these

results were, it is more important to realize that creep in straw bales is not well understood and cannot be safely ignored.

The Stak Block

The Stak Block, invented and patented by Cal Poly graduates Ben Korman (ARCH) and Jay Ruskey (AGB) (Korman, et al., 2005) and produced under the company name Oryzatech Inc., is a solution intended to address the shortcomings of straw bales and the need to use significant amounts of straw. Simply put, 30 pounds of rice straw are treated with an adhesive binder, compressed into a mold, baked in an oven to cure the binder, and finally removed from the mold. Figure 2 shows what the finished Stak Blocks look like, and Figure 3 shows the general dimensions. The outer surfaces are planar, smooth, and stiff compared to the straw bale. They can be cut with regular carpentry tools used to cut wood.

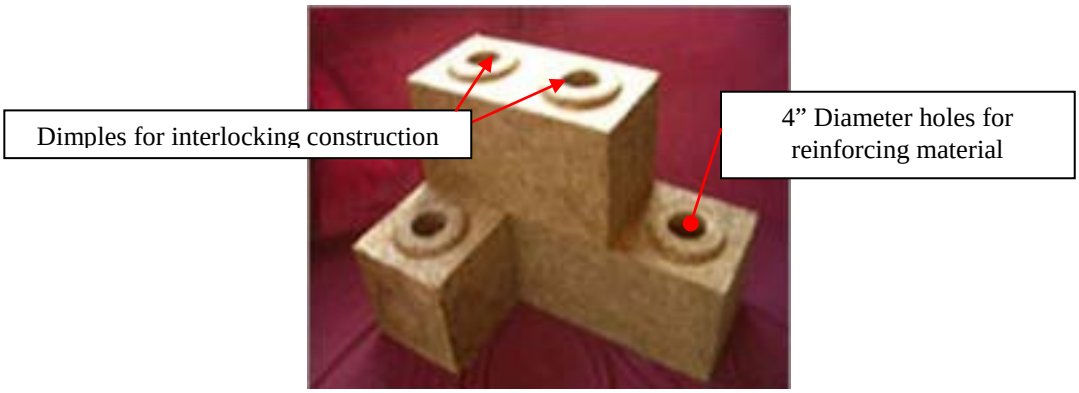

Figure 2. The Stak Block. Photo courtesy of Oryzatech, Inc.

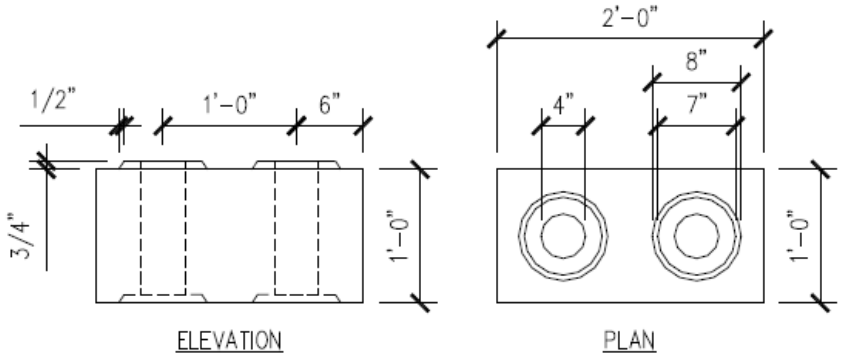

Figure 3. Stak Block dimensions. Drawing from Camann (Camann, 2009). Reproduced with permission.

Overview of Stak Block's Use

The Stak Block's raised "dimples" on top (with corresponding female impressions on the bottom) are intended to make the block easier to stack and interlock to form walls – like toy bricks (e.g., LEGO®s). To form walls, the blocks are stacked in a running bond pattern, as shown in Figure 4. The dimples along the top row are sawed off just before the wooden board is secured on top. A washer, nut, and threadbar (solid steel rod with screw threads) are used with the wooden board and together precompress the wall to stabilize it before the roof is installed. The threadbar is used at prescribed intervals, fits inside the Stak Block's vertical holes and is anchored to the concrete foundation. The face exposed to the outside would be coated with an appropriate skin such as stucco or plaster.

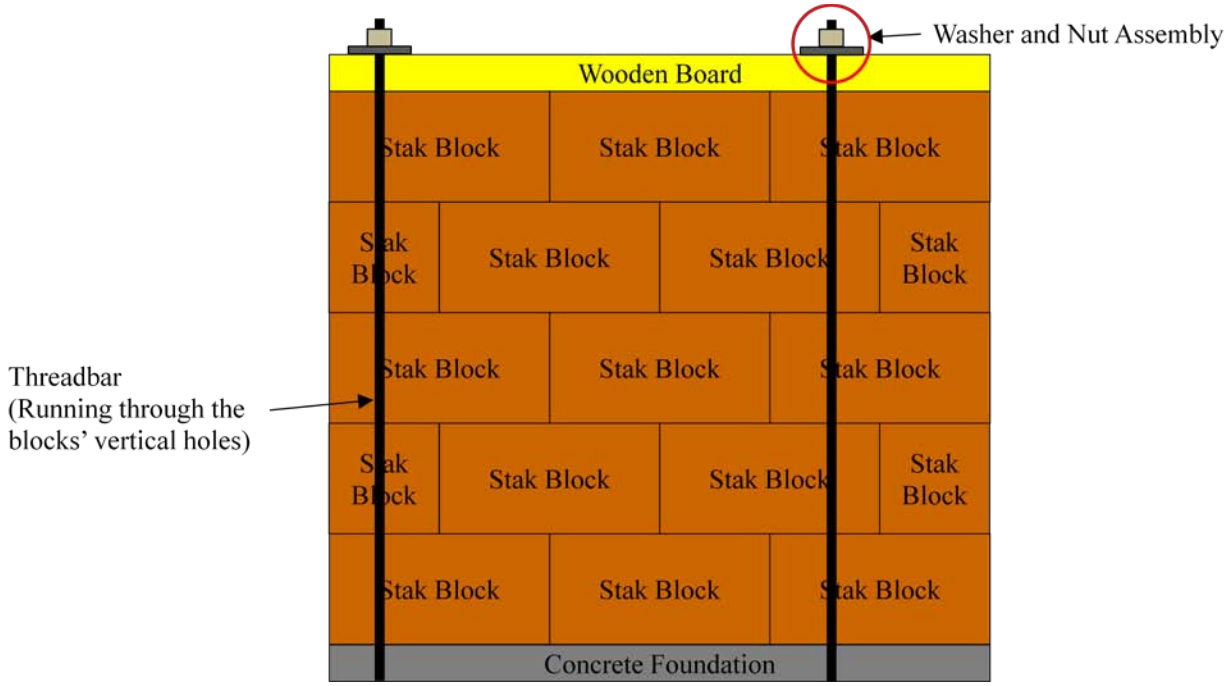

Figure 4. Schematic of possible Stak Block's use in wall systems.

This system has been successfully tried for one wall of a tool shed located at a private residence in Goleta, CA. Figure 5 shows the interior of the wall with the Stak Block exposed and well-fit with the window, roof, and conventional wall system surrounding it. Figure 6 shows the washer and board assembly in context.

Figure 5. Interior wall photo of actual Stak Block wall.

Figure 6. Photo of wooden board, nut, and washer pre-compression system.

There are several other suggested methods to reinforce the Stak Block wall, including a variety of coatings (e.g. stucco, plaster) and pouring concrete down the vertical holes. These are the subject of continuing investigation.

Stak Block's Potential to Address Straw Bale's Challenges

Unpublished data collected by Cal Poly materials engineering undergraduates (May 2008) showed that the manufacturing process yields a block with predictable and repeatable mechanical properties – and therefore surpassed the straw bale in this category. The undergraduates used the load measured when a full-sized Stak Block was compressed by 1.2" (10% strain) as a metric. Their data fit a normal curve centered about 9000 lb_f as shown in the Minitab plot in Figure 7.

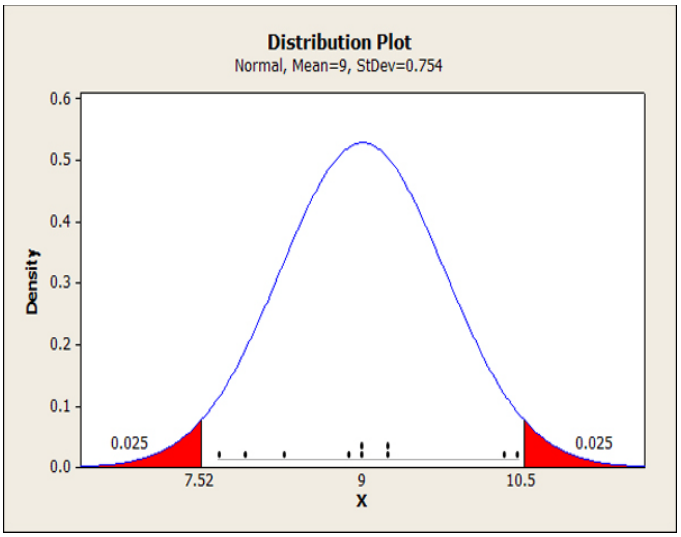

Figure 7. Distribution plot of measured load (kips) at 10% strain deformation of Stak Block.

Moreover, they found the elastic modulus to be 900 psi (lb_f/in^2) and the yield strength to be 23 psi (lb_f/in^2). These results indicate that the Stak Block is stiffer than a straw bale but may have around the same yield strength.

Other testing suggests that the Stak Block may match or exceed the performance of straw bales in other categories considered part of the straw bale's strength. In the same May 2008 undergraduate study referenced earlier, students determined that the fire resistance of the Stak Block exceeded straw bales (see Figure 8 and Figure 9).

Figure 8. Initial state of simulated straw bale and Stak Block walls.

Figure 9. Final state of simulated straw bale and Stak Block walls.

With regards to insulation value, a materials engineering undergraduate student determined the Stack Block's R-value to be 3.89/inch (Monell, 2008) compared to 1.45/inch for straw bales (King, 2006). Thus, the Stak Block is stronger, stiffer, more consistent, and a better insulator than the straw bale.

Improving Carbon Footprint and Development for Appropriate Technologies

The current and planned future manufacturing processes call for electrically powered ovens to cure the block at 300°F for approximately 1 hour. The shortfall in this method is that it is unwise to assume enough

electricity derived from renewable and reliable sources is available wherever the Stak Block is produced – using electricity derived from fossil fuels (or even fission) would easily defeat the carbon advantages of using rice straw.

An obvious solution employs solar thermal energy to directly heat the block. This introduces two main challenges: (1) collecting enough light to convert into thermal energy, and (2) keeping the oven insulated to maintain prescribed temperatures. To address these challenges it is worth investigating whether the block can cure at a lower temperature; it might mean complex light collection and thermal insulation systems are not needed. If this is true, then a simple solar oven could be made in countries that lack advanced manufacturing capabilities of developed countries – effectively increasing the Stak Block's rapid deployment.

It is not unrealistic to expect that the binder can cure at a lower temperature if given more time. The chemical reaction may be driven by the amount of energy entering the binder/straw mix. A lower temperature would mean that energy enters the binder at a slower pace, and to compensate the block should be baked at that temperature for a longer period of time. In this way the same amount of energy is used to cure the block, albeit at a slower pace than the current manufacturing method.

Thesis Statement

The time and temperature relationship needed to cure the adhesive binder with rice straw is not well understood. The goal of this thesis is to study straw cubes to discern a time-temperature relationship needed to cure the binder.

CHAPTER 2: CURING OF pMDI AND STRAW

Oryzatech uses a binder known as polymeric diphenylmethane diisocyanate (pMDI). This binder is produced by various companies under different trade names and is becoming more prominently used as an adhesive in wood-based composites such as oriented strand board (OSB) (Effect of moisture content on curing kinetics of pMDI resin and wood mixtures, 2005) (Cure chemistry of wood/polymeric isocyanate (PMDI) bonds:Effect of wood species, 2007). What makes this adhesive more attractive than others is that it does not contain formaldehyde, a compound the State of California recognizes as a carcinogen. Products containing formaldehyde typically release this compound into the atmosphere in small but still harmful amounts over time and therefore pose a threat to human health.

pMDI consists of long polymer chains and is a viscous liquid at room temperature, but the polymers will crosslink to form larger molecules when heat, moisture, or both are added (Effect of moisture content on curing kinetics of pMDI resin and wood mixtures, 2005). The resulting product has a higher melting point than the original liquid, and consequently the binder changes phase into a solid form. The polymers also interact and form covalent bonds with the wood (or possibly straw if appropriate), and it is this 3-D network of bonds that holds the straw together.

Although pMDI has been studied for some time, there remains disagreement on the curing kinetics (Evaluation of the cure kinetics of the wood/pMDI bondline, 2001). Moreover, pMDI has been studied with wood but not straw . Thus, the purpose of this section is to provide an overview of the reaction kinetics, relevant findings, and how these findings influence this thesis.

General Characteristics

pMDI is known to be reactive with water, and it is suggested that it reacts with the hydroxyls found in wood to cure (Effect of moisture content on curing kinetics of pMDI resin and wood mixtures, 2005). When curing with wood, several products are formed before the adhesive forms covalent bonds with wood (Cure chemistry of wood/polymeric isocyanate (PMDI) bonds:Effect of wood species, 2007). Harper et al. recognized that the complex nature of the curing process rendered first principle approaches to modeling the reaction very difficult, and instead focused on empirically derived curing models (Evaluation of the cure kinetics of the wood/pMDI bondline, 2001). For increased accuracy, their experiments were intended to simulate the heat, pressure, and moisture conditions

found in actual manufacturing in order to best understand the curing process. To begin with they assumed pMDI cured according to a basic curing model that relates a rate constant k with a function of the degree of cure $f(\alpha)$ ($0 \leq \alpha \leq 1$), and the rate of cure $\frac{d\alpha}{dt}$ at a constant temperature (Equation 1).

$$\frac{d\alpha}{dt} = kf(\alpha) \qquad (1)$$

The rate constant was assumed to depend on several other parameters according to an Arrhenius relationship (Equation 2)

$$\ln k = \ln A - \frac{E}{RT} \qquad (2)$$

where E is the activation energy, A is the Arrhenius frequency factor, R is the ideal gas constant, and T is the absolute temperature. Equations 3 and 4 show the two possible models for the cure function $f(\alpha)$.

$$f(\alpha) = (1 - \alpha)^n \qquad (3)$$

$$f(\alpha) = \alpha^m(1 - \alpha)^n \qquad (4)$$

In Equation 3, n is the reaction order and in Equation 4 the sum of exponent m and n is the reaction order. Reactions in which $\frac{d\alpha}{dt}$ is at a maximum at the onset of cure are usually characterized by Equation 3. Autocatalyzed reactions generally have $\frac{d\alpha}{dt}$ reach a maximum when $0.30 \leq \alpha \leq 0.40$, and are better described by Equation 4. Harper et al. assumed that pMDI follows most curing reactions (the rate of cure reaches a maximum around 45-55% completion) and therefore reasoned Equation 4 would more accurately model the curing. Following their experiments with the wood species Aspen (*Populus tremuloides*), they concluded the reaction followed an autocatalyzed first order model.

Moreover, experiments and modeling conducted by He & Yan show that moisture present in the wood increases the activation energy and reaction enthalpies but likely reduces the curing time (Effect of moisture content on curing kinetics of pMDI resin and wood mixtures, 2005). As an explanation they suggested that the isocyanates comprising the pMDI reacted with the water in the wood more frequently than the hydroxyls (also in the wood); water may have a greater mobility in wood and could reach the pMDI faster than the hydroxyls. Thus the overall effect would be a reduction in curing time compared to completely dried wood. However, their models predicted that the moisture content needs to be on the order of 12% by weight before it makes a significant impact, and there was very little improvement in cure time when the moisture content was increased to 50%.

The actual time it took for the curing reaction to occur was much less than the time Oryzatech uses to cure the block. The mathematical model Harper et al. developed from their experiments was compared to the experimental data they collected, and it showed that the model approximated the experimental data reasonably well despite predicting a shorter curing time. But more importantly, the reaction itself occurs on the order of a couple of minutes – about 30 times less than the time Oryzatech uses.

The magnitude of these curing times was also observed in experiments by He and Yan in their investigation on the effect of using different wood species with pMDI (Effect of moisture content on curing kinetics of pMDI resin and wood mixtures, 2005) (Curing kinetics of polymeric diphenylmethane diisocyanate with different wood species, 2007). The details are more appropriately discussed in the next section. However, it is worth mentioning that the relatively short reaction times imply that the curing reaction itself is not the rate-limiting step when curing the Stak Block.

The temperatures used in the experiments conducted by Harper et al. and He & Yan are also lower than that used by Oryzatech. In both Harper and He's studies the pMDI was successfully cured with the wood samples at temperatures ranging from 92.2°C to 164.5°C depending on a combination of other factors (Evaluation of the cure kinetics of the wood/pMDI bondline, 2001) (Effect of moisture content on curing kinetics of pMDI resin and wood mixtures, 2005). These results suggest that Oryzatech's need to heat the block to 150°C (300°F) may not be driven by the actual curing temperature.

Effect of Different Wood Species

In each of these studies only wood was cured with pMDI, leaving it ambiguous how applicable the conclusions are to curing pMDI with rice straw. He and Yan's experiments on pMDI curing kinetics with different wood species suggest these results could in fact be applied to straw. By comparing the activation energy, reaction enthalpy, and reaction times they concluded that the reaction kinetics was not significantly different among wood species – if moisture was present in the wood (12% moisture content by weight). Although Harper et al. did not report the moisture content in their samples He and Yan's curing times are still close to Harper's.

These results imply that if enough moisture is present in the straw it could be considered a type of "wood." Therefore the curing times and temperatures between pMDI and rice straw could be expected to be close to those used and determined by Harper et al. and He & Yan.

CHAPTER 3: MODELING OF HEATING PROCESS

A product such as the Stak Block that has good thermal insulation properties must conversely have a very low thermal conductivity. It would therefore be expected that, for the size of the Stak Block, the core was significantly cooler than the surface for most of the time it was in the oven. If this was true then the low thermal conductivity could be considered the limiting factor, and it would be possible to cure the Stak Block at temperatures used by Harper et al. and He & Yan – albeit for a longer time in the oven. The purpose of this chapter is to report and explain the heat transfer closed-form estimations and finite element (FE) modeling prior to experimentation. (This chapter will use SI units because they are more straightforward to use when solving heat transfer problems, a technique consistent with a majority of heat transfer analyses. Where appropriate, U.S. customary unit equivalent values will be provided).

Closed Form Estimations for the Stak Block

The Biot number is a standard metric that can be used to determine how safe it is to assume a uniform temperature distribution for any object undergoing convection to or from a fluid. It is calculated as:

$$\boldsymbol{Bi} = \frac{\boldsymbol{hL_c}}{\boldsymbol{k}} \qquad (5)$$

where L_c is the volume to surface area ratio (i.e. characteristic length), h is the convection coefficient, and k is the material thermal conductivity. Generally, if $Bi < 0.1$ then it is safe to assume that the object has a uniform temperature distribution at any point in time. Approximating the Stak Block simply as a 1' x 1' x 2' rectangular prism with two 4" diameter through holes yielded $L_c = 0.04737$m. The thermal conductivity was calculated to be 0.11 W/m^2-K based on the R-value determined by the May 2008 study. This was considered a better estimate than using the R-value calculated in the 2009 senior project; the senior project accounted for the cylindrical holes in the Stak Block and would therefore not accurately represent the material.

It is worthwhile to briefly explain the heating process in order to develop estimates for remaining parameters. As mentioned previously, Stak Blocks were placed into molds (Figure 10) with approximately 1/8" wall thicknesses.

Figure 10. Stak Block mold.

The steel mold may be safely neglected in this approximation for two reasons. First, the volume of a simplified steel mold with a 1/8" wall thickness would constitute less than 8% the volume of the Stak Block. Second, the thermal conductivity estimates for the steel (k = 60.5 W/m-K) (Incropera, et al., 2007) were more than 100 times the Stak Block estimate. Therefore, the steel mold was considered negligible and the block was modeled as having direct convection interactions with the oven air.

Two molds are typically stacked in the oven and baked concurrently. It can be inferred from the photo in Figure 11 that there is very little room for forced convection when two molds are baked.

Figure 11. One Stak Block mold in oven. Second molds were stacked on top of the first.

For this reason free convection was a reasonable assumption. The oven wall was assumed to be 422K (300°F) – the temperature Oryzatech sets the oven. 300K (80°F) was chosen as reasonable initial temperature. As an approximation, all surfaces were assumed to have a uniform convection coefficient. Based on the orientation of the mold in the oven, the mold was modeled as a vertical flat plate .3048m (1') tall to determine the convection coefficient. Thermophysical properties of air and the Churchill & Chu Nu-Ra correlation (Incropera, et al., 2007) were used to determine a convection coefficient of $11 W/m^2\text{-}K$.

Substituting these values into Equation 5 the Biot number was found to be 4.74 for the Stak block. This high number strongly indicates that the Stak Block cannot be assumed to have a transient uniform temperature distribution. The combination of the three-dimensionality of the block and the transient nature of the problem already made a closed-form study very difficult – even after simplifying the block geometry. Therefore, a numerical approach was more appropriate at this point.

Preliminary Heat Transfer Finite Element Model of Stak Block

Abaqus Standard 6.7 was the commercial finite element analysis software used to create a heat transfer FE model for the full sized Stak Block. The purpose of this study was to estimate the transient temperature distribution within the block.

Simplifications and Assumptions

A simplified three-dimensional FE model was created in order to save computation time. The dimples and corresponding female impressions would have required the use of a very complex mesh to accommodate three dimensionally round features and were therefore not included. Since the dimple's height was less than 5% of the block's height this was considered a reasonable approximation. The resultant "block" was symmetrical across the x, y, and z axes and consequently permitted the use of only a one-eighth (6" x 6" x 12") model of the Stak Block (Figure 12) without significant loss of information about the entire block. A 2 inch radius hole free to interact with the oven air was modeled in its appropriate location. Quadratic heat transfer elements were used (768 hexahedron and 352 wedge elements), with a seed size of 0.0375m. Mesh convergence studies showing the appropriateness of this seed size can be found in Appendix A.

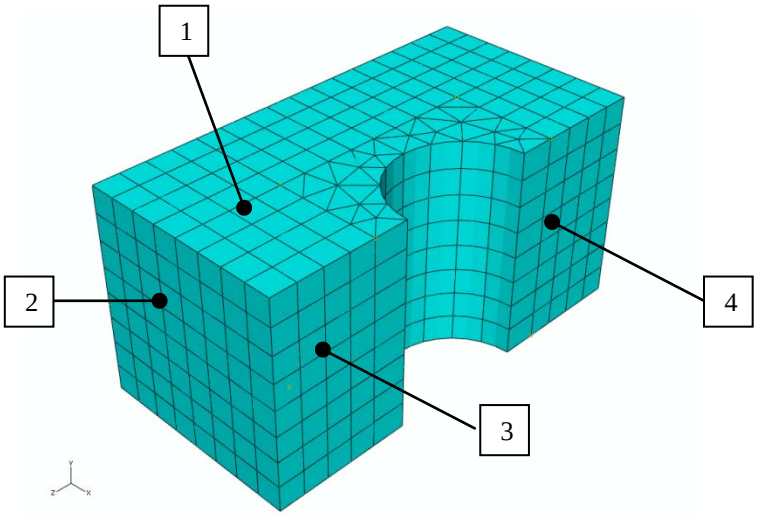

Figure 12. One-eighth model of Stak Block. Overall dimensions are 6" x 6" x 12". Numbered faces indicate those internal to the Stak Block but exposed via cross-sectioning in the FE model.

A value for specific heat was not available and so C_p = 1300 J/kg-K was estimated based on comparable wood-based building materials (Incropera, et al., 2007). In addition, ρ = 263 kg/m^3 was assumed as a uniform average density based on a 30 lb block. This was a reasonable assumption because (1) a cross section photo (Figure 13) did not reveal an obvious density variation and (2) the straw compression process did not intuitively have a density bias.

Figure 13. Cross-section photo of Stak Block.

The Stak Block was heated in a steel mold (Figure 11) which was then placed in an oven (Figure 12). As in the Biot approximation, for simplification the steel mold was not considered in the analysis. The specific heat of steel ($434 \leq C_p \leq 480$ J/kg-K) is less than half the specific heat estimate for the Stak Block, and the thermal conductivity of steel is much greater than the straw. Conduction from the oven floor to the mold was considered negligible because (1) the surface area contact was very small (2) it was likely there was a high contact resistance between the oven and the mold and (3) heat flux was also limited by the welds that connect the fin-like features to the mold. Figure 10 and Figure 11 visually support these assumptions.

The oven was modeled as pre-heated to 422K (300°F), and the block having an initial temperature of 300K (80°F). The convection coefficient and thermal conductivity calculated earlier were also applied to this model. An absorptivity of 0.95 was chosen based on materials similar to black painted steel (Incropera, et al., 2007), and its close value to 1.0 represents the black steel mold's near-perfect ability to absorb all radiation. The mold's emissivity (i.e., a factor considered for radiation heat loss) was not a concern because the oven is always hotter than the mold and the oven completely encloses the mold, therefore there cannot be a net heat loss from the block to the oven.

However, the most significant assumption made for this FE analysis was that any nonlinearities caused by chemical reactions or other unforeseen factors could be considered negligible. The results of the analysis shed light on the validity of this assumption.

Results and Discussion of Preliminary FE model

A temperature contour plot of the Stak Block after 1 hour is shown in Figure 14. The blue-colored regions indicate temperatures approximately 300 – 340K (80 – 150°F). This result confirms that (1) the block's temperature cannot be considered uniform after 1 hour and (2) a significant portion of the block is much cooler than the oven temperature. Taking into account that the binder had been cured at 377K (219°F) with wood (Curing kinetics of polymeric diphenylmethane diisocyanate with different wood species, 2007), additional contour plots revealed that a significant portion of the block still did not reach this temperature after 30 minutes (Figure 15) and even 60 minutes (Figure 16). (377K was rounded down to 375K, and therefore regions cooler than 375K are shown in black).

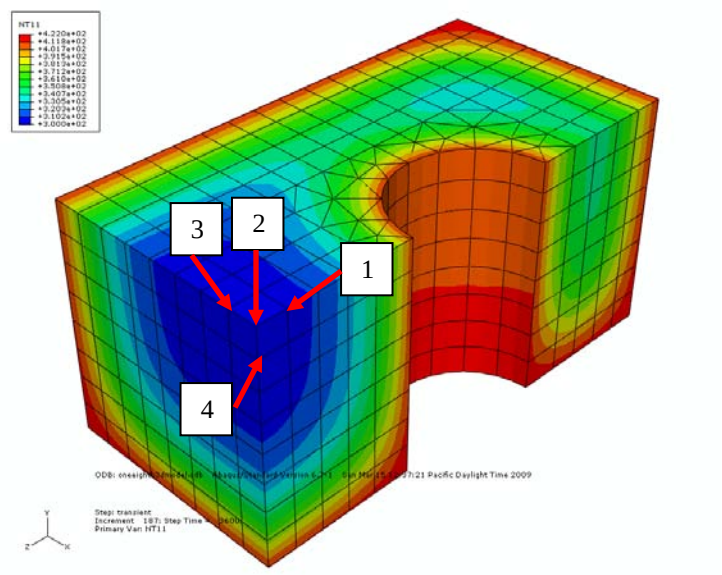

Figure 14. Temperature Contour Plot in Kelvin of 3-D Transient FE Model.

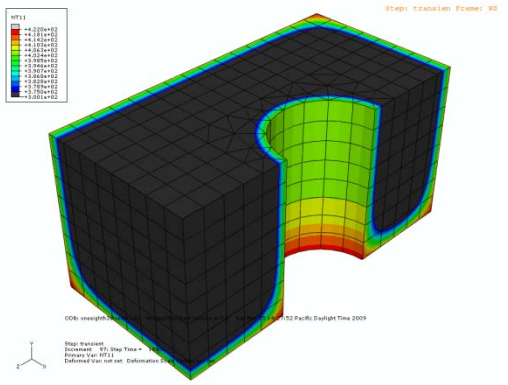

Figure 15. Block Temperature contour plot at t = 1800s. Black regions indicate temperatures below 375K.

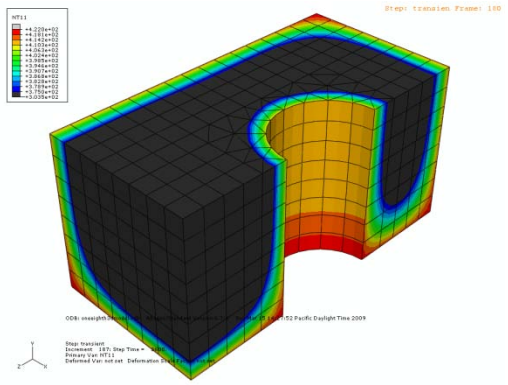

Figure 16. Block temperature contour plot at t = 3600s. Black regions indicate temperatures below 375K.

The small change in the proportion of the Stak Block volume that reached 375K from 30 minutes to 60 minutes supported the idea that cure times are more strongly influenced by how fast heat propagates through the material rather than how much energy is needed to sustain the binder curing reaction itself. More importantly, the vast black-colored regions of Figure 15 and Figure 16 suggested that a large proportion of the block is left uncured. By contrast Oryzatech reported that most, if not all, of their blocks were cured. Such a discrepancy called into question the accuracy of the thermal conductivity and specific heat estimations. Additional simulations were performed by varying thermal conductivity and specific heat individually (ceteris paribus) to study their effects on the temperatures of four core nodes (shown in Figure 14). Their temperatures were recorded after a simulated period of 1 hour, and the results are presented in Figure 17 and Figure 18.

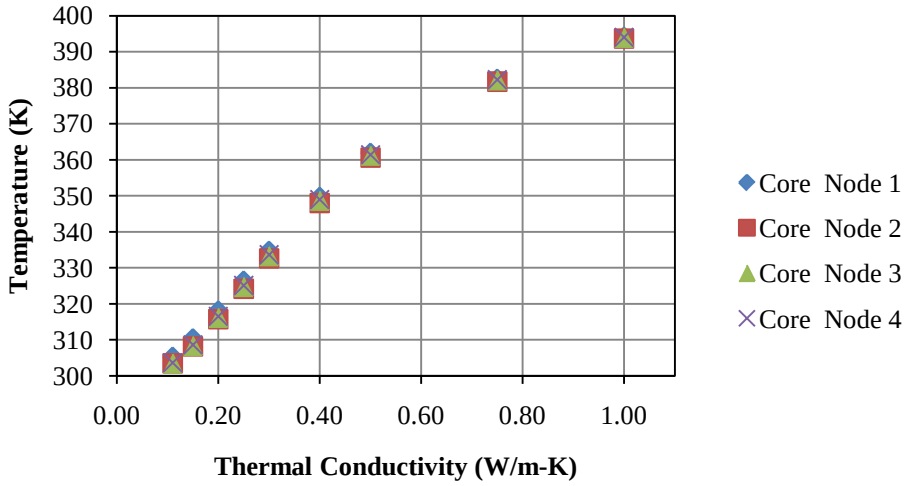

Figure 17. Effect of thermal conductivity on core nodal temperatures after 1 simulated hour.

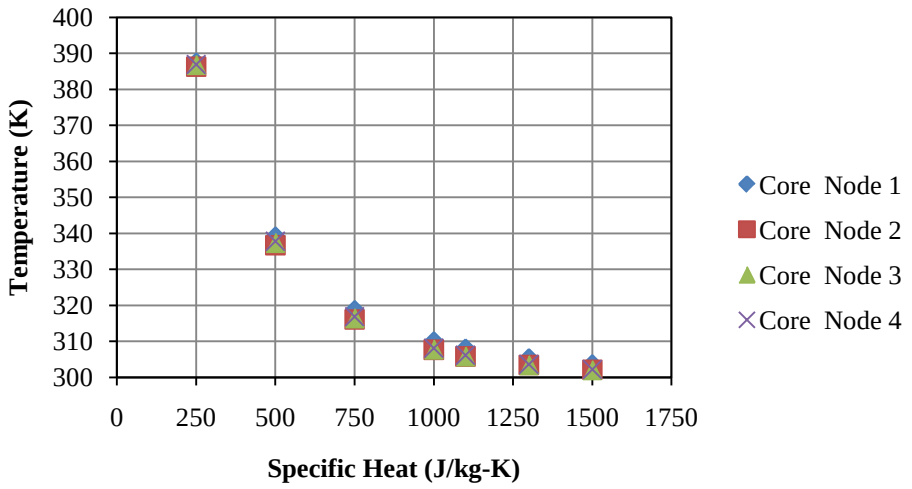

Figure 18. Effect of specific heat on core nodal temperatures after 1 simulated hour.

It is unlikely that more accurate modeling of the oven would have produced significantly different results. The graphs showing the effect of emissivity and the convection coefficient (Figure 19 and Figure 20) support this conclusion.

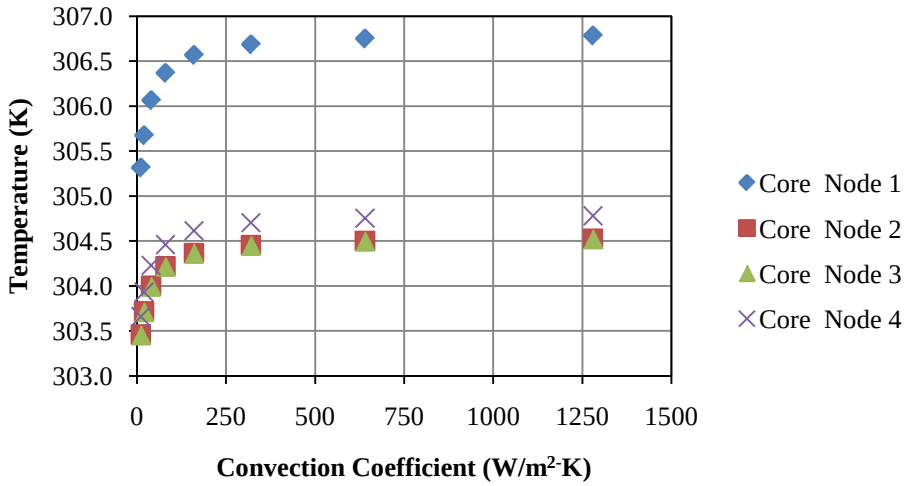

Figure 19. Effect of convection coefficient on core nodal temperatures after 1 simulated hour.

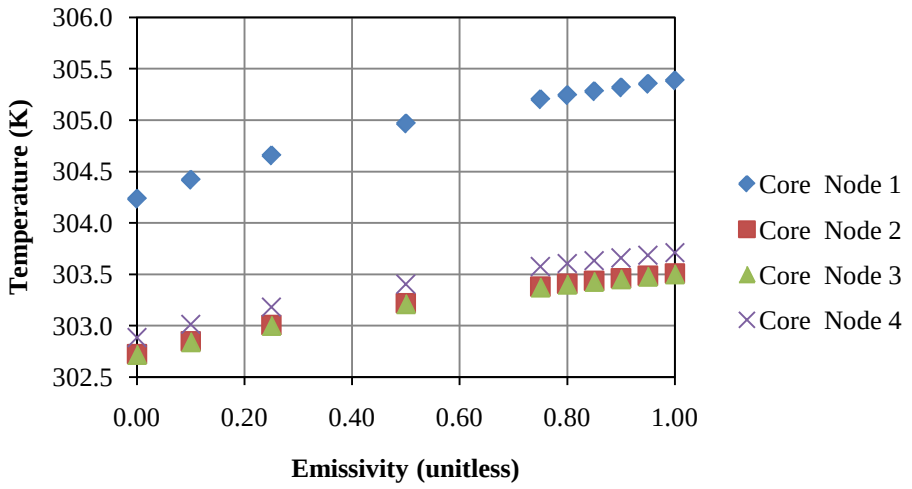

Figure 20. Effect of emissivity on core nodal temperatures after 1 simulated hour.

Clearly, to achieve a temperature of 375K the thermal conductivity needed to be near 0.60 W/m-K. This meant that the actual R-value needed to be one-sixth (R = .21/in) of the experimentally determined R-value of the Stak Block (R = 1.25 /in, calculated without the air void) – assuming constant properties. As an alternative the actual specific heat could be close to 300 J/kg-K. However both of these values for thermal conductivity and specific heat were not considered reasonable for the material in question. These FE results therefore raised the question whether the Stak block cured at a lower temperature, and whether other considerations (e.g., exothermic binder chemical reaction, changing material properties, etc.) were not negligible. More importantly, this meant that the FE results alone could not be used to estimate curing times, and further investigation was needed to understand the curing process.

CHAPTER 4: EXPERIMENTAL METHODS AND MATERIALS

Previous chapters clearly outline that current information was insufficient to understand the proper curing times and temperatures needed. If the block did not cure at a lower temperature, then other effects – such as the reaction enthalpy of the binder curing – may have influenced the curing process. However, the size of the Stak Block, the resources needed to make and study it made it impractical to directly study for this thesis – and therefore the curing behavior of smaller cubes was studied instead. This chapter explains the materials and methods used in the experiments intended to better understand this phenomenon.

Experimental Design

A split-plot design was used to complete the entire experiment within the time frame available. Initially 3 temperatures were selected to bake the cubes (150°C, 100°C, 50°C) at 4 different times (1hr, 2 hrs, 3hrs, 4hrs). For each experiment run, four molds were baked simultaneously at the same temperature. One mold was randomly selected to be removed at each specified time, and the cube inspected for cure using a chemical dye. In this first iteration, only the 100°C temperature was run twice to demonstrate repeatability in the results. But it was later decided for the remaining iterations to perform each experimental run twice, and the results of the cube curing evaluations were used to inform the time-temperature combinations tested in the next iteration to develop sufficient granularity in the data. Temperatures above 150°C or below 50°C were not tested. After sufficient granularity in the data was found, three optimized (i.e., minimum time at set temperature) time-temperature combinations were identified (low, medium, and high temperatures). Four cubes were subsequently cured simultaneously at each of the optimized time-temperature combinations. The specimens were subjected to mechanical property evaluations to determine the modulus of elasticity and yield strength. The modulus of elasticity and yield strength for cubes baked at different times and temperatures were compared to discern if they had cured.

Straw Cube Fabrication

The cube forming and processing methods were designed to mimic the Stak Block manufacturing process as accurately as possible. The following describes the materials and methods used.

Binder Treatment

110g of rice straw was measured using a triple beam balance and placed into a treatment chamber (Figure 21). The treatment chamber lid was removed enough to permit an atomizer airstream to enter it. Approximately 4mL of pMDI binder was measured into a graduated cylinder (which also served as a reservoir for the atomizer). Binder was drawn from the graduated cylinder reservoir up into the atomizer using the Venturi Effect created by a high pressure airstream (120 psi) which atomized the binder into a mist. The atomizer, tube, and graduated cylinder setup is pictured in Figure 22. In this method, only enough straw was treated with binder to form 1 cube.

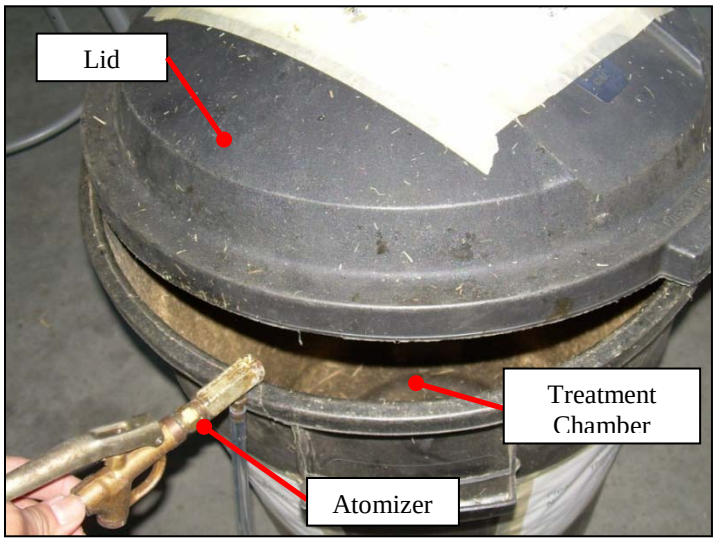

Figure 21. Set-up used to treat straw with atomized pMDI

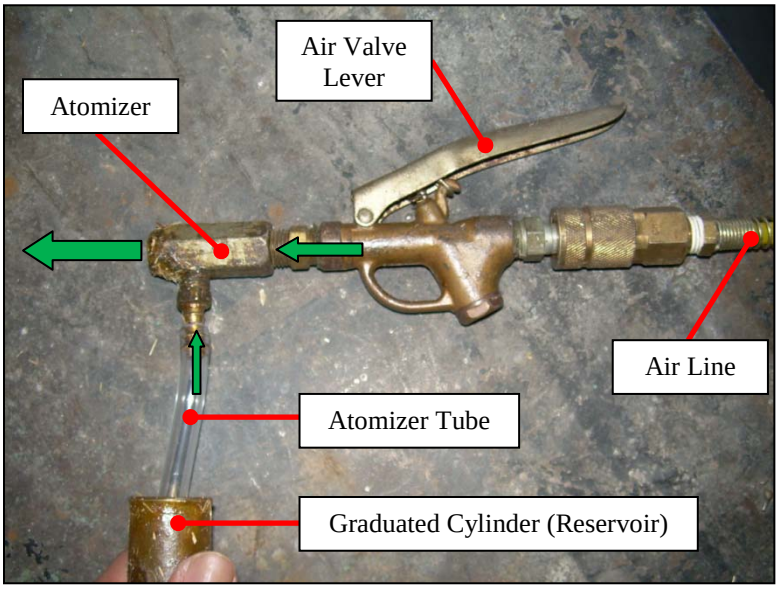

Figure 22. Atomizer configuration.

The atomized binder was applied in short 2-3 second bursts of with the atomizer aimed at the straw. Between each burst, the lid was replaced onto the chamber and manually shaken vertically 12-15 times so that the straw was sufficiently mixed with each burst of binder.

Mechanical Compression to Size

100g of binder treated straw was compressed into molds that formed cubes with 2.75 inch side lengths. Although this gives a higher average density (293 kg/m^3) than the Stak Block (263 kg/m^3), from several trial runs it was determined that inputting 100g of straw yielded cubes weighing about 90g (264 kg/m^3) after they were baked in an oven for 4 hours. The difference in mass was assumed to be caused by the amount of straw lost when transferring it from the balance into the mold. Moreover, it was decided that it was better to err on the side of a denser block – curing times were expected to be longer because of the extra mass and therefore provide a more conservative estimate of curing times.

A custom press (Figure 23) was designed and built to achieve this task. Details of the straw press construction can be found in Appendix H. Molds for each cube were made from a square tube and two compression plates. The square tube section (Figure 24) confined 4 of the 6 cube faces, while the 2 compression plates (Figure 25) confined the remaining two cube faces. A schematic of how this process works is shown in Figure 26 through Figure 29. A total of 8 molds were fabricated for use and labeled with a Roman numeral. For each experiment run the molds chosen for use and order they were filled were randomized. Each mold was filled within 2 hours of the binder being applied to the straw.

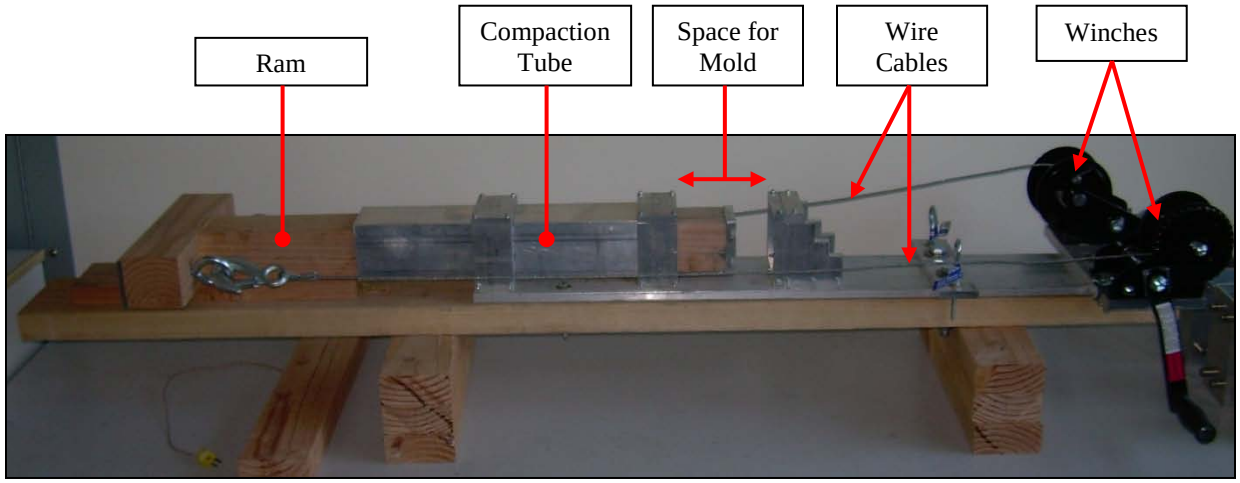

Figure 23. Straw cube press.

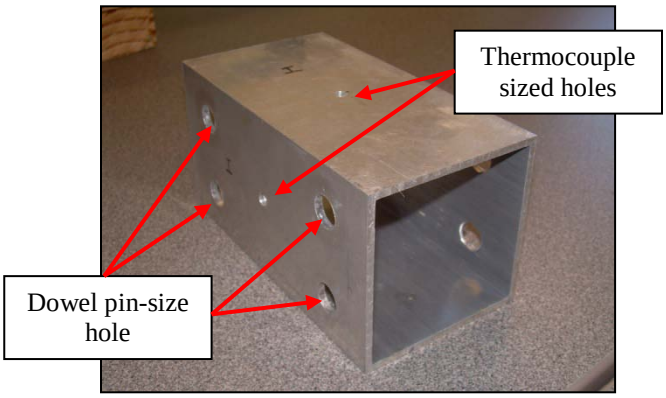

Figure 24. Square tube component of mold.

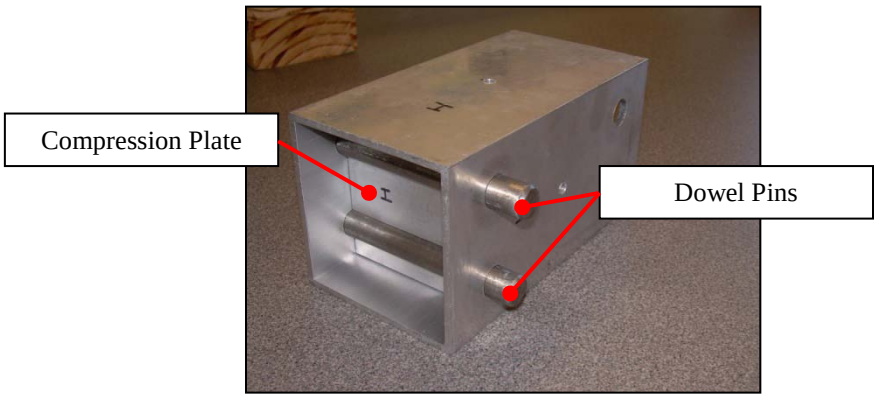

Figure 25. Mold with 1 compression plate (rear plate removed to contrast with installed plate).

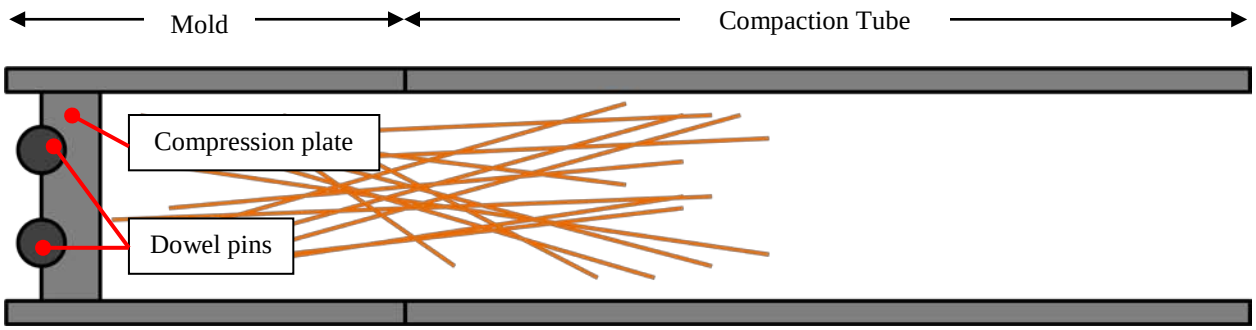

Figure 26. Loose straw is stuffed into the mold via the compaction tube. Cross-section view.

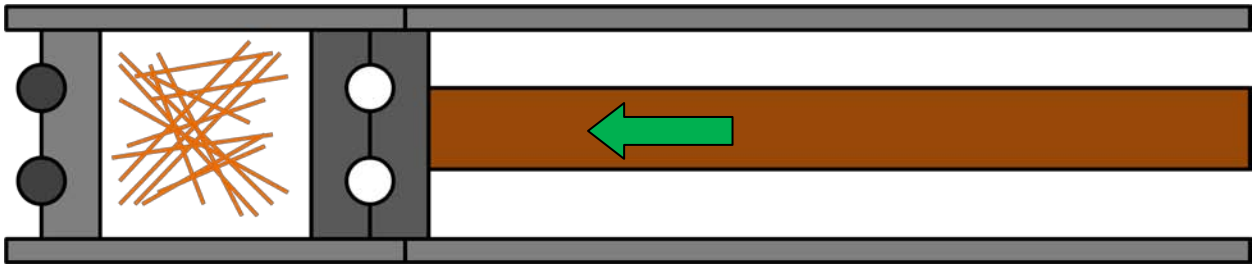

Figure 27. A winch-powered ram compresses the straw to desired size. Winch not pictured.

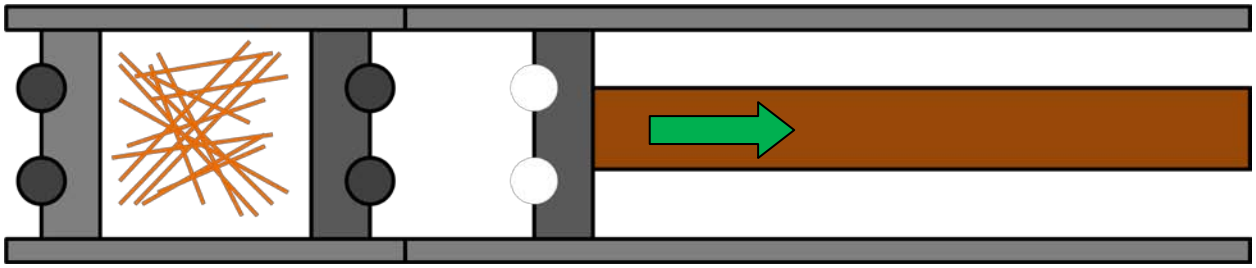

Figure 28. Dowel pins are inserted to hold the compression plate in place, and then the ram is withdrawn.

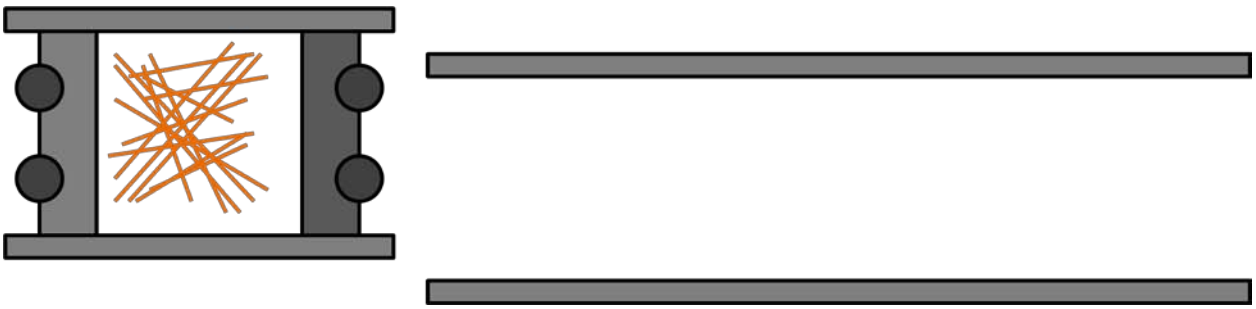

Figure 29. The completed mold is removed from the press and is ready to be placed in the oven.

Curing

Molds, filled with appropriate amounts of binder-treated straw, were placed in a Fischer Scientific 851F isothermic precision low-temperature oven (capable of temperatures ranging 50 – 300°C, 122 – 572°F). The oven was preheated to the temperature prescribed by the experiment. The oven consisted of two racks as pictured in Figure 30. The molds were randomly placed in a staggered pattern (Figure 31) to limit the effects of molds shielding each other from convection currents or thermal radiation. Molds were placed in the oven within 2 hours from when they were filled. The oven interior dimensions were 18" x 26.5" x 18" (width, height, depth) and the rack dimensions were 18" x 18". The lower rack was spaced 8" above the oven bottom, and the upper rack 8" above the lower rack. Each mold had a 3" x 5.75" footprint on the rack.

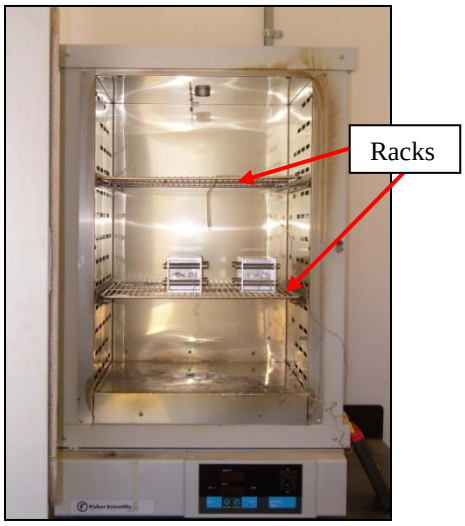

Figure 30. Fischer Scientific 851F precision low temperature oven.

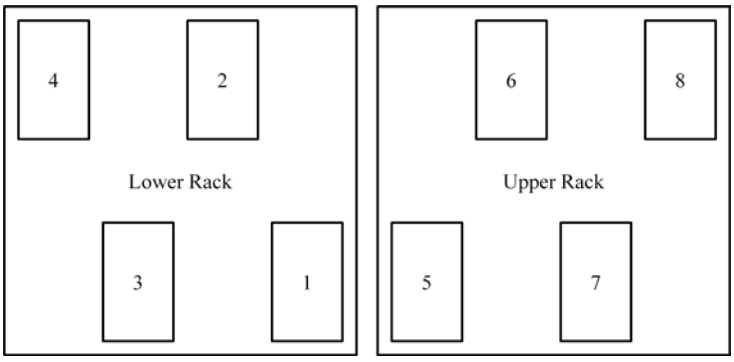

Figure 31. Mold positioning on oven racks.

Cube Retrieval

Once each mold cooled enough in ambient air to be safely handled with bare hands, the cubes were retrieved from their molds using the same press that compressed them to size. Figure 32 and Figure 33 show how this works schematically. Mass and dimensions were recorded for each cube. The cubes were stored at room temperature (approximately 18°C - 29°C, 65°F-85°F) for 24-72 hours prior to evaluation for curing.

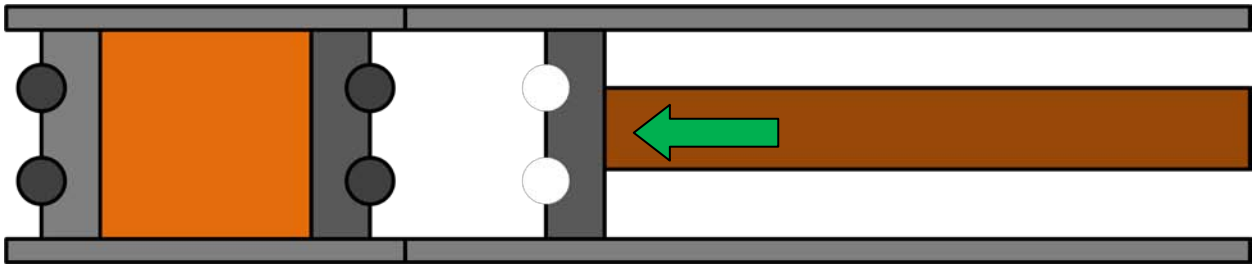

Figure 32. The baked mold is placed back into the press, and the ram is re-inserted into the compaction tube.

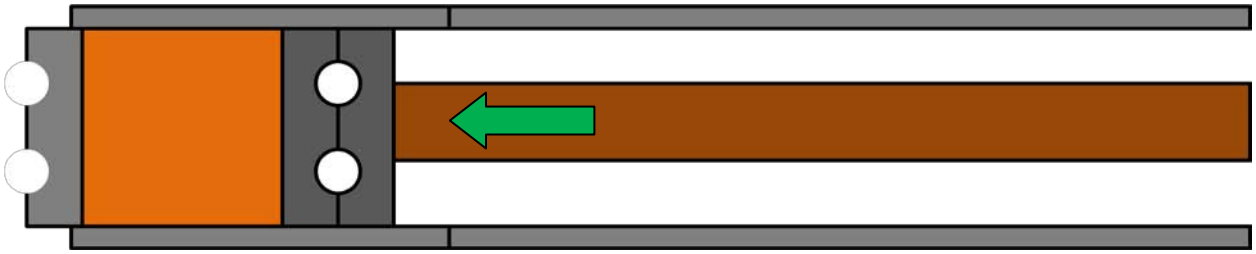

Figure 33. All dowel pins are removed, and the finished cube is pushed out.

Curing Evaluation Using Chemical Dye

Cubes were cut into 2 equal halves using a vertical band saw so that the cutting plane was perpendicular to the axis used to compress the straw. Once the cross-section was exposed, a chemical dye (that indicates the presence of uncured binder) was sprayed onto the cross-sectioned face and its response was recorded. If any part of the cross-sectioned face changed colors from yellow to red its response was recorded as “uncured,” and if there was no color change its response was recorded as “cured.” Figure 40 is an example of the cross-section of a halved cube.

Curing Evaluation Using Mechanical Properties

Cubes prepared specifically for mechanical property evaluation were tested in accordance with Procedure A of ASTM C165-07: the test standard for measuring compressive properties of thermal insulations. This standard

was considered the most appropriate, and Procedure A was selected over Procedure B based on the load-displacement curves for full-sized Stak Blocks. Key differences between methods prescribed by ASTM C165-07 and those used in this thesis are explained below, and their influence on the results is discussed Chapter 6. Values for the modulus of elasticity and yield strength were calculated also in accordance with ASTM C165-07 §8.1.

Test Apparatus and Test Fixture

An Instron 3369 universal tester was used as the test device (Figure 34). A custom designed and built compression test fixture for the cube compression tests was fabricated and installed (Figure 35 and Figure 36). The custom fixture differs from the schematic illustrated in Figure 4 of ASTM C165-07 mainly because the custom fixture's spherical surface radii are significantly smaller. This was done to fit the budget and machining capability available to the thesis. Furthermore, the standard did not specify or provide guidelines on the dimensions of the spherical surface. The validity of using smaller radii spherical surfaces is more appropriately discussed in the Procedural Differences subsection.

Figure 34. Instron 3369 universal tester. (Test fixture used in this thesis not installed).

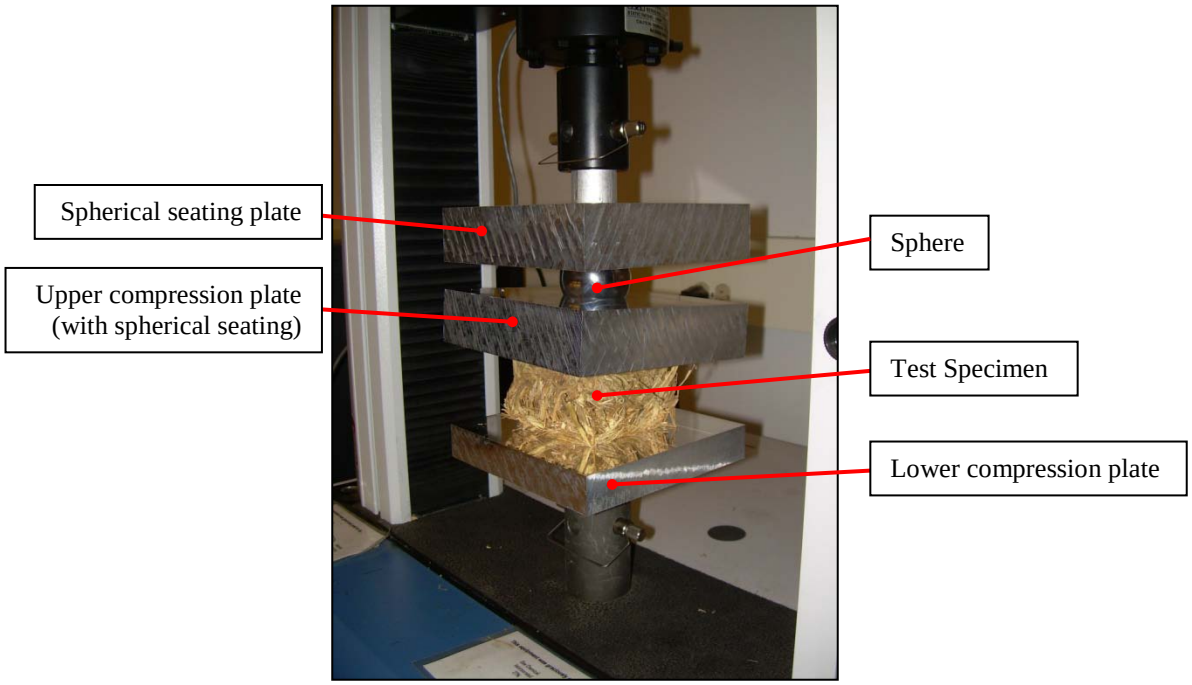

Figure 35. Custom test fixture installed on Instron.

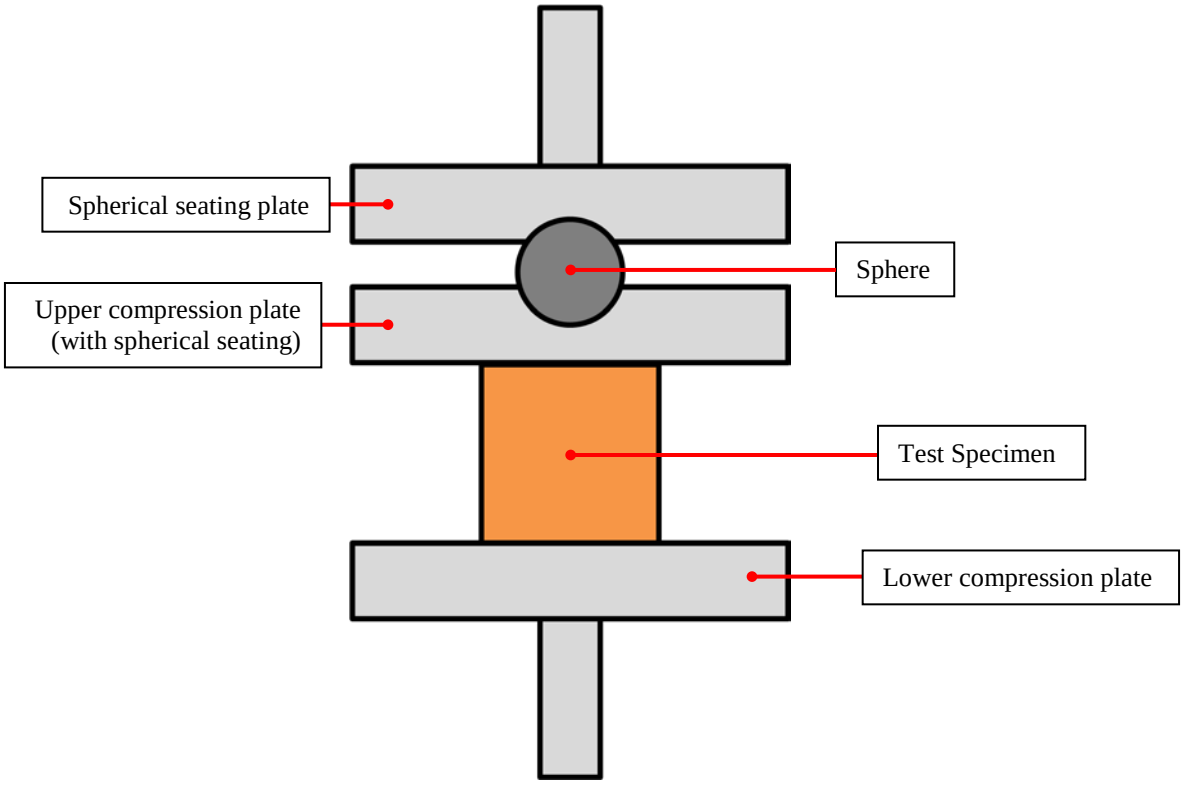

Figure 36. Schematic of custom test fixture used on Instron.

Test Specimens

Because heating to 250°F (121°C) would have adversely affected the samples, ASTM C165-07 required that samples be left to condition at 73.4 ± 1.8°F (23 ± 1°C) for a minimum of 40 hours. Conditioning at such precise conditions was beyond the resources of the thesis, and instead the samples were left for at least 40 hours to condition at 71 ± 1°F (22 ± 0.6°C) in a laboratory room.

ASTM C165-07 also required that the specimen thickness not exceed its width or depth. Typically, cubes made for this thesis had straw protruding along the edges – but not the entire face – of the top (and occasionally bottom) surfaces of the cube, as pictured in Figure 37. Although this protrusion made the specimen thicker than permitted by the standard, it was assumed to be negligible and left on the cube during compressive testing.

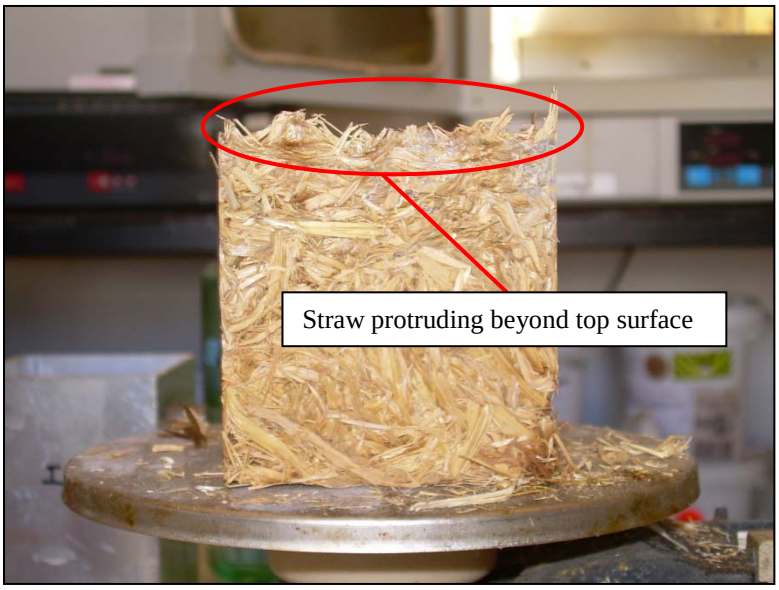

Figure 37. Typical shape of sufficiently cured straw cube.

Procedural Differences

ASTM C165-07 required that the spherical surfaces be lubricated prior to testing. Although the fixture was not lubricated, 4 aspects of the design would have compensated for its absence:

1. Because the spherical radius was much smaller than the design pictured in Figure 4 of ASTM C165-07 the sphere acted partly as a pivot for the upper compression plate. The anticipated result was that it would be easier to angularly displace the upper compression plate.

2. The steel sphere was polished to a mirror finish with a ±0.0002 inch diameter tolerance, and the aluminum spherical surfaces were considered to be very smooth. Therefore friction between the aluminum and steel would still be small and make it easier to angularly displacing the upper compression plate.
3. The total area of spherical surfaces in contact was still less than the fixture that would have been made based on the design in ASTM C165-07. This meant that fewer defects (that would cause a rougher surface) were present, and effectively reduced the energy required to overcome friction and angularly displace the upper compression plate.
4. The use of an actual sphere (instead of only spherical surfaces) introduced additional degrees of freedom (Figure 38) than the design in ASTM C165-07. Both mating surfaces must bind to prevent angular deflection in the upper compression plate, effectively making it easier to angularly deflect than the design in the ASTM standard.

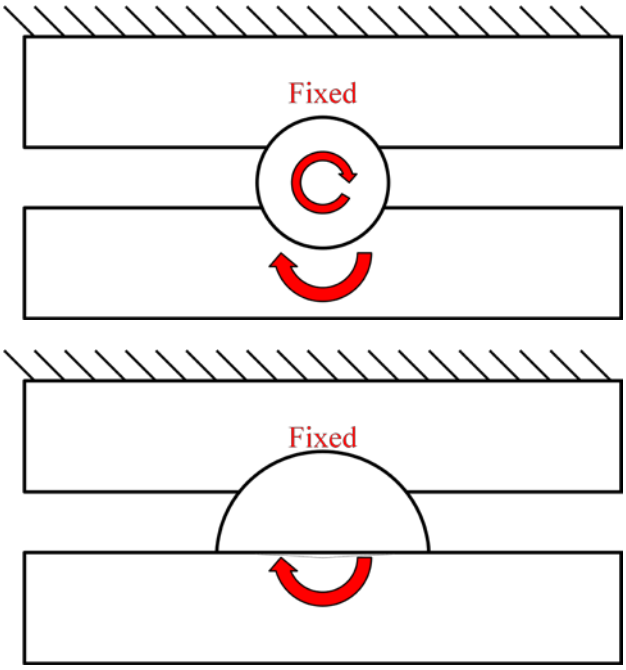

Figure 38. Schematic design differences between thesis fixture (top) and suggested fixture (bottom).

The Instron's crosshead speed was programmed at 0.1375 inches/min as according to the calculation recommended by ASTM C165-07 §7.1.3 for materials lacking a prescribed speed. That is, "the speed shall be 0.05 in./min (1.27 mm/min) for each 1 in. of specimen thickness." The nominal thickness (2.75 inches) was used to determine the crosshead speed.

ASTM C165-07 §7.1.4 does not require a preload, but requires one to be reported if used and that it be less than 2% of final load. The straw cube was compressed with a total preload of approximately 11.0 lb_f, which was still less than 2% of the final load. This included both the weight of the test fixture (steel sphere and upper compression plate) as well as the crosshead induced preload. Each test was not terminated until the cube deformed by 0.75 inches (this displacement was selected arbitrarily to ensure a complete load-displacement curve) along the compression axis.

ASTM C165-07 §6.2 requires test specimens to be chosen at random, but this required each cube to be baked one at a time and would have taken an unreasonable amount of time to complete the experiment. Thus, the cubes were baked in batches appropriate to their prescribed temperature and time. It was assumed that variation caused by baking the cubes in this way was negligible. However, the order the cubes were baked and tested was completely randomized.

Because no specification could be found for testing straw cubes, a sample size of 4 was chosen for each sample group. This was in direct accordance with ASTM C165-07 §6.2.

Temperature Profiles

Type K thermocouples linked to HH306 Omega dataloggers were inserted into molds that contained binder-treated straw to develop temperature profiles while the cubes were baked. One thermocouple located at the surface and a second positioned at the core were linked to one datalogger. The thermocouple wire leads were strung through a ceramic shield to more accurately place the thermocouple. Either a CNC or drill press was used to drill holes to permit the insertion of thermocouples into the core. Figure 39 shows a schematic of this setup. The datalogger manual indicated that the thermocouple error was approximately ± (.2% reading + 1°C).

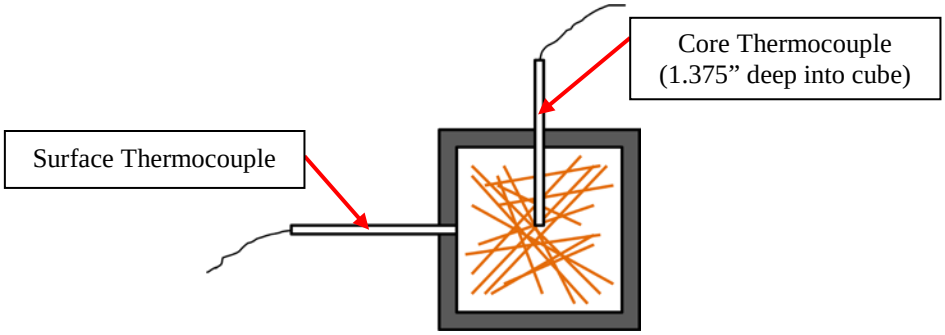

Figure 39. Schematic of thermocouple configuration. Cross-section view.

A third thermocouple was randomly positioned to dangle from the top rack and linked to a second HH306 Omega datalogger. This was intended to monitor the oven air temperature for irregularities. For this regimen the molds were placed in the oven preheated to 150°C (300°F) and left to heat for 4 hours. This procedure was used for 2 molds containing treated straw. Cubes cured under this procedure (with or without binder) were not evaluated for curing.

Figure 40. Cross-sectioned cube.

Cube and Stak Block FE simulations

Abaqus 6.7 Standard (Finite Element Analysis software) was used to simulate the core temperatures of binder-treated straw cubes being heated in the oven – assuming no chemical reaction or other endo/exothermic processes. For reasons explained in Chapter 4 the density ρ was changed to 264 kg/m^3 to reflect the increased density. The thermal conductivity and specific heat were adjusted until the simulated core temperature sufficiently matched the experimentally determined core temperatures. The simulation was then run again (using k and C_p fitted to the experimental data) to predict the curing times for both the experimental cubes and the full size Stak Block.

For these simulations, the aluminum mold was included since its volume was equal to about 75% of the cube's volume – significant enough to require consideration. Since Abaqus was only capable of simulating gray surfaces, the mold was assigned an emissivity of 0.95 to represent its ability to absorb more radiation than it emits. The Fisher Scientific oven included a fan to ensure the entire cavity remained at approximately the same temperature. However, since it produced no discernable draft, free convection was assumed to be a reasonable approximation. Assuming an oven temperature of 423K and an initial mold temperature of 300K, the appropriate Nu-Ra correlations (Incropera, et al., 2007) gave a convection coefficient of $h = 8$ W/m^2-K for the sides and bottom, and 2 W/m^2-K for the top. But since the oven cavity was claimed to be at approximately the same temperature, it was decided to assume the fan stirred the air enough to raise the convection coefficient. Therefore a convection coefficient of 10 W/m^2-K was assigned to all surfaces. The mold was modeled without the steel dowel pins or holes. However, once again symmetry about all three orthogonal axes (x, y, and z) permitted modeling only one-eighth of the cube and mold assembly. Quadratic heat transfer elements were used with a seed size of .004. Mesh convergence studies showing the suitability of this seed size are in Appendix C. An example of the shape modeled is shown in Figure 41.

The FE model was then fit to the experimental core temperature data by adjusting the convection coefficient, straw thermal conductivity and specific heat. The resulting model was then run again to predict the curing times for the curing temperatures tested and adjusted to fit if necessary. The parameters fitted to the curing model were then used in the Stak Block FE model to extrapolate curing times.

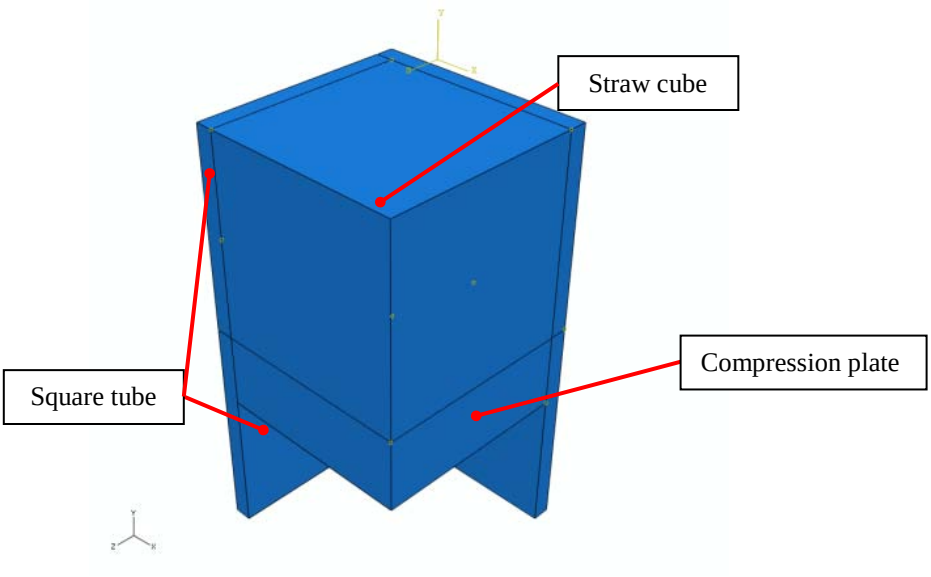

Figure 41. Shape modeled of cube and mold. One-eighth model.

CHAPTER 5: RESULTS

As summarized earlier, data on curing, temperature, and mechanical testing were collected and reported. The following sections present the data with remarks on its presentation. Interpretations of the data will be left to the discussion and conclusion sections.

Curing Evaluation Using Chemical Dye

The results of the curing responses were presented in graphical form as shown in Figure 42. Each data point represented a particular time-temperature combination a cube was baked at: blue dots indicate the cube was fully cured and a red "x" indicates it was not. Because all responses were plotted on this graph some data points show both a red "x" and a blue dot. It was found that the model assuming temperature and time were inversely proportional produced a graph that best fit the data. To calculate this curve, the time between cured and uncured cubes was averaged, and this new data point was used to calculate the regression curve. For example, a cube was not cured at (0.25, 423) but cured at (0.50, 423), and the two times were averaged to produce the point (0.375, 423). Ambiguous time-temperature combinations (that produced both cured and uncured cubes) were considered as "uncured" and this assumption will be discussed in the next chapter. The points used in this regression are summarized in Table 3. The full results can be found in Appendix C.

Table 3. Points used to calculate regression curve.

Temperature (K)	Time (hrs)
423	0.375
398	0.375
373	0.625
358	0.875
348	1.50
338	1.75

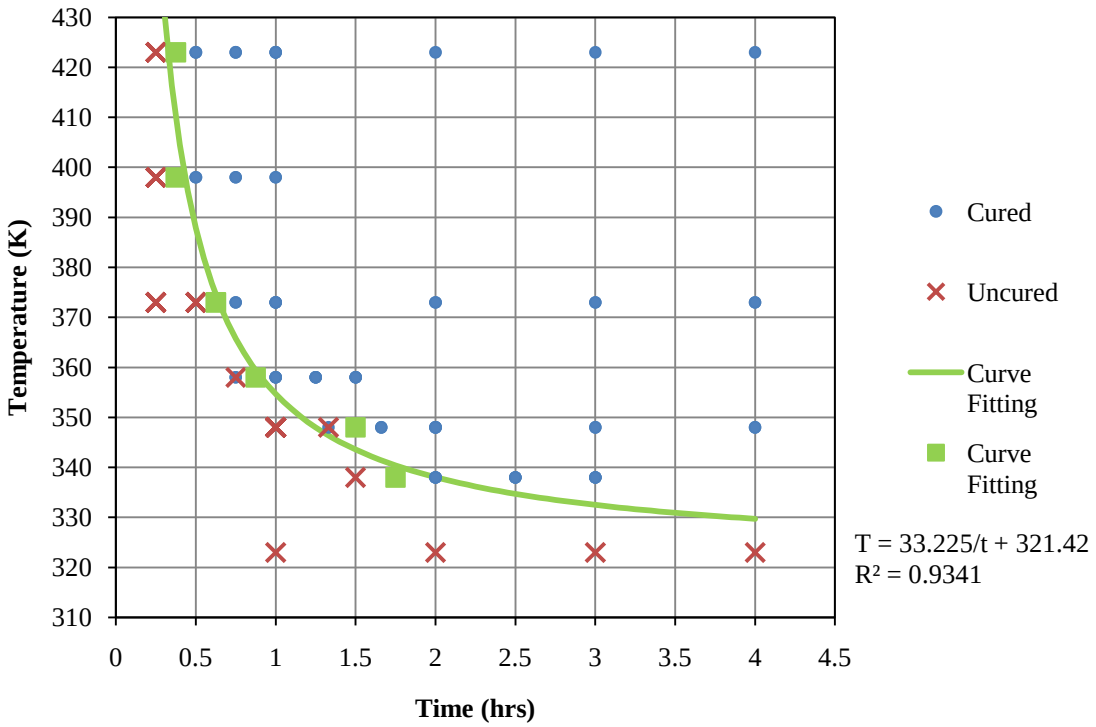

Figure 42. Plot of Curing Evaluation Results. Green data points were used to calculate the green curve fit.

Curing Evaluation Using Mechanical Testing

Mechanical testing was used to confirm the results obtained by inspecting cubes with a chemical dye. This was based on the assumption that the stiffness and yield strength for cured cubes was the same ,regardless of the time and temperature used to cure them. Load-displacement data of the crosshead was obtained directly from the Instron universal tester software and converted into stress/strain curves for each cube. Displacement contributions made by the aluminum test fixture were considered negligible compared to those made by the straw cube. The yield strength and modulus of elasticity for each cube were calculated from the stress-strain curves per ASTM C165-07. A distance of 3% was used to calculate the yield strength. Refer to the ASTM standard to understand how the 3% was used. The results are summarized in Table 4. The full set of stress-strain curves can be found in Appendix F.

Table 4. Modulus of Elasticity (E) and yield strength (σ_y) of straw cubes fabricated for mechanical testing.

	Cube	E (psi)	σ_y (psi)
150°C, 0.50 hr	III - UC4	1300	34
	V - UC4	1000	28
	VI - UC4	1600	42
	VIII - UC4	1200	30
65°C, 2.0 hr	I - UC5	1200	32
	V - UC5	1000	29
	VII - UC5	1200	30
	VIII - UC5	1400	38
100°C, 0.66 hr	II - UC6	1700	43
	VI - UC6	1000	27
	VII - UC6	1600	41
	VIII -UC6	1100	30

An ANOVA analysis was performed to determine if the modulus of elasticity and yield strength were significantly different for the cubes cured at different time-temperature combinations. The null and alternate hypotheses were formalized as:

$$H_{0,\sigma_y}: \mu_{150\,℃} = \mu_{100\,℃} = \mu_{65\,℃}$$

$$H_{0,E}: \mu_{150\,℃} = \mu_{100\,℃} = \mu_{65\,℃}$$

$$H_{a,\sigma_y}: At\ least\ two\ of\ the\ \mu's\ are\ different$$

$$H_{a,E}: At\ least\ two\ of\ the\ \mu's\ are\ different$$

The following assumptions were made in order to perform the analysis:

- Baking cubes simultaneously rather than one-by-one had no effect on the results. Assuming this is true, the experiment could still be considered sufficiently randomized.
- The standard deviations of each sample group were approximately the same. To make this assumption the ratio of the largest to the smallest sample group variance should generally not exceed 4. This ratio was 4.625 for the modulus of elasticity and 3.872 for the yield strength.
- The sample groups were approximately normally distributed. This was checked by showing that normal quantile plots looked sufficiently linear.

The ANOVA analysis produced a test statistic of F = 0.32 and 0.23 for the modulus of elasticity and yield strength respectively. Both of these values gave P-values of 0.74 and 0.80 respectively. Because both values were not less than a P-value of 0.10, the null hypothesis was failed to be rejected.

Temperature Profiles

Surface and core temperature data from the dataloggers were plotted as shown in Figure 43, along with the core and surface temperatures of the FE model that best fit the binder-treated straw. The FE model was fitted to the experimental data for a binder-treated cube by adjusting the convection coefficient, thermal conductivity, specific heat – determined to be h = 10 W/m^2-K, k = 0.1 W/m-K and Cp = 2000 J/kg-K. Of the range of simulations tried, this was found to be the best fit, but was expected to overestimate curing times because of the time visible time delay.

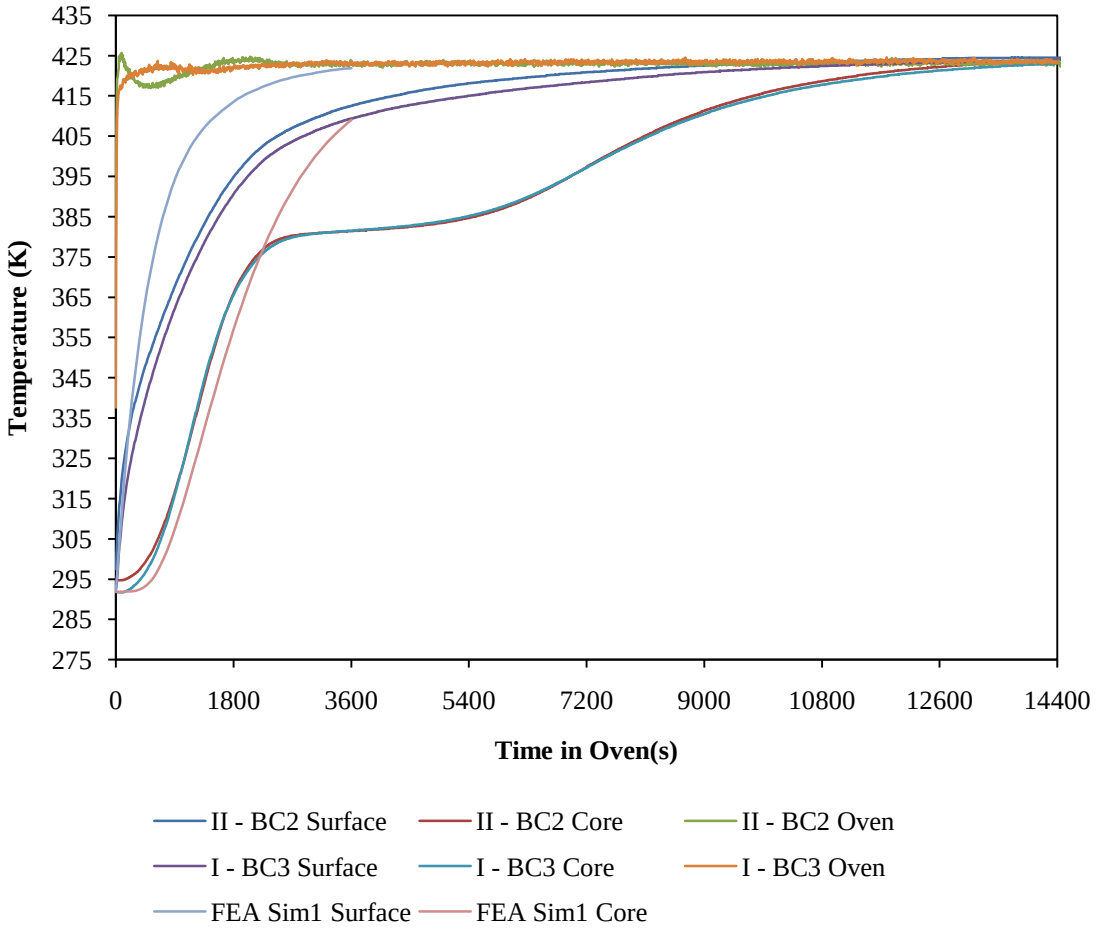

Figure 43. Temperature plot with FE prediction up to 3600s. k = 0.1 W/m-K C_p = 2000 J/kg-K.

Predicted Cube Curing Times

Both the regression curve and the FE model were used to predict curing times. The regression curve was assumed to represent optimized curing conditions; it predicts the shortest time needed to cure the cube at a particular temperature. Curing times in the FE simulations were predicted by determining the time needed for the core to reach 65°C – this was the lowest temperature the cubes were observed to cure. The same values for specific heat and thermal conductivity used to fit the FE model to the temperature profile in Figure 43 were also used to predict the curing times. Because these FE curing times were lower than expected, more simulation found that using C_p = 3000 J/kg-K (instead of 2000 J/kg-K) predicted curing times thought to be more accurate overall. The results are summarized in Table 5. Note that experimental data are presented as intervals. The experimental times were not

more precisely determined because (1) the granularity in the data was considered sufficient and (2) testing additional cubes required more time than available. The FE graphs used to predict curing times are in Appendix E.

Table 5. Comparison of experimental and predicted curing times. Blue indicates overestimation, red is underestimation, and green indicates within range of experimental times.

Oven Temp	Experimental (hrs)	Inverse Curve (hrs)	FEA Model 1 C_p = 2000 J/kg-K (hrs)	FEA Model 2 C_p = 3000 J/kg-K (hrs)
65°C	1.50 – 2.00	2.00	1.68	2.37
75°C	1.33 – 1.66	1.25	0.83	1.15
85°C	0.75 – 1.00	0.91	0.67	0.92
100°C	0.50 – 0.75	0.64	0.55	0.77
125°C	0.25 – 0.50	0.43	0.47	0.62
150°C	0.25 – 0.50	0.33	0.40	0.55

Extrapolation to the Stak Block

Following the results of the cube curing FE simulations, it was determined that FE models to extrapolate curing times to the Stak Block could still yield meaningful results. These simulations used k = 0.1 W/m-K and C_p = 3000 J/kg-K for material properties. For all simulations, the block core was significantly cooler than the 65°C temperature known to cure. Therefore to determine if the block had "cured," a brief comparison was made with the contour plot of a Stak Block simulated to bake in a 150°C oven for 1 hour, as shown in Figure 44. That is, the time it took for a temperature of at least 65°C to penetrate to the same depth in the same location shown in Figure 44 was recorded as the "curing" time. For comparison, Figure 45 shows a temperature contour plot of a simulated Stak Block baked at 398K for 9.67 hrs. The FEA predicted curing times for the full-sized Stak Block are summarized in Table 6.

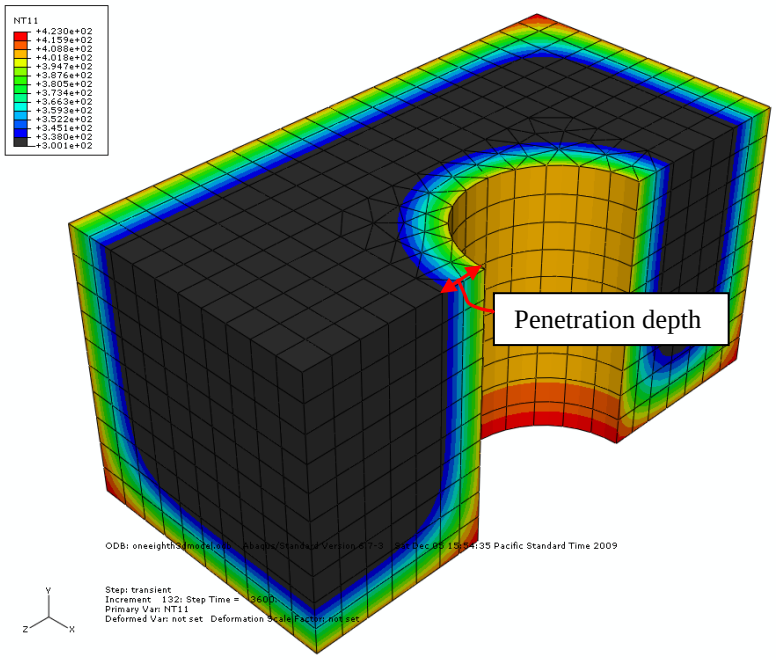

Figure 44. Temperature contour plot of simulated Stak Block after 1 simulated hour at 422K (150°C). Black regions represent temperatures cooler than 338K (65°C).

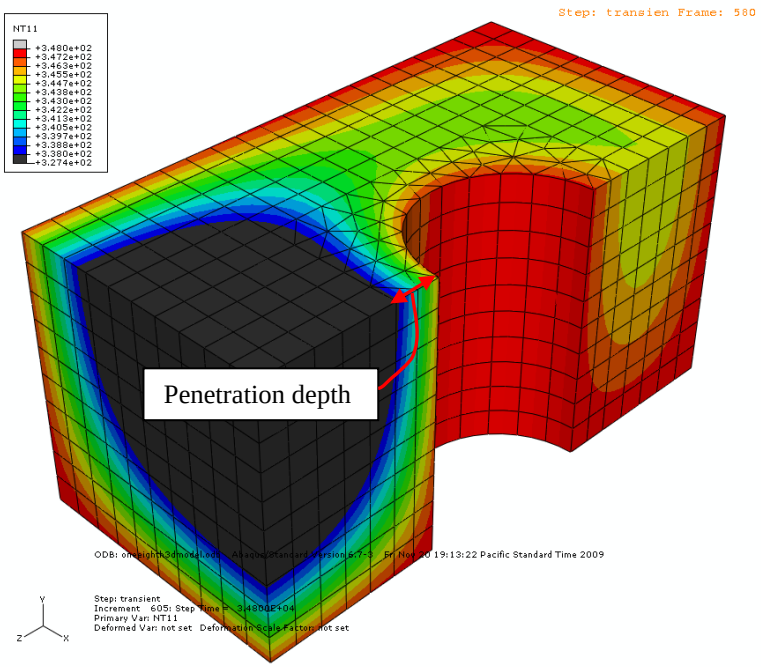

Figure 45. Temperature contour plot of simulated Stak Block after 9.67 simulated hours at 398K (125°C). Black regions represent temperatures cooler than 338K (65°C).

Table 6. Stak Block curing times predicted by FE model.

Oven Temp	Curing Time (hrs)
65°C	14.00
75°C	9.67
85°C	6.27
100°C	3.67
125°C	1.79
150°C	1.00

CHAPTER 6: DISCUSSION

The results of the experiments and simulations did not always match expectations. Moreover, these discrepancies introduced new questions of how the curing process really works. This chapter discusses the results of each portion of the thesis and on the results overall.

Cube Curing Responses Using Chemical Dye

The results of the cube curing experiments were not entirely expected. Although the overall pattern shown in Figure 42 was reasonable, the individual data often went against intuition. For example, Figure 46 showed a nonsymmetrical distribution of red dye at the cross-sectioned surface – typical of all samples.

Figure 46. Image of cross-sectioned cube. Note that the reddish parts denote the presence of uncured binder.

It is expected that for a reaction limited by thermal conductivity only the center of the cube would be uncured and that the distribution be symmetrical about all 3 orthogonal axes. However Figure 46 shows that the straw in the center and a significant region along the bottom edge is uncured. To be sure, the chemical dye was sprayed over the entire surface, and so any uncured binder present should have reacted and turned red. An uneven application of the binder could explain this result, but this requires that a large proportion of straw does not have binder. Based on the binder application process this is quite unlikely.

There are two plausible causes that could be studied to better understand this phenomenon. The odd distribution could mean that heat moved slower through the bottom face than the other faces, either by variation in thermal conductivity throughout the solid or non-uniform heat transfer from the mold to the straw. The other cause could be the way the cube was cut when evaluated. That is, the cube was cut against the grain rather than with the grain. Although the straw was stuffed into the mold without a preferred direction, when the straw was compressed it

formed layers rather than remaining truly random-directional. Therefore, cutting against the grain (i.e. perpendicular to the layers) was more likely to expose cross-sections of straw fibers that had no way of being exposed to binder treatment instead of straw sides that were treated with binder. From Figure 46 we see that the reddish areas were located where the straw *surface* was exposed, while the brown areas were located where straw *cross-sections* were exposed. However, the decision to cut against the grain was considered justified because it would suffer less damage from the cutting blade in this direction than if it were cut with the grain (i.e. parallel to the layers).

It was originally hoped that image analysis could be used to determine the percent area of the cross-sectioned face that had cured (for partially cured cubes) and fit the data to a logistic growth or other appropriate model for extrapolation. But quite obviously it was not meaningful to do this for the resulting data; the cross-sectioning may not have accurately reflected the degree which the cube had cured. Therefore only binary responses (i.e. "cure" and "not cured") were recorded.

Regression Curve

The observed time-temperature relationship was expected – a higher oven temperature yielded a shorter curing time. An inverse relationship between time and temperature was postulated as the most appropriate model compared to linear, logarithmic, power, and exponential models. More importantly an inverse model has the expected response characteristics: a negative correlation, one vertical asymptote, and one horizontal asymptote.

It was assumed that the curing time was influenced by the amount of energy reaching the block. Thus, for a lower curing temperature either (1) energy penetrated through the cube more slowly or (2) the chemical reaction takes place more slowly or (3) a combination of both 1 and 2. In each case, the result is that the cube would take longer to cure, and this was reflected by the negative correlation.

A vertical intercept would imply that a cube cured *instantaneously* if it is placed in a hot enough oven. This intuitively did not make sense nor was this behavior observed in this study. Therefore, it was more appropriate that the graph had a vertical asymptote. Without further understanding the curing process at even greater temperatures, it was acceptable to leave the vertical asymptote at $t = 0$. However, it was less significant to understand these high temperatures because the focus was on lower temperatures.

A horizontal intercept would have implied that the cube could cure at absolute zero. This cannot be true both intuitively and through observation, and thus it was more appropriate for the graph to have a horizontal asymptote. The horizontal asymptote at T = 321K (48°C, 118°F) implies that, if left for an infinitely long enough time, the binder will cure with the straw. This could be true and is not beyond reason, but more importantly this asymptote is at a reasonable value.

The plot in Figure 42 includes ambiguities – points that show that a particular time-temperature combination yielded both cured and uncured cubes. This result was interpreted to mean that factors with random variations were significant enough at this time-temperature combination to produce conflicting results. Therefore it was assumed that a disagreement in the results indicated that the probability of curing was much less than 1 at the respective time and temperature, and these points were considered as "uncured" when calculating the regression curve according to the method described in the previous chapter. Because of the small sample size this conservative assumption was considered appropriate. The cube's density/material properties and the amount of binder present are factors with random variations that are likely the cause.

Significant variation in heat transfer to the cubes is not likely. The spacing and placement of the molds was chosen as a compromise to balance the need to minimize radiation/convection shielding with the need to ensure different parts of the oven had an equal chance of being used. Radiation shielding may not be significant since radiation may not constitute a significant proportion of the total heat transfer. Equation 6 and 7 show the equations for radiation and convection heat transfers assuming diffuse and gray surfaces.

$$\boldsymbol{q_{radiation}}'' = \boldsymbol{\alpha\sigma\left(T_\infty^{\,4} - T_s^{\,4}\right)} \qquad (6)$$

$$\boldsymbol{\overline{q}_{convection}}'' = \boldsymbol{\overline{h}(T_\infty - T_s)} \qquad (7)$$

Where α is the absorbtivity of the mold, σ is the Stefan-Boltzmann constant (5.670×10^8 W/m^2-K^4), T_∞ is the oven temperature, T_s is the mold surface temperature, and h is the average free-convection coefficient (Incropera, et al., 2007). If the absorbtivity of the aluminum mold is estimated as 0.15 (Incropera, et al., 2007), the oven wall to be 423K, the mold to be 300K, and an average heat transfer coefficient of 5 W/m^2-K (recall from Chapter 4) then the radiation heat transfer is equal to 33% of the convection heat transfer. But as reported in Chapter 5, a convection coefficient of 10 W/m^2-K was deemed appropriate. Using this new convection coefficient, the heat transfer by radiation was less than 15% of the total heat transfer – small enough that it could be negligible. It was reasonable to assume that the oven fan caused this increase in convection, and this subsequently implied that the oven temperature

was approximately uniform throughout and that the convection coefficients were approximately the same for all cubes.

Alternately, oven temperatures can also affect heat transfer. Three temperatures (100, 75, and 50°C) were randomly selected to determine the repeatability and accuracy of the oven temperature. The results plotted in Figure 47 indicated that the oven temperatures were repeatable and constant, but were generally 2°C cooler than the target temperature. Recalling from Chapter 4 that the thermocouple error was approximately ± (.2% reading + 1°C), the actual temperature was likely within 1°C. Despite this discrepancy, the 1-2°C was not considered significant enough to affect the heat transfer.

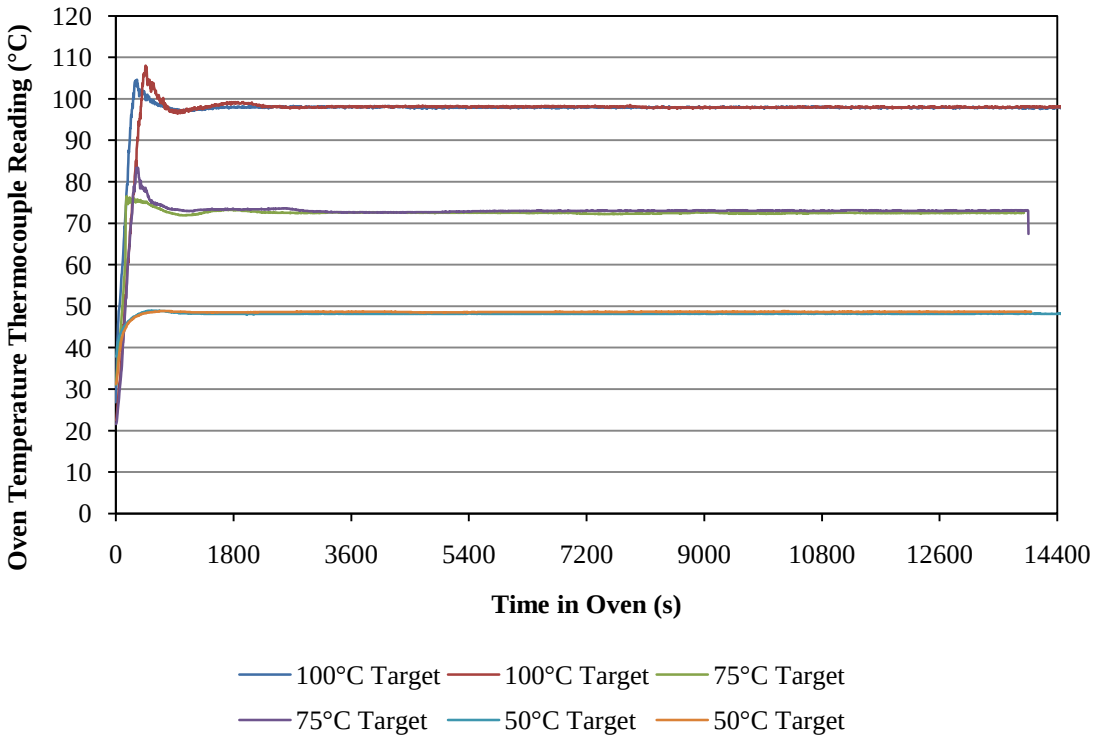

Figure 47. Repeatability of oven temperatures.

Through analysis the inverse regression model was a very good fit and yielded a high coefficient of determination ($R^2 = 0.9341$). Moreover, it can be seen from Figure 42 and Table 5 that the curing times predicted closely matched those that were experimentally determined. This showed that the inverse regression model was a reasonable approximation.

Curing Evaluation Using Mechanical Testing

The purpose of mechanical testing was to confirm the results obtained via the chemical dye method. It was assumed that the mechanical properties would not be significantly different for cubes cured at different optimized times and temperatures – baking for any longer period of time may not increase the strength since all the binder should have reacted and may actually promote decay of the straw or the binder. As reported in Chapters 4 and 5 three groups of four cubes were fabricated at selected time-temperature combinations and mechanically tested: (0.25 hrs, 150°C), (0.75 hrs, 100°C), and (2 hrs, 65°C). These represented optimized times for cure as determined through the chemical dye inspection method. Thus, it was expected that the modulus of elasticity and yield strength would not be significantly different among the 3 groups.

ANOVA results in context

The ANOVA analysis did support the null hypothesis: cubes cured at different optimized time-temperature combinations have the same yield strength and modulus of elasticity, as was expected. To recap from Chapter 5, this statement can be formalized in statistical language, where μ represents the mean of a sample group:

$$H_{0,\sigma_y}: \mu_{150\,℃} = \mu_{100\,℃} = \mu_{65\,℃}$$

$$H_{0,E}: \mu_{150\,℃} = \mu_{100\,℃} = \mu_{65\,℃}$$

$$H_{a,\sigma_y}: At\ least\ two\ of\ the\ \mu's\ are\ different$$

$$H_{a,E}: At\ least\ two\ of\ the\ \mu's\ are\ different$$

The results can be summarized again in Table 7.

Table 7. Summary data of compression testing.

	E (psi)		σ_y (psi)	
	Mean	Std. Error	Mean	Std. Error
150°C (0.50 hr)	1275	250	33.5	6.19
100°C (0.66 hr)	1200	163	32.25	4.03
60°C (0.20 hr)	1350	351	35.25	7.93

P-values for both the modulus of elasticity and yield strength (0.74 and 0.80 respectively) were significantly greater than 0.10 – a very liberal criterion used to determine whether the null hypothesis should be rejected. If the statistical assumptions were valid it can be said with confidence that the different time-temperature combinations yielded samples with the same yield strength and modulus of elasticity.

One may claim that since the ratio of the largest sample variance to the smallest sample variance (4.625) for the modulus of elasticity data was greater than 4 an ANOVA analysis may not be valid. However, this was a general rule, and because the ratio did not exceed this amount that much the results cannot be immediately labeled invalid. In addition, ANOVA required that the samples were fabricated independently of each other. But as explained in Chapter 4 this required much more time than available and so the samples were made in batches. ANOVA can still be used if it was assumed that no variation in the results is caused by the oven. In other words, it needs to be assumed that the heat transfer to the cubes would still be the same regardless if the cubes were baked individually or if they were baked in groups. But from the reasoning given in the Regression Curve section of this chapter, this assumption is valid.

Even with the assumptions in context, the results and analysis showed that baking cubes at different optimized times and temperatures likely did not produce straw cubes with a significantly different yield strength and modulus of elasticity. Therefore, the mechanical testing supported the results obtained through the chemical dye inspection method. More interestingly, it also supported the possibility that the yield strength and modulus of elasticity may not be significantly different for Stak Blocks cured at different optimized times and temperatures.

Suitability of Test Methods and Materials

Stress-strain curves were derived from the original load-displacement plots, and Figure 48 shows a typical example. There were three meaningful regions in the graph: a toe region, a linear elastic region, and a strain softening region. The toe region was characterized by an initially low but increasing stiffness. The linear elastic region was characterized by a relatively constant stiffness. The strain softening region was characterized by a continually decreasing stiffness. The presence of a linear elastic region confirmed that it was correct to follow Procedure A of ASTM C165-07. This allowed a good approximation for the modulus of elasticity, as indicated by the red straight-line approximation. More importantly, all the cubes' modulus of elasticity values were much less

than aluminum ($E_{Al} \approx 10^7$ psi (Beer, et al., 2006), $E_{straw} \approx 10^3$ psi), and therefore it was acceptable to ignore the strain contribution from the aluminum test fixture.

The ASTM standard suggests – but does not require – using distances of 5% or 10% to calculate yield strength. A distance of 3% strain was used because it would give a reasonable result. (Refer to ASTM C165-07 §8.1.3 to see how the 3% strain metric was used). Using any larger distance would place the yield stress further into the strain softening region, and any smaller distance would place the yield stress in the proportional region.

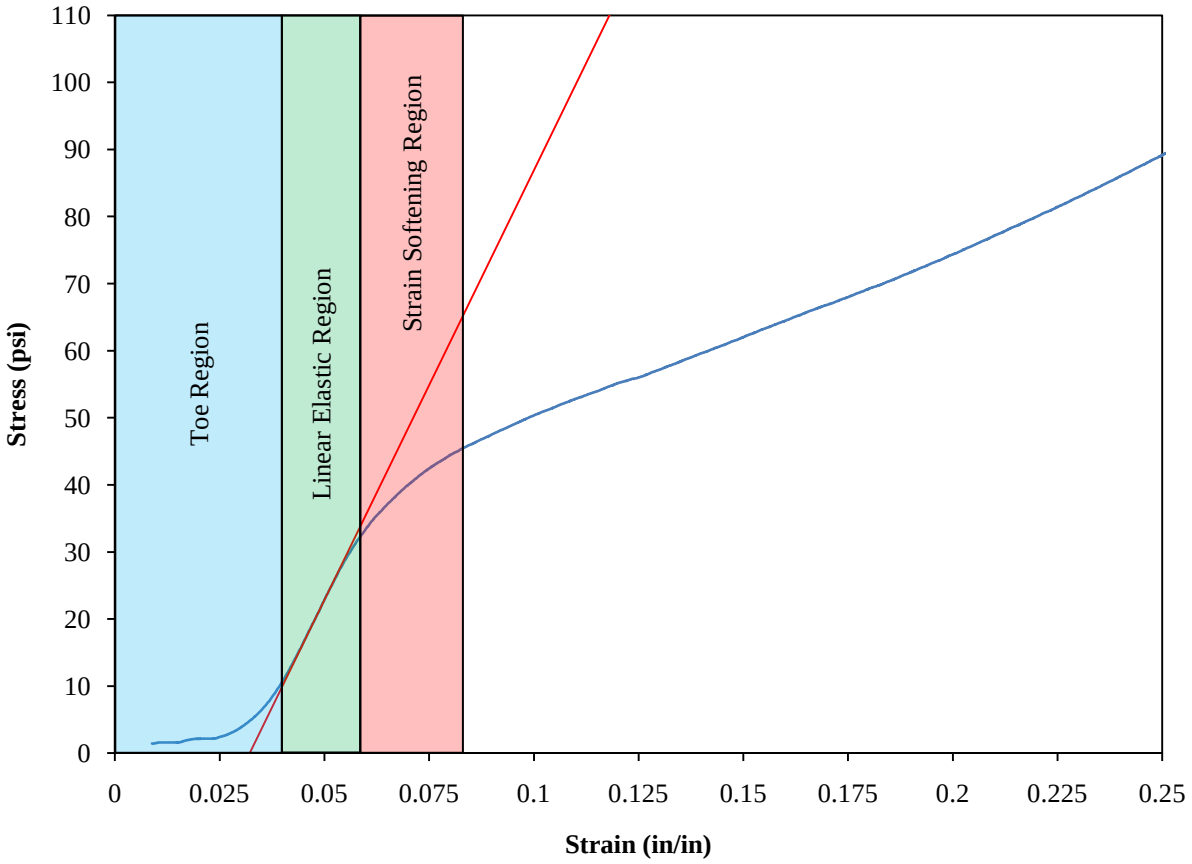

Figure 48. Example stress-strain curve from Cube III – UC4.

The test results are still valid despite the minor design difference from the schematic in Figure 4 of ASTM C165-07. The purpose of having a lubricated spherical surface is to ensure that straw surfaces in contact with the fixture experience a uniform pressure distribution, and as long as the upper compression plate pivots under a reasonable load the test fixture should considered acceptable. Figure 49 and Figure 50 were typical examples of pre- and post-testing conditions, and they showed that the test fixture was capable of remaining approximately plane as

well as angularly deflecting. It could be argued that a lower stiffness may be recorded if the sample moved off-center, but again this was not observed to happen.

Figure 49. Example compression test setup before the test. Cube I – UC5.

Figure 50. Example compression test setup after the test with angular deflection. Cube I – UC5.

Figure 51. Example compression test setup after the test without angular deflection. Cube VII – UC5.

Temperature profiles

The temperature profiles produced interesting and insightful results. Figure 43 shows three distinct regions in the experimental core data, with both tests strikingly repeatable. The graph followed very close to a logistic growth function in the first 0-1800 seconds and begins to plateau from 3000 to 4800 seconds. Surprisingly this exact behavior was also seen in temperature profiles for cubes not treated with an adhesive, denoted with an "L." (Temperature profiles for untreated cubes were not meant to be part of the experiment, but were used to test the thermocouple set-up before testing binder-treated cubes). A comparison is shown in Figure 52. The important observation is that all the curves exhibited nearly the same shape.

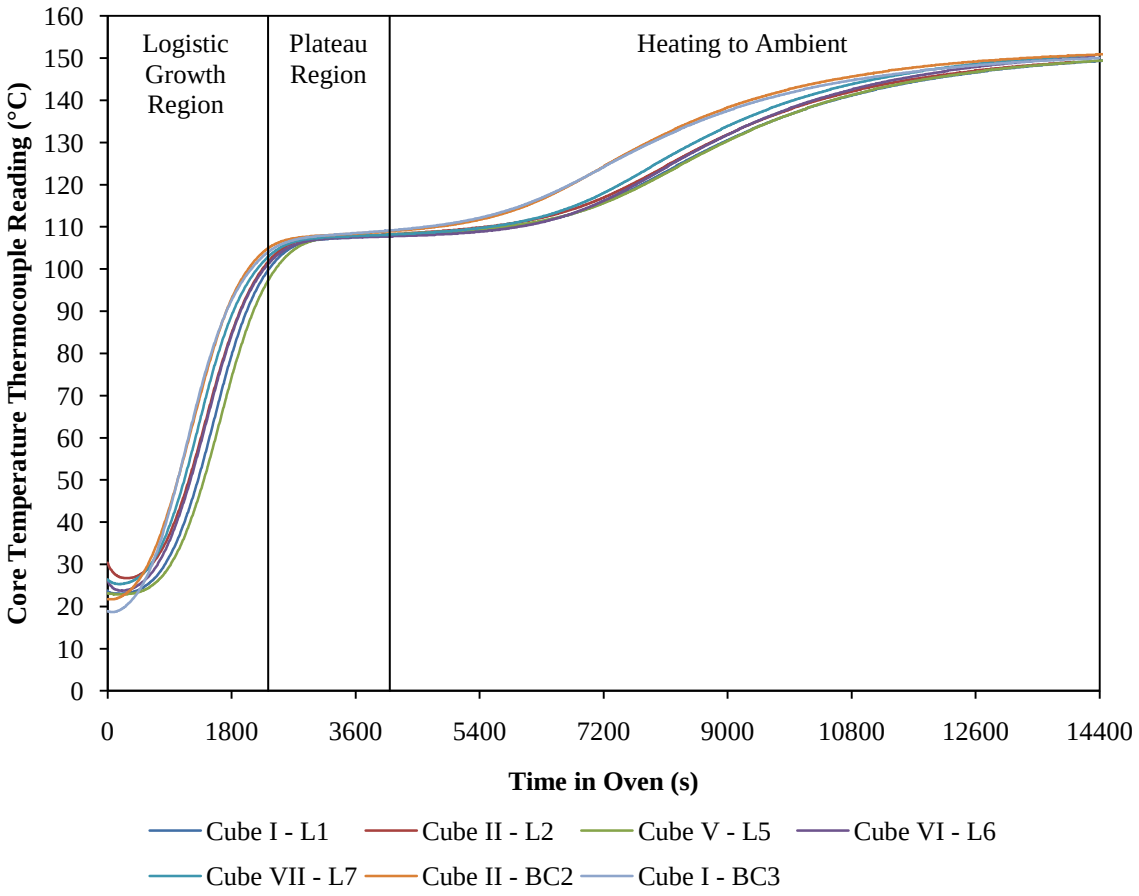

Figure 52. Core temperatures for cubes with and without binder. "BC" designation indicates binder.

The striking similarity between the cured and uncured temperature profiles strongly supports the hypothesis that curing a cube (or actual Stak Block) is limited by how fast heat propagates through the straw. If the curing process was limited by the chemical reaction itself, then it would be expected that the cubes with binder would heat

up at a much slower rate. The absence of pre-heating could have caused the time delay for core temperatures of binderless cubes. If this were assumed, then a re-plot of the data (Figure 53) where each curve is shifted to the left (by the amounts indicated in Table 8) showed that the shape of the logistic growth part of the curve was virtually identical for all cubes. Surface temperatures plotted with the same time compensation (Figure 54) were less repeatable. These results may be more of a result in variation of the thermocouple's placement, and that they were significant enough to affect surface temperature readings. A plot of the oven temperatures and a re-plot (using the same time shift in Table 8) are shown in Figure 55 and Figure 56. The near-same oven temperature profiles in the re-plot supports the idea that the time shifts were a result of not pre-heating. Note that the "L" series measured an oven set to 149°C (300°F), but for the real experiment the "BC" series measured an oven set to 150°C (considered to be a better "round" number than 149°C). Recall from Chapter 4 the thermocouple error was approximately ± (.2% reading + 1°C). This meant that the oven set to 149°C could have been 2-3 degrees cooler than its intended target. However, the oven set to 150°C met its target. As explained previously, this discrepancy was unlikely to significantly affect the results.

Table 8. Amount of time (in seconds) temperature profiles are shifted to the left for pre-heat compensation.

Cube I - L1	300
Cube II - L2	180
Cube V - L5	390
Cube VI - L6	210
Cube VII - L7	105

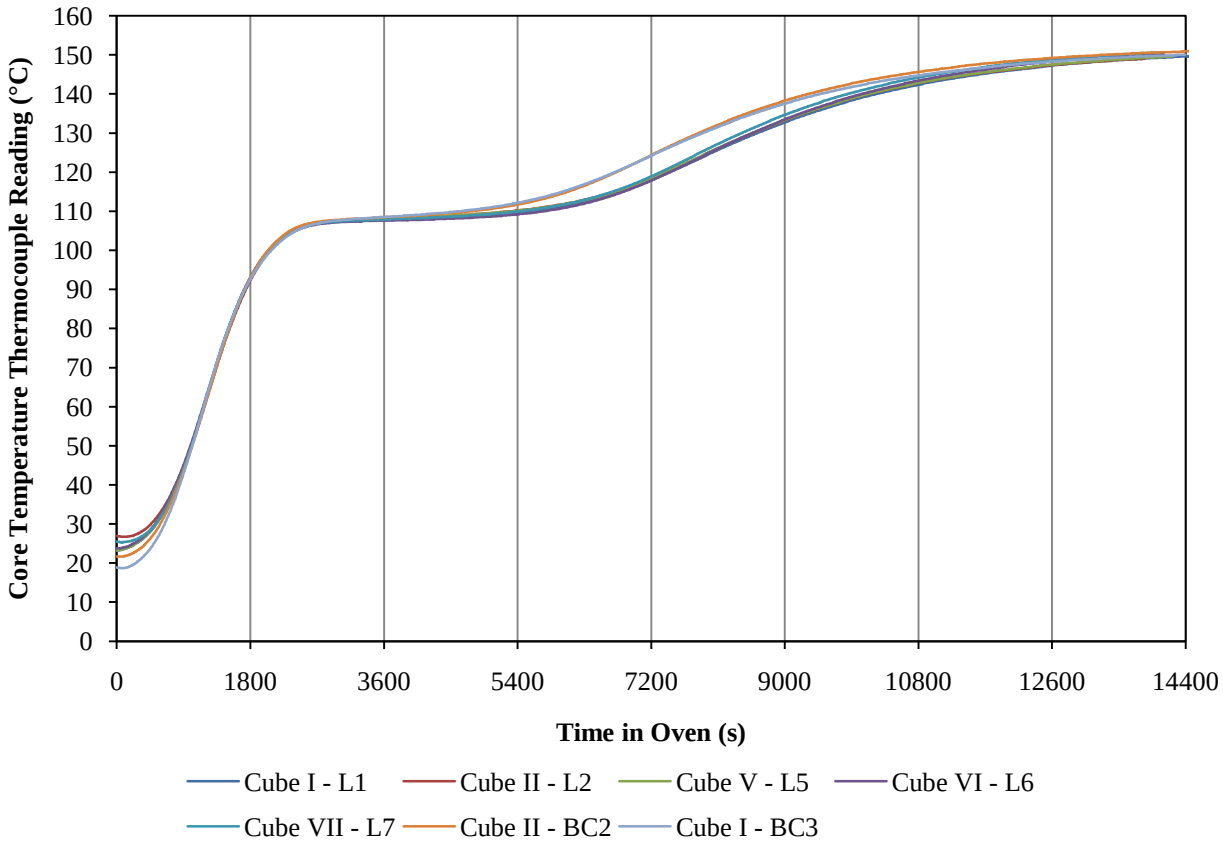

Figure 53. Core temperatures for cubes with and without binder. Adjusted for time delay.

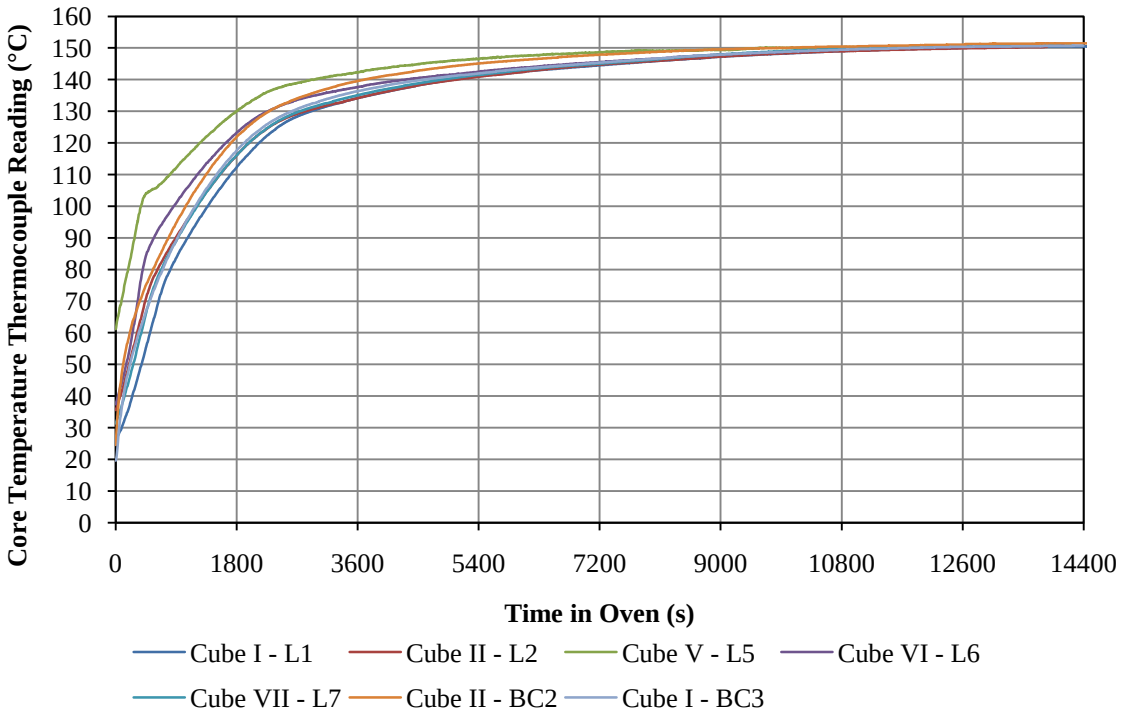

Figure 54. Surface temperatures for cubes with and without binder. Adjusted for time delay.

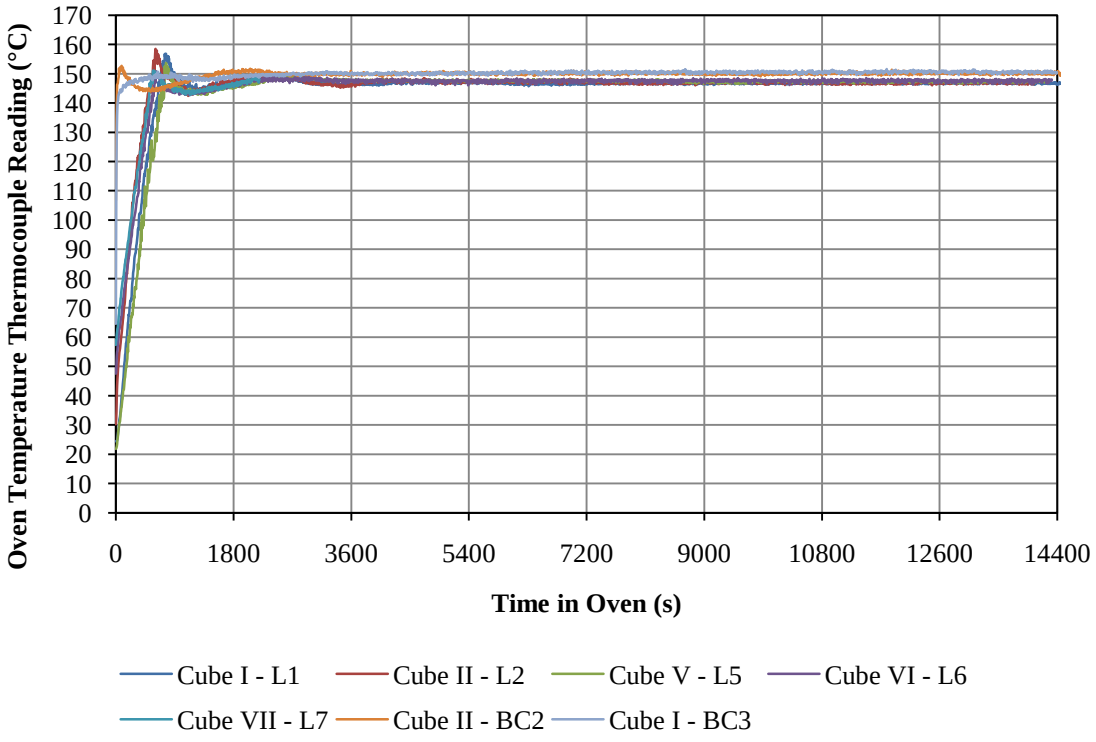

Figure 55. Oven temperatures for cubes with and without binder.

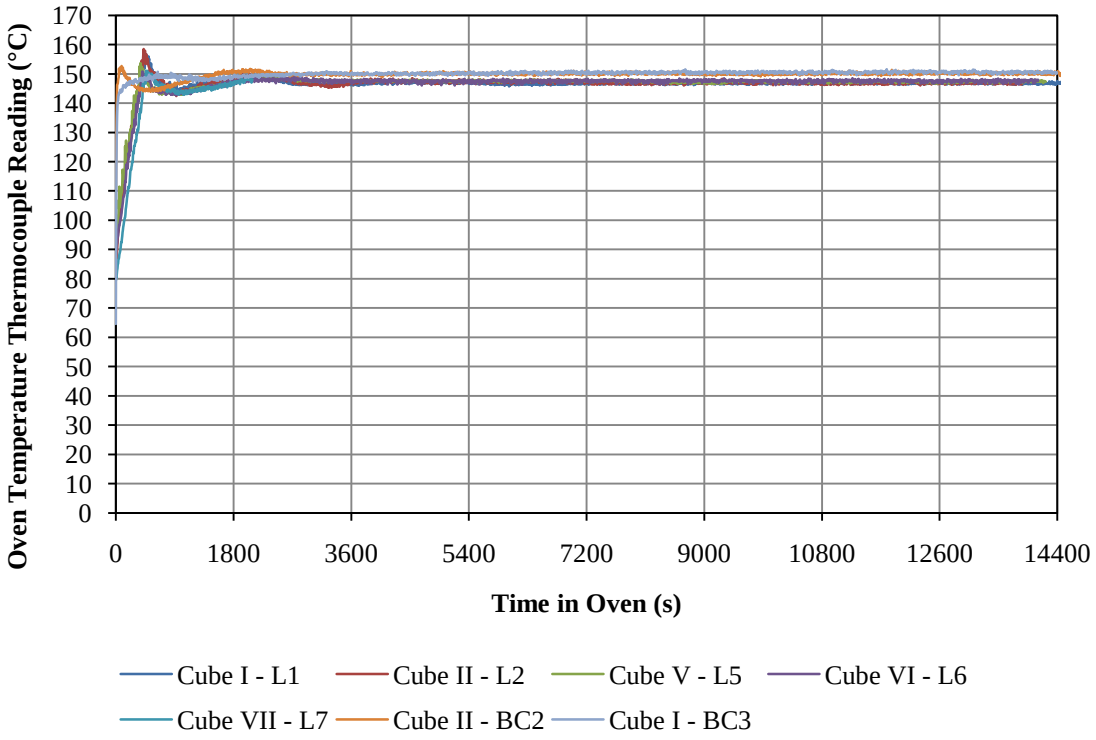

Figure 56. Oven temperatures for cubes with and without binder. Adjusted for time delay.

It is worthwhile to explain the temperature plateau at about 107°C; this characteristic was observed in all cubes regardless of binder treatment. This temperature was quite close to the boiling point of water and supposing that the temperature leveling off was caused by moisture vaporizing from the straw could be a valid explanation. Generally there are two methods to raise the boiling point of water beyond 100°C: (1) increase the pressure and/or (2) add impurities (such as salt) to the water. It is unlikely that a pressure significantly greater than the atmosphere built up in the mold; gaps between the compression plates and the mold were large enough to permit steam to escape. Consequently, any pressure increase would be negligible and make no significant contribution to the boiling point elevation. As an alternative explanation, if an impurity such as common salt (NaCl) was the cause, then the concentration must be reasonable. If it is assumed that the boiling point elevation equation for liquid solutions is applicable to the cube then we can use Equation 8:

$$\Delta T_b = K_b m \qquad (8)$$

where ΔT_b is the change in boiling point, K_b is the molal boiling point elevation constant, and m is the molality. Substituting 7°C for ΔT_b, 0.512 °C/m for K_b (value for water) (Silberberg, 2003), it can be easily shown that m = 13.5. Furthermore, if it is assumed that the moisture content by mass is 8.5% (based on measurements from a

moisture probe) it would be anticipated that about 6.7g of common salt (NaCl) is in a cube with a 100g initial mass. From a brief approximation viewpoint this does not seem unreasonable, although a much more comprehensive study should be done to investigate this.

Further informal evidence supports the moisture hypothesis; it was noted and predicted that the cube's mass would always be significantly lighter than the straw mass measured on the balance. Straw was inevitably lost when it was transferred from the balance to the mold, and this was assumed to be solely responsible for the mass change. But this assumption may not have been valid because the straw input mass was calibrated based on baking cubes (without binder) in the oven for over 2 hours – long enough to drive out most of the moisture. If the straw moisture content was 8.5% by weight, it would be expected that a 100g straw input would yield a cube with a 91-92g mass after baking in the oven for over 2 hours. These values were close to those mentioned in the Chapter 4 when calibrating the setup to account for the supposed loss of straw in transit between the scale and the press.

Moreover, a comparison of the experimental temperature data with an exact (infinite series) mathematical solution also suggested that the temperature plateau could be a result of moisture. The equation, a summary of its development, and the parameters used is given in Appendix D. The core temperature profile predicted by the exact solution was fit to the experimental core data by varying k, and the result is plotted in Figure 57. Although the exact solution modeled a straw cube that experienced convection directly with the oven (i.e., no mold), this was still considered a reasonable approximation.

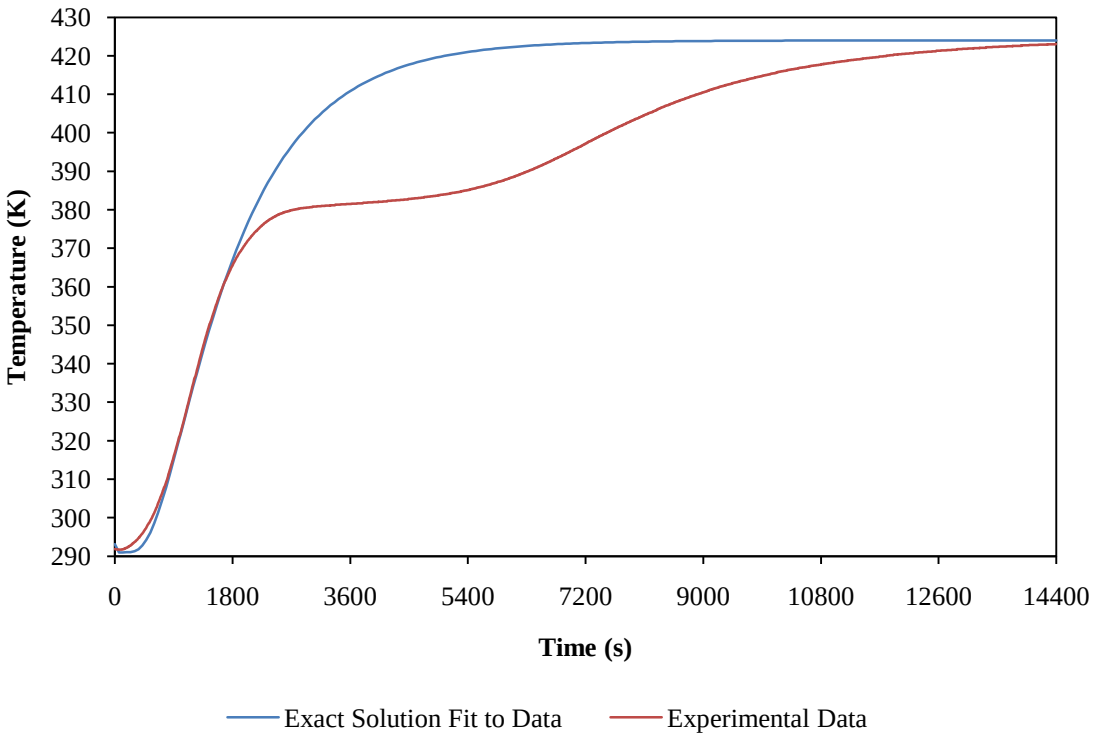

Figure 57. Comparison of exact solution and experimental data. In the exact solution k = 0.07 W/m-K, C_p = 1300 J/kg-K, ρ = 263 kg/m^3, and h = 10 W/m^2-K.

The straw was assumed to have a 10% moisture content by mass, and a weighted average of specific heat of straw (estimated at C_p = 1000 J/kg-K) with the specific heat of water yielded a composite specific heat of approximately C_p = 1300 J/kg-K, which was used in the exact solution fitted to the data. The density was adjusted to account for a cube formed with 95g of straw – this assumed that up to 5g of straw was lost in transit from the scale to the press, and that any further loss of mass was caused by the vaporization of moisture when the cube was in the oven. More importantly, if water was being vaporized then the energy that would have gone into heating the cube from approximately t = 1730s to 5625s should be equal to the amount of energy needed to vaporize a given quantity of water at atmospheric pressure. Using the equations in Appendix D, it was found that the approximate amount of energy that went into vaporizing water was 5270 J. From thermodynamic tables, the ΔH_{vap} for water at atmospheric pressure is 2257 kJ/kg (Moran, et al., 2004), which would mean that approximately 2g of water was vaporized. Although 2g would constitute about 2% of the cube's mass, it should be considered that this measurement may only reveal the mass of water vaporized near the thermocouple and not the entire cube, and is therefore still a reasonable value.

Despite the similarities between the temperature profiles of cubes with and without binder there is a discernable difference. Once beyond the plateau region it is clear the binder-treated cubes heated up faster – likely caused by either an exothermic reaction or a change in thermal properties. An exothermic reaction may result from binder decomposing at a temperature close to 107°C. On the other hand the thermal conductivity of a binder treated cube may increase once the temperature plateaus around 107°C. Moreover, these hypotheses should be studied further to better understand this phenomenon.

As reported in the results, using k = 0.1 W/m-K and C_p = 2000 J/kg-K as the parameters yielded an FE model that best fit the data even though it was expected to over-predict curing times. Error resulting from the approximation would likely be constant: a simple time shift less than 5 minutes. It is worth noting that the simulated surface temperature was only a good approximation for the experimental data in the first 300 seconds. This is likely a result of the actual convection coefficient decreasing with the temperature difference between the surface and the oven, whereas the FE model assumed a constant coefficient. However, this was not considered to significantly affect the curing predictions – the key concern was fitting the FE model to the core data. Nevertheless, this was still expected to reasonably estimate curing times of the cube.

Predicting Cube Curing Times with FE Model

The results in Table 5 show that the FE model with C_p = 2000J /kg-K gave liberal estimates of the curing times for temperatures below 100°C. They were lower than the times predicted by the regression curve and for 75°C and 85°C it completely underestimated the curing time. However, it was still acceptable that it fit better with the regression curve and the experimental data for the hotter oven temperatures.

At the time of the simulations, it was decided that this under prediction may have been a result of a variable thermal conductivity or specific heat, and it was decided keep the thermal conductivity constant and increase the specific heat to compensate. The curing times predicted by the C_p = 3000J/kg-K model were therefore sufficiently conservative. (These parameters were used to extrapolate to the Stak Block.)

One later hypothesis suggested that the vaporized moisture effectively increased the thermal conductivity in the straw. Therefore, for oven temperatures lower than 100°C, the effective thermal conductivity would be much lower since little to no moisture was vaporized. However, an informal experiment demonstrated that this is likely

not the case. Figure 58 shows a cube without binder heated in the oven to 422K, allowed to cool afterward, and then re-heated again.

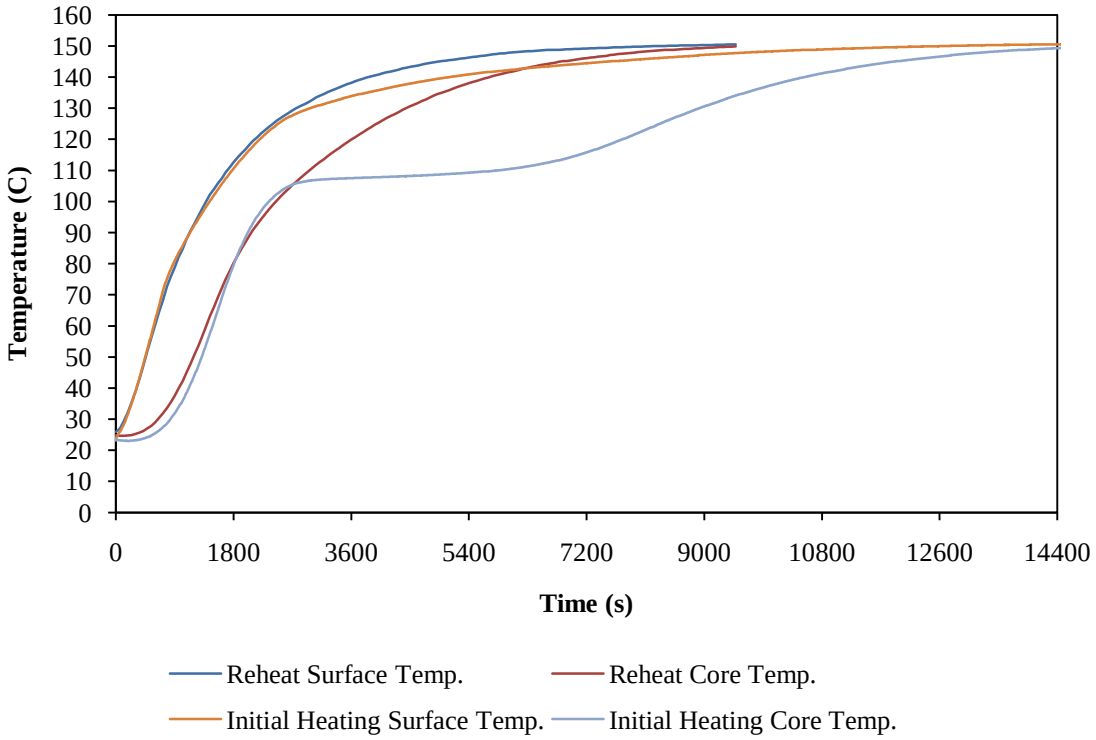

Figure 58. Comparison of initial heating of cube without binder, and subsequent re-heating.

It was noted that the core temperature profile of the reheat still followed relatively closely to the initial heating curve. If the thermal conductivity was effectively increased due to moisture, then it would be expected that the core would take much longer to heat up when reheated; no moisture should be present to vaporize and effectively increase the thermal conductivity. Because the reheated core temperature profile was not significantly different from the initial heating core temperature profile in the first 1800s, it was considered unlikely that vaporized moisture would have led to an increased thermal conductivity.

Moreover, it is quite likely that the under prediction in curing times from the FE model resulted from a simulated convection heat transfer rate that was much greater than the actual value. Recall that the surface convection coefficient h = 10 W/m^2-K was calculated based upon an oven temperature of 422K – although it was applied to simulations of all oven temperatures. However, at cooler oven temperatures it is most likely that the convection coefficient was significantly smaller and resulted in a slower heat transfer rate in the actual experiment.

Extrapolation to the Stak Block

Of particular interest is a simple extrapolation to the Stak Block using the same FE parameters determined to be a good fit for the experimental data (k = 0.1 W/m-K and C_p = 3000 J/kg-K). The simulation for the current curing process predicted that the Stak Block core still did not reach the curing temperature of 65°C after 1 hour (Figure 44) – a counterintuitive result because Oryzatech observes this is sufficient for their Stak Block to cure.

It is plausible that moisture may effectively raise the thermal conductivity significantly more for the Stak Block than for the cube. Recall Figure 17 shows that the thermal conductivity may need to be around 0.40 W/m^2-K for the core to reach 65°C. The rise in thermal conductivity for the Stak Block might be caused by more moisture trapped in the block. Although the moisture content by weight should be the same for the cubes as the Stak Block, there is a significant difference in surface area to volume ratio (0.54 for the Stak Block and 1.45 for the cube). Vaporized moisture maneuvering through the straw may be more likely to be lost to the surroundings for the cube than for the Stak Block.

Another possibility is that an exothermic reaction during the heating process becomes significant when curing on the scale of the Stak Block but not on the scale of the cube. Recall Figure 53 shows a discernable temperature profile difference beginning in the plateau region. In this area the cubes with binder heated up faster than those without. On the scale of the Stak Block this may create significant heat generation. Although the heat generation would begin on the outside before moving inward to the core, it may be enough to hasten the overall heating rate. An exothermic reaction taking place around 107°C (the plateau) may still be able to contribute significantly to helping heat the block, as it is still below the 150°C ambient temperature.

One other scenario is that the baking process is not sufficient to cure the block, but the overall process is. That is, while the blocks cool down the binder continues to cure via some unknown mechanism, possibly moisture continuing to move through the straw. Therefore, by the time Oryzatech cut open the blocks for inspection all the binder had reacted.

Even though the FE model for the Stak Block may not accurately model the actual curing process, it can still be used to meaningfully estimate curing times. As explained in Chapter 5, the FE model for the current process can be compared to the FE model for lower temperatures based on how deep in the block the 65°C curing temperature can be found. As would be expected, the curing times are quite longer, and curing at temperatures below 85°C using a solar oven may not be practical since the times required are generally longer than the number of

daylight hours. Moreover, these results suggest that the curing process may need to be better understood in order to develop a more accurate finite element model.

CHAPTER 7: CONCLUSIONS

This thesis sought to study straw cubes to discern if there was a time-temperature relationship needed to cure the binder. More importantly, this thesis achieved these objectives and several conclusions can be drawn from the results of this study. They are summarized below:

- Curing times are likely more dependent on the rate at which energy passes through the straw than by how much energy is required to cure the adhesive.
- Straw cubes can be cured with oven temperatures lower than 150°C if left for sufficiently longer periods of time.
- The time and temperature needed to cure the straw cubes with pMDI binder are inversely proportional, and can be approximated by the equation in Figure 42.
- The modulus of elasticity and yield strength among binder-treated straw cubes baked at different optimized time-temperature combinations is likely not significantly different.
- The effect of other variables in the bulk curing of straw and pMDI binder are likely to significantly influence the curing process on a macro scale and needs to be better understood.
- Parameters found to give a good approximation for the straw cube FE models may not be applicable to the FE model of the Stak Block.
- Data from experiments with the Stak Block is needed to validate current FE models for the Stak Block or develop more accurate ones.

CHAPTER 8: RECOMMENDATIONS FOR FUTURE WORK

Despite the achievements of this thesis, there are several opportunities for future work to better predict the curing times and temperatures of the Stak Block. These are summarized below.

- FE simulations of the cube curing experiments with lower convection coefficients should be run to estimate curing times.
- An experimentally determined transient temperature distribution of the Stak Block curing in the oven is recommended to discern whether the core is significantly hotter than current FE models predict.
- It is recommended that the Stak Block curing process – both the time spent in the oven and time cooling – should be characterized experimentally to identify and understand unknown variables significant for curing straw on this size magnitude.
- Experiments characterizing the curing kinetics between straw and pMDI are recommended to discern and understand factors significant to curing straw with MDI from those that become significant only when cured on a large scale.
- The convection, radiation, and conduction heat transfer the Stak Block and its mold experience should be experimentally investigated.
- Finally, it is recommended that the experimental data from the above recommended work be used to develop more accurate computer models, including ones capable of simulating chemical reactions if appropriate.

LIST OF REFERENCES

Abbott, Betsy, et al. 2006. Waste Today, Wall Tomorrow: Assessment of an Innovative Straw Block for Residential Construction. Goleta : University of California, Santa Barbara, 2006.

Beer, Ferdinand P., Johnston, E. Russel and DeWolf, John T. 2006. *Mechanics of Materials.* San Francisco : McGraw Hill, 2006. 0-07-298090.

Bill, Steen, David, Bainbridge and Steen, Athena Swentzell. 1994. *The Straw Bale House.* White River Junction : Chelsea Green Publishing Company, 1994. 0-930031-71-7.

Camann, Kevin Robert. 2009. *Design and Performance of Load Bearing Shear Walls Made from Composite Rice Straw Blocks.* San Luis Obispo : California Polytechnic State University, 2009.

Cure chemistry of wood/polymeric isocyanate (PMDI) bonds:Effect of wood species. Das, Sudipto, Malmberg, Michael J. and Frazier, Charles E. 2007. 3, s.l. : International Journal of Adhesion & Adhesives, 2007, Vol. 27.

Curing kinetics of polymeric diphenylmethane diisocyanate with different wood species. He, Guangbo and Yan, Ning. 2007. 3, s.l. : International Journal of Adhesion and Adhesives, 2007, Vol. 27.

Effect of moisture content on curing kinetics of pMDI resin and wood mixtures. He, Guangbo and Yan, Ning. 2005. 5, s.l. : International Journal of Adhesion & Adhesives, 2005, Vol. 25, pp. 450-455.

Evaluation of the cure kinetics of the wood/pMDI bondline. Harper, David P., Wolcott, Michael P. and Rials, Timothy G. 2001. 2, s.l. : International Journal of Adhesion & Adhesives, 2001, Vol. 21.

Granata Design Limited. 2009. *CES Selector Version 5.1.0.* [Software] Cambridge, United Kingdom : s.n., 2009.

Hrynchuk, Lesha. 1998. *Rice Straw Diversion Plan.* 1998.

Incropera, Frank P., et al. 2007. *Introduction to Heat Transfer.* Hoboken : John Wiley and Sons, 2007. 978-0-471-45727-5.

Intergovernmental Panel on Climate Change. 2007. *Climate Change 2007 - The Physical Science Basis.* Cambridge : Cambridge University Press, 2007. Assessment Report.

King, Bruce. 2006. *Design of Straw Bale Buildings.* San Rafael : Green Building Press, 2006. 0-9764911-1-7.

Korman, Benjamin Z., Ruskey, III, John A. and Priest, Doug C. 2005. *Culm Blocks. 6,951,080 B2* United States of America, October 4, 2005. Utility Patent.

MatWeb. 2010. *Material Property Data.* [Online Database] Blacksburg, Virginia : Automation Creations, Inc., 2010.

Monell, Justin. 2008. *Determination of R-value for a new Straw Based Composite Material.* San Luis Obispo : California Polytechnic State University, 2008.

Moran, Michael J. and Shapiro, Howard N. 2004. *Fundamentals of Engineering Thermodynamics.* s.l. : John Wiley and Sons, 2004. 0-471-27471-2.

Silberberg, Martin S. 2003. *Chemistry.* San Frnacisco : McGraw Hill, 2003. 0-07-239681-4.

Steinicke, Horst. 2005. *Straw As a Building Material.* San Luis Obispo : California Polytechnic State University, 2005.

APPENDIX A: Stak Block FE mesh convergence graphs

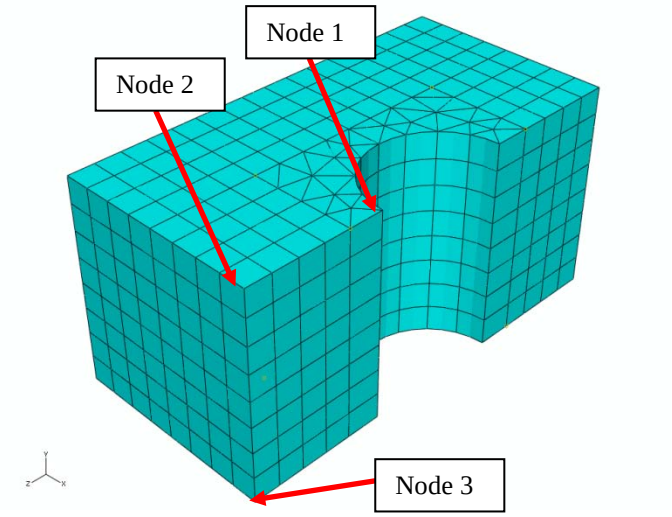

Figure 59. Nodes used in FE mesh convergence.

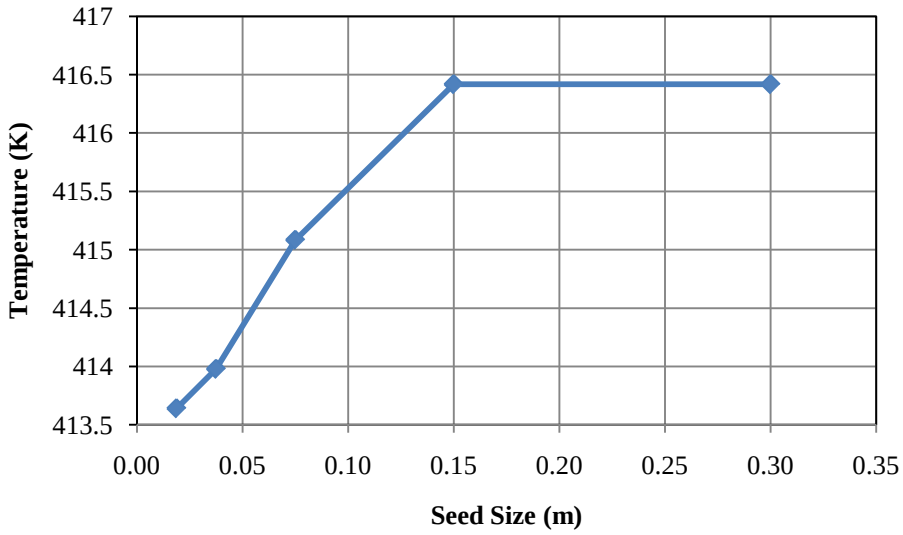

Figure 60. Mesh Convergence Plot at Node 1.

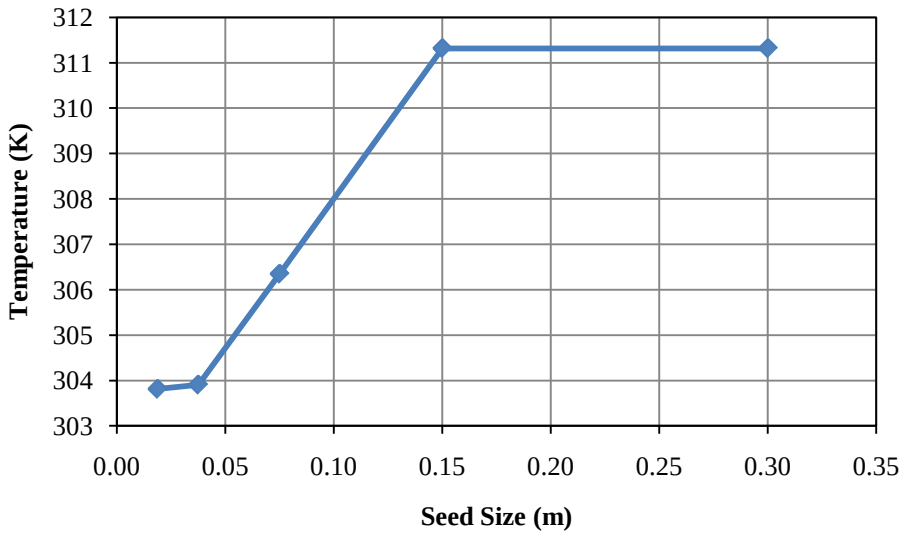

Figure 61. Mesh Convergence Plot at Node 2.

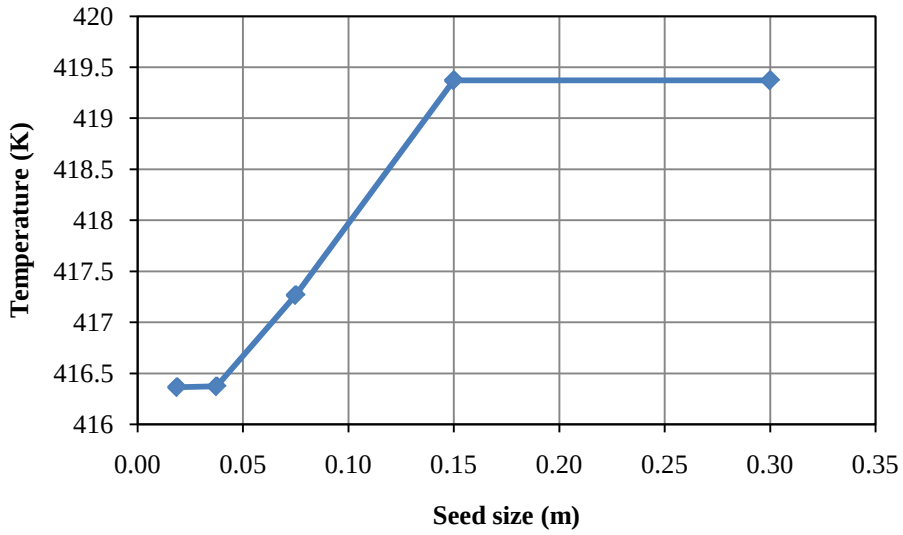

Figure 62. Mesh Convergence Plot at Node 3.

APPENDIX B: Cube FE mesh convergence graphs

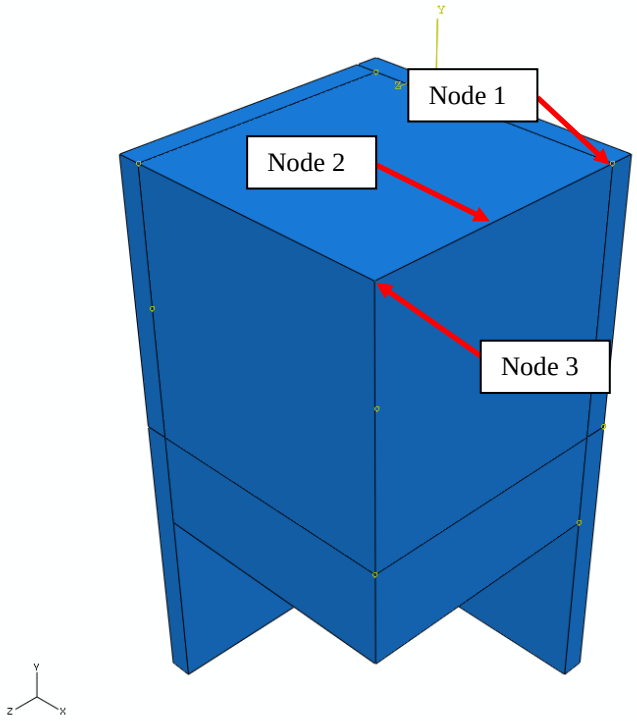

Figure 63. Node locations for mesh convergence study.

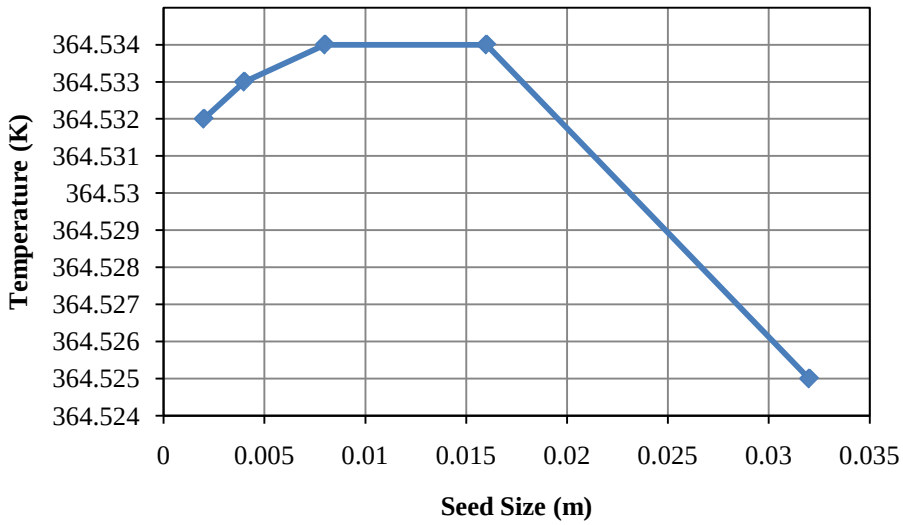

Figure 64. Mesh Convergence Plot at Node 1.

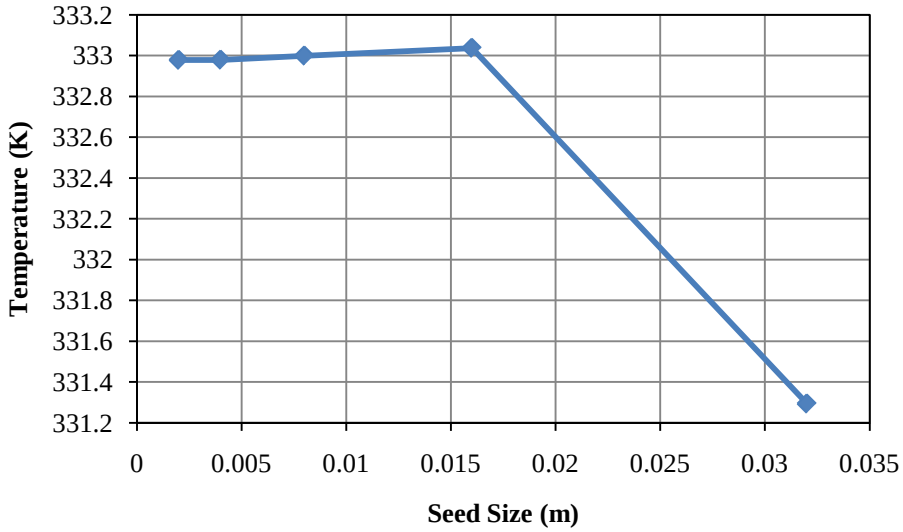

Figure 65. Mesh Convergence Plot at Node 2.

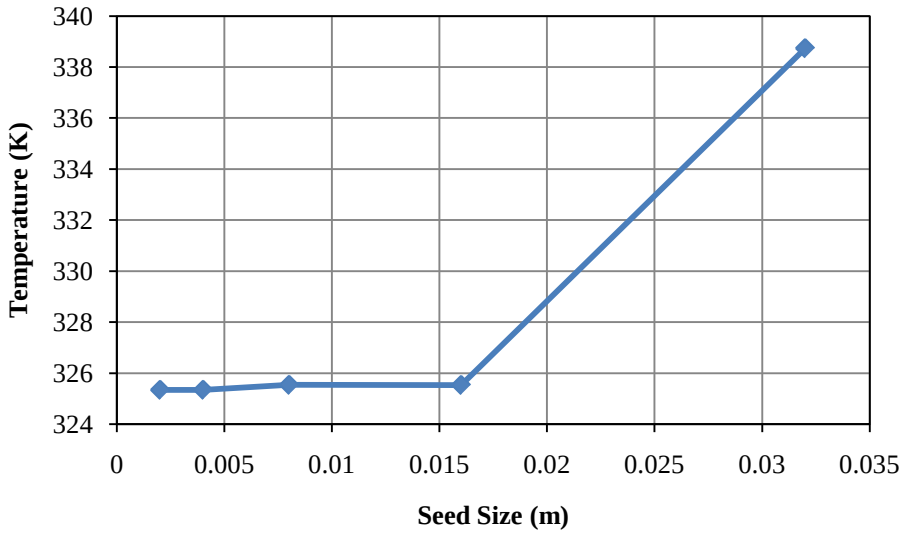

Figure 66. Mesh Convergence Plot at Node 3.

APPENDIX C: Full results of cube curing evaluation

Table 9. Cube responses in first iteration. Uncured = 0, Cured =1.

Cube Name	Temperature	Time	Response
VII - RT1	150	1	1
III - RT1	150	4	1
VIII - RT1	150	2	1
V - RT1	150	3	1
III - RT2	50	1	0
II - RT2	50	2	0
VI - RT2	50	3	0
VII - RT2	50	4	0
II - RT3	100	1	1
I - RT3	100	2	1
III -RT3	100	3	1
VII - RT3	100	4	1
VII - RT4	100	1	1
VIII - RT4	100	2	1
IV - RT4	100	3	1
III - RT4	100	4	1

Table 10. Cube responses in second iteration. Uncured = 0, Cured =1.

Cube Name	Temperature	Time	Response
IV - RT5	75	1	0
III - RT5	75	2	1
VII - RT5	75	4	1
VI - RT5	75	3	1
III - RT6	75	1	0
I -RT6	75	2	1
VIII - RT6	75	3	1
VII - RT6	75	4	1

Table 11. Cube responses in third iteration. Uncured = 0, Cured =1.

Cube Name	Temperature	Time	Response
III - RT7	75	1	0
VII - RT7	75	1.33	0
VI - RT7	75	1.66	1
I - RT7	75	2	1
II - RT8	75	1	0
III - RT8	75	1.33	1
V - RT8	75	1.66	1
VIII - RT8	75	2	1
IV - RT9	100	0.25	0
VIII - RT9	100	0.5	0
III - RT9	100	0.75	1
V - RT9	100	1	1
II - RT10	150	0.25	0
V - RT10	150	0.5	1
IV - RT10	150	0.75	1
VIII - RT10	150	1	1

Table 12. Cube responses in fourth iteration. Uncured = 0, Cured =1.

Cube Name	Temperature	Time	Response
I - RT11	65	1.5	Not usable
II - RT11	65	2	Not usable
IV - RT11	65	2.5	Not usable
III - RT11	65	3	Not usable
VII - RT12	65	1.5	Not usable
III - RT12	65	2	1
I - RT12	65	2.5	1
VI - RT12	65	3	1
VIII - RT13	85	0.75	1
V - RT13	85	1	1
VI - RT13	85	1.25	1
II - RT13	85	1.5	1
III - RT14	85	0.75	0
VIII - RT14	85	1	1
V - RT14	85	1.25	1
IV - RT14	85	1.5	1
VI - RT15	65	1.5	0
I - RT15	65	2	1
III - RT15	65	2.5	1
IV - RT15	65	3	1

Table 13. Cube responses in fifth iteration. Uncured = 0, Cured =1.

Cube Name	Temperature	Time	Response
III - RT16	150	0.25	0
VII - RT16	150	0.5	1
II - RT16	150	0.75	1
VI - RT16	150	1	1
IV - RT17	100	0.25	0
II - RT17	100	0.5	0
VIII - RT17	100	0.75	1
VII - RT17	100	1	1

Table 14. Cube responses in sixth iteration. Uncured = 0, Cured =1.

Cube Name	Temperature	Time	Response
I - RT18	125	0.25	0
II - RT18	125	0.5	1
III - RT18	125	0.75	1
VIII - RT18	125	1	1
VII - RT19	125	0.25	0
I - RT19	125	0.5	1
IV - RT19	125	0.75	1
VI - RT19	125	1	1

APPENDIX D: Summary of exact mathematical solution to cube.

In mathematical terms, the temperature of the cube is described as:

$$\boldsymbol{T = T(x_1, x_2, x_3, t)}$$

Where x_1, x_2, and x_3, are rectangular coordinates (in meters) relative to the geometric center of the cube and t is time (in seconds). This is related to the one-dimensional solutions of plane walls with convection:

$$\frac{T(x_1, x_2, x_3, t) - T_\infty}{T_i - T_\infty} = P(x_1, t) \cdot P(x_2, t) \cdot P(x_3, t)$$

Where $P(x_1, t)$, $P(x_2, t)$, $P(x_3, t)$ are each the dimensionless temperatures for one-dimensional plane walls with convection on both sides. T_i and T_∞ are the initial and fluid temperatures respectively. Each dimensionless temperature is calculated by the infinite series, although summing first four terms is usually sufficient:

$$P(x_1, t) = \sum_{n=1}^{\infty} C_n \exp(-\zeta_n^2 Fo) \cos(\zeta_n x_1^*)$$

Where ζ_n is a positive characteristic root of the equation:

$$\zeta_n \tan \zeta_n = Bi$$

Where Bi is the Biot number following Equation 5 and C_n is calculated from ζ_n:

$$C_n = \frac{4 \sin \zeta_n}{2\zeta_n + \sin(2\zeta_n)}$$

Where Fo is the Fourier number (dimensionless time):

$$Fo = \frac{\alpha t}{L^2}$$

L is half of the width (or length or height as appropriate) of the parallelepiped, t is time, and α is the thermal diffusivity:

$$\alpha = \frac{k}{\rho C_p}$$

Where k is thermal conductivity, ρ is density, and C_p is specific heat. x_1^* is calculated as:

$$x_1^* = \frac{x_1}{L}$$

Where x_1 is the actual rectangular coordinate.

A comparison of the exact solution with the appropriate FE model (i.e. a cube heating up without a mold) gave virtually identical results, as shown in Figure 67.

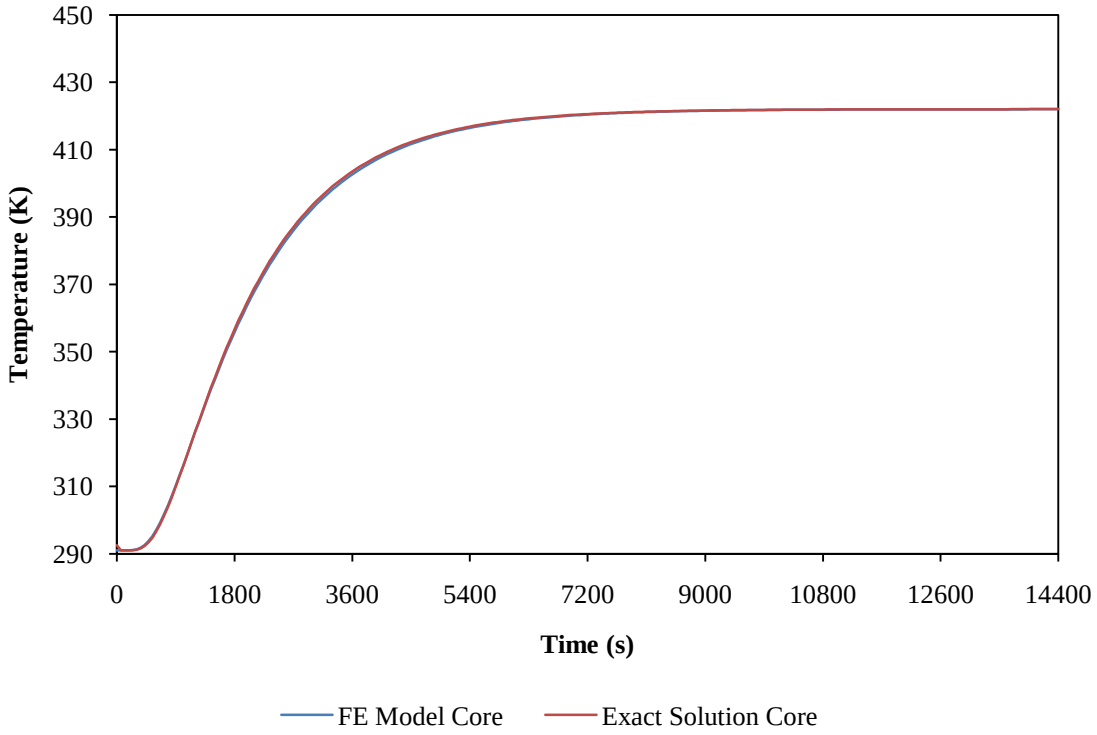

Figure 67. Comparison of exact solution with appropriate FE model. C_p = 2000 J/kg-K, k = 0.1 W/m-K, ρ = 263 kg/m^3, h = 10 W/m^2-K.

However, it was demonstrated that an FE model of a cube in an aluminum mold produced results different from the closed-form solution for a cube without a mold – under the same oven conditions. These differences eventually became significant, as shown in Figure 68.

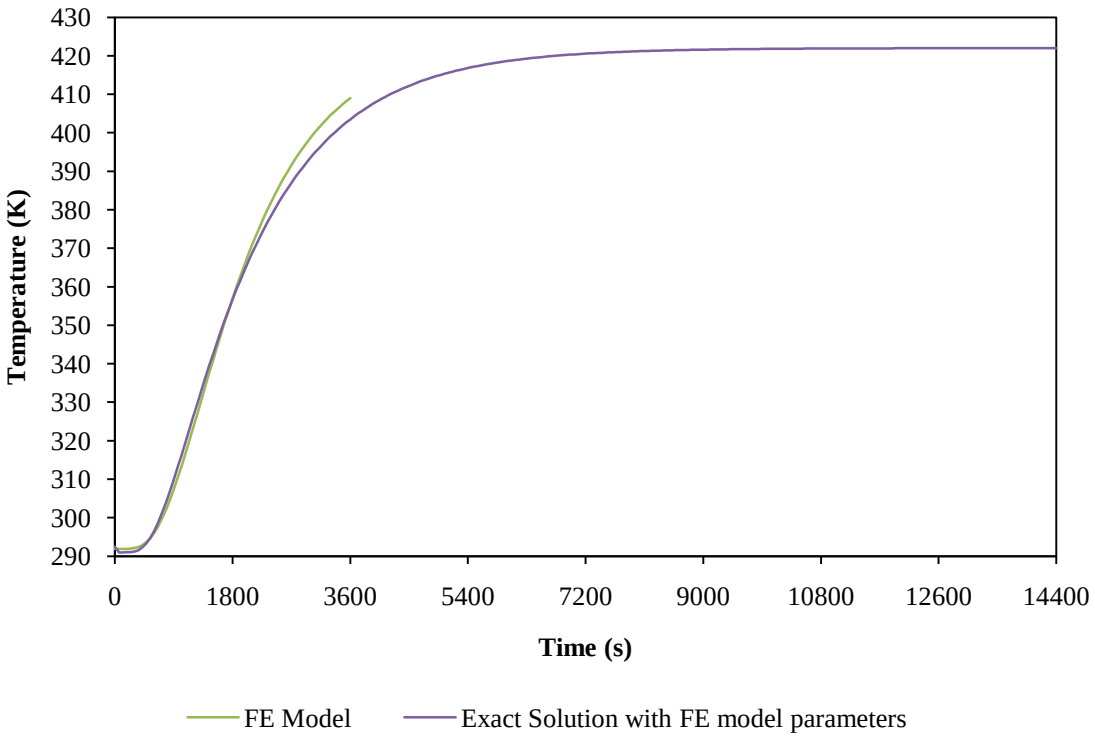

Figure 68. Comparison of FE model with exact solution. C_p = 2000 J/kg-K, k = 0.1 W/m-K, ρ = 263 kg/m^3, h = 10 W/m^2-K.

Similarly, the energy absorbed by the cube is also the product of three one-dimensional solutions, each of which is given by:

$$\frac{Q}{Q_0} = 1 - \frac{\sin \zeta_1}{\zeta_1} \theta_0^*$$

Where Q represents the total energy absorbed from $t = 0$ to $t = t_1$, Q_0 represents the maximum possible energy that can be absorbed, which is given as:

$$Q_0 = \rho c V (T_i - T_\infty)$$

Where ρ is the material density, c is the specific heat, V is the volume, T_i is the initial temperature, and T_∞ is the oven temperature. Note that the Fourier number Fo must be greater than 0.2 to use this equation, since it is based on the first term approximation of the infinite series solution to the transient temperature distribution. Appropriately,

$$\theta_0^* = C_1 \exp(-\zeta_1^2 Fo)$$

APPENDIX E: Finite element model temperature profiles used to calculate straw cube curing times

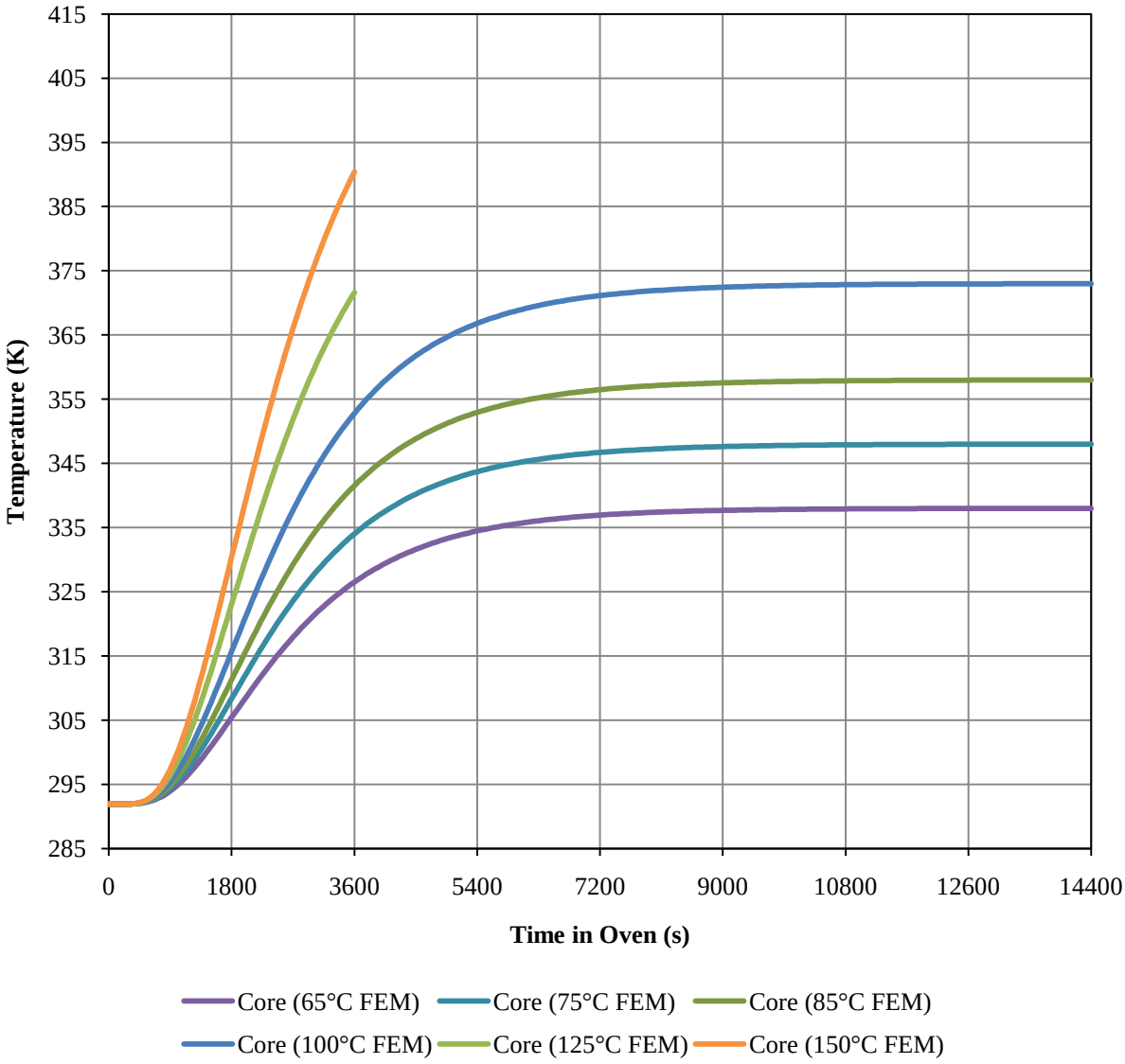

Figure 69. Straw Cube finite element model predictions of core temperatures for different oven temperatures (°C).

APPENDIX F: Finite element model temperature contour plots used to extrapolate Stak Block curing times

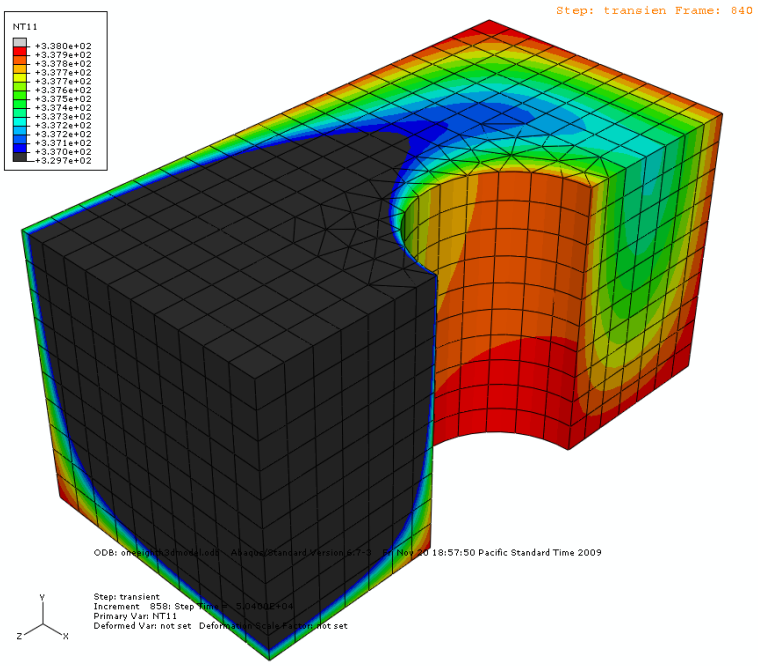

Figure 70. Stak Block contour plot for T = 338K and t = 50400s.

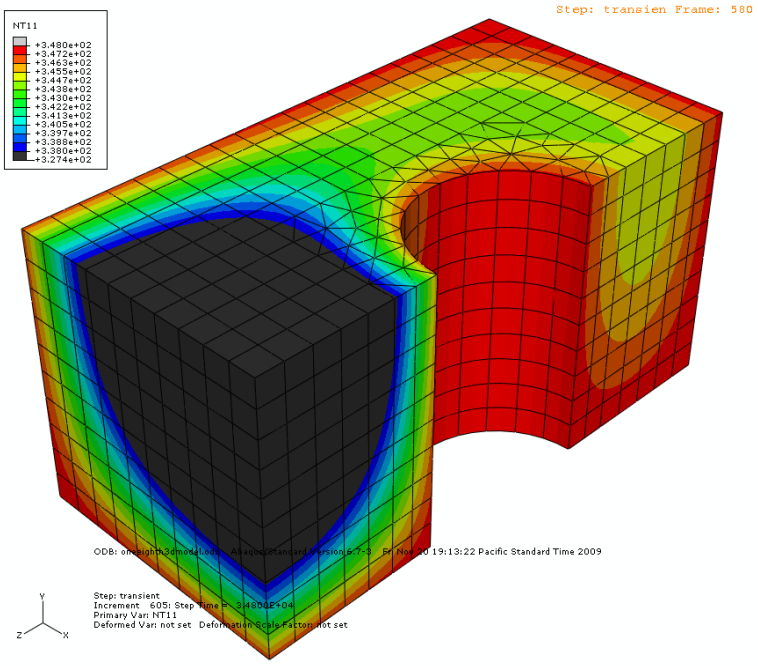

Figure 71. Stak Block contour plot for T = 348K and t = 34800s.

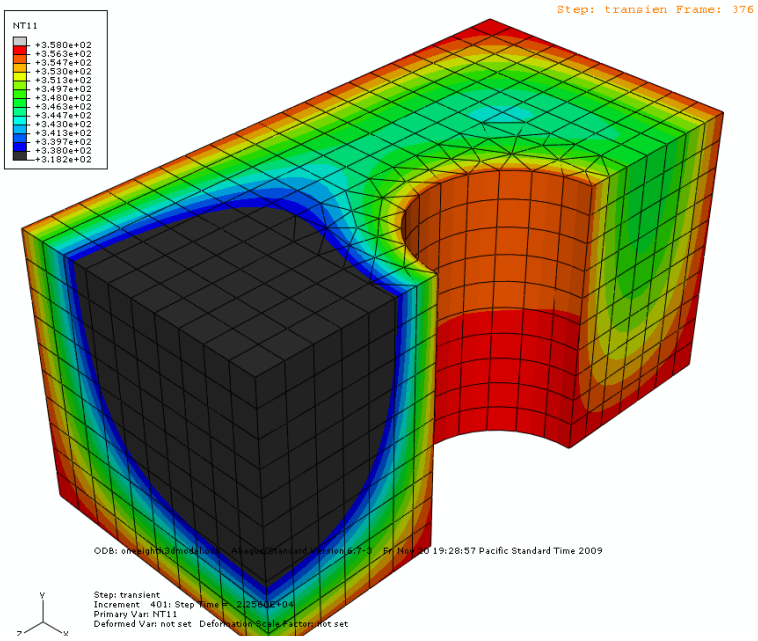

Figure 72. Stak Block contour plot for T = 358K and t = 22560s.

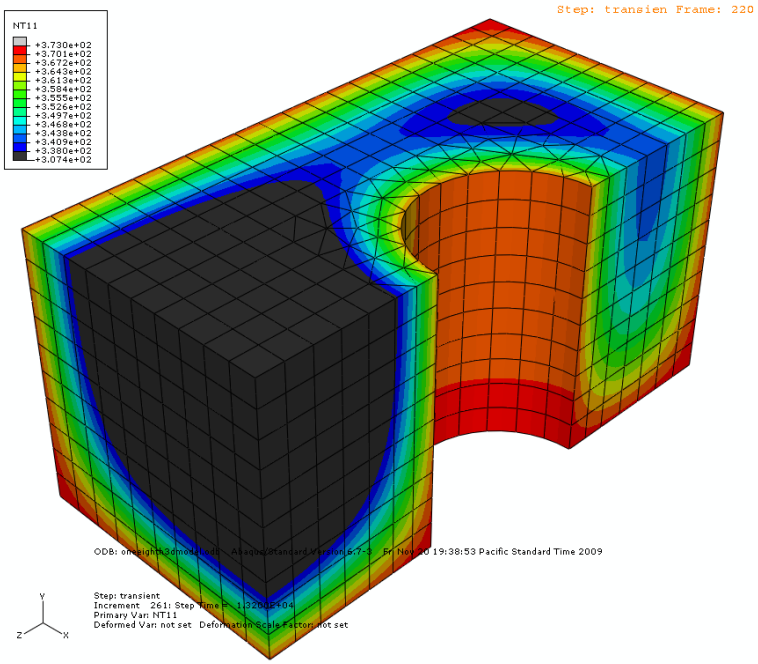

Figure 73. Stak Block contour plot for T = 373K and t = 13200s.

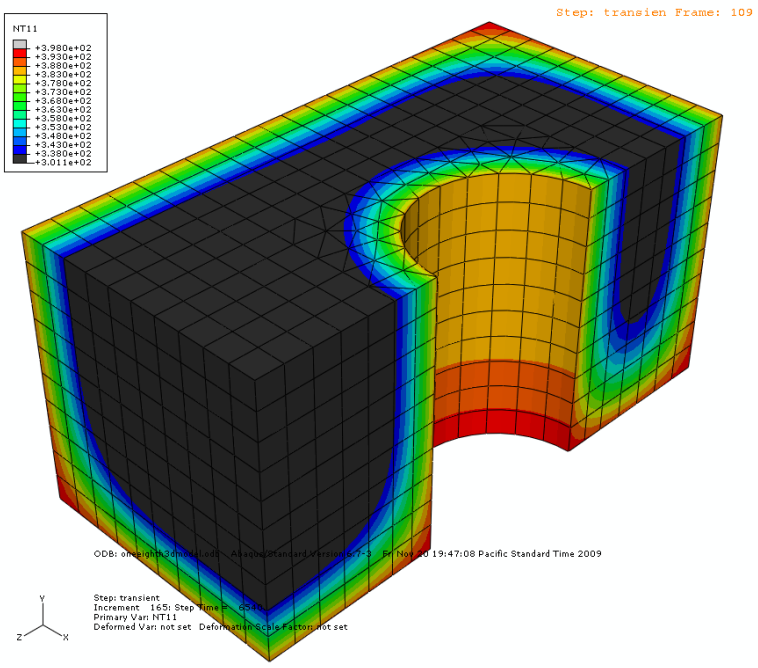

Figure 74. Stak Block contour plot for T = 398K and t = 6540s.

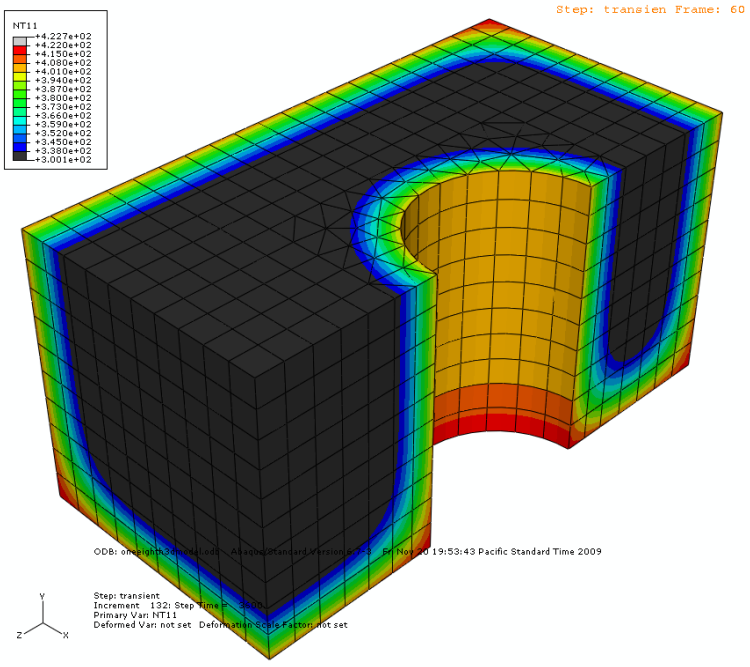

Figure 75. Stak Block contour plot for T = 423K and t = 3600s.

APPENDIX G: Stress-strain curves for all cubes

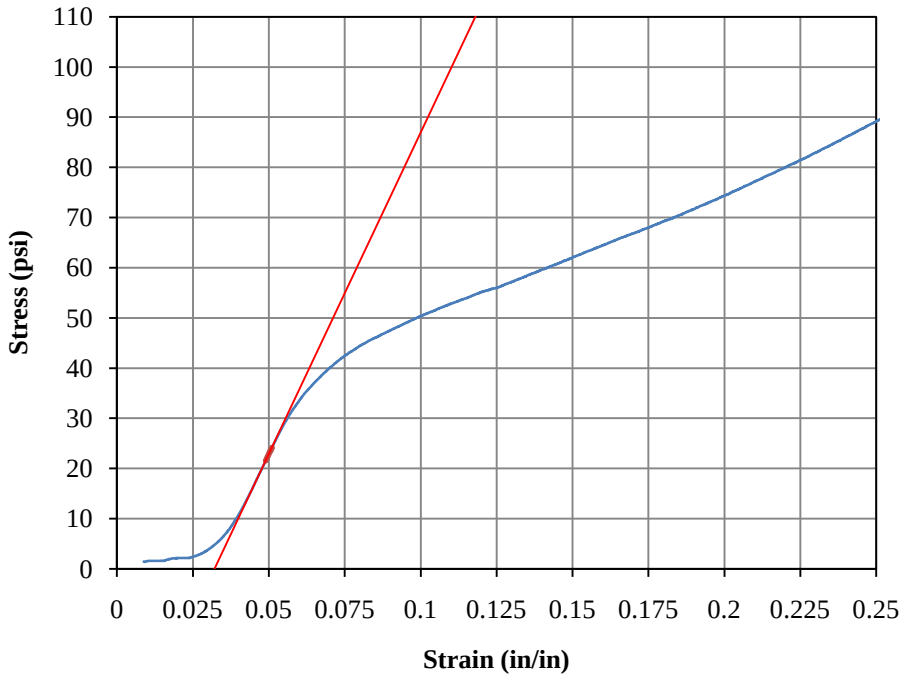

Figure 76. Stress-strain graph. Cube III - UC4.

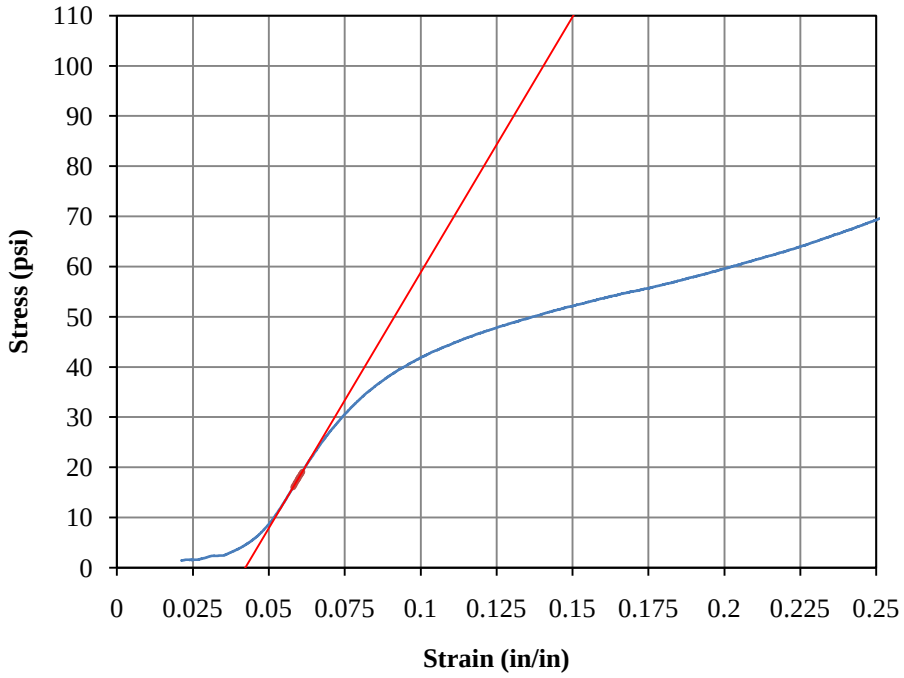

Figure 77. Stress-strain graph. Cube V - UC4.

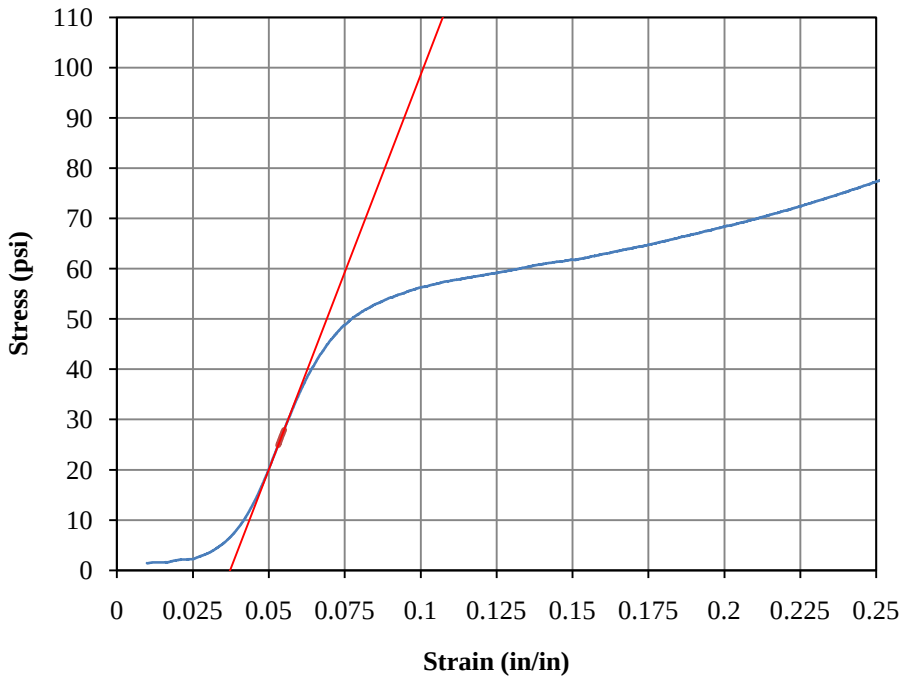

Figure 78. Stress-strain graph. Cube VI - UC4.

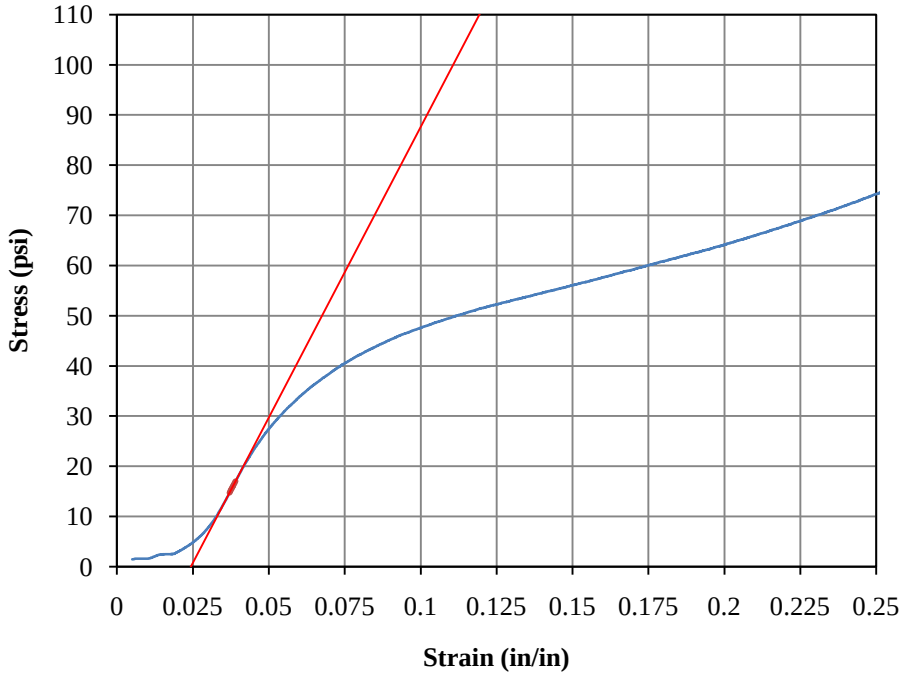

Figure 79. Stress-strain graph. Cube VIII - UC4.

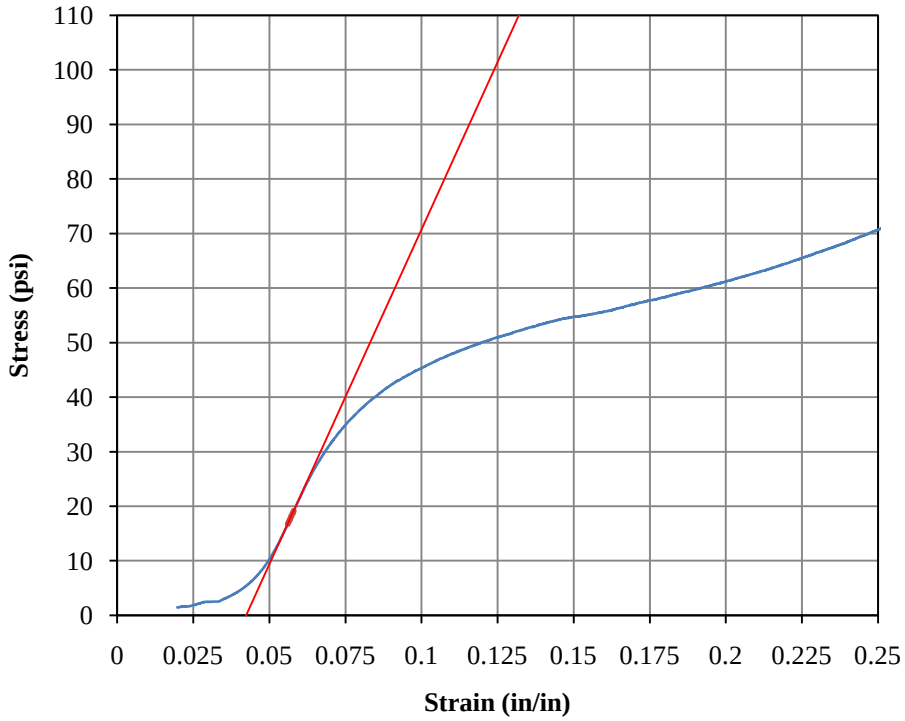

Figure 80. Stress-strain graph. Cube I - UC5.

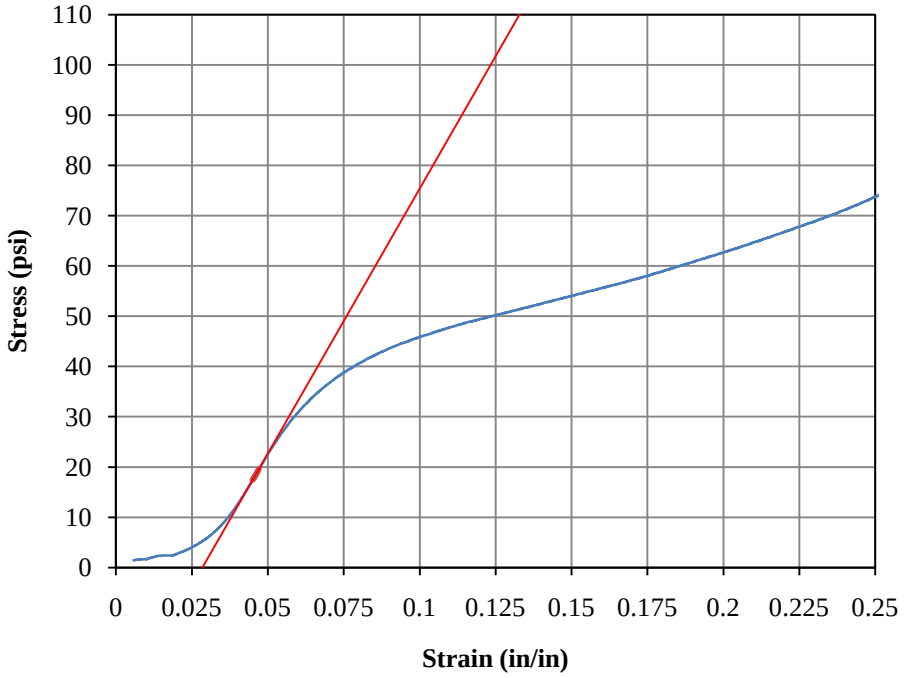

Figure 81. Stress-strain graph. Cube V - UC5.

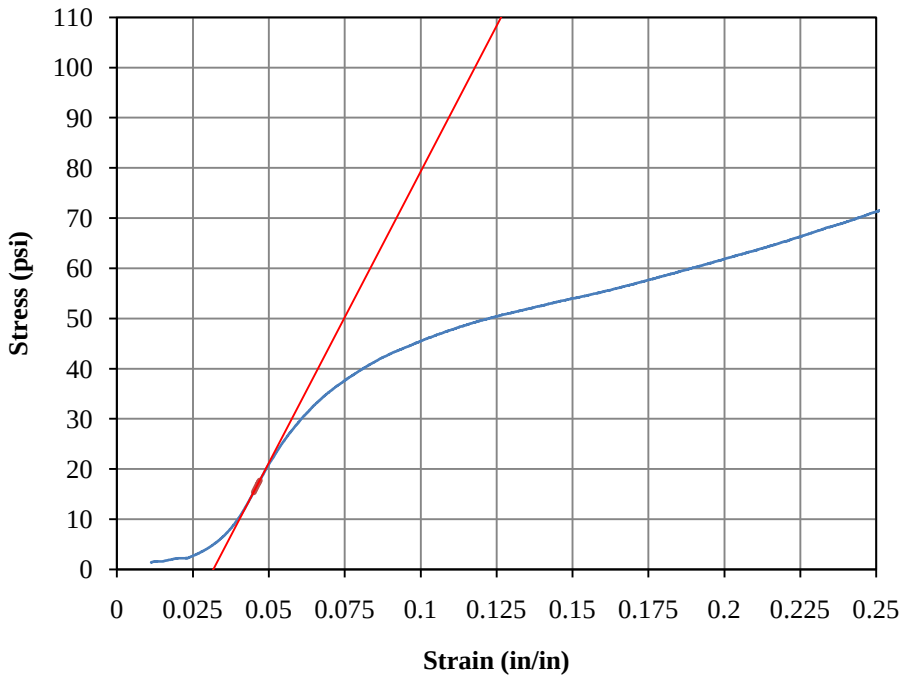

Figure 82. Stress-strain graph. Cube VII - UC5.

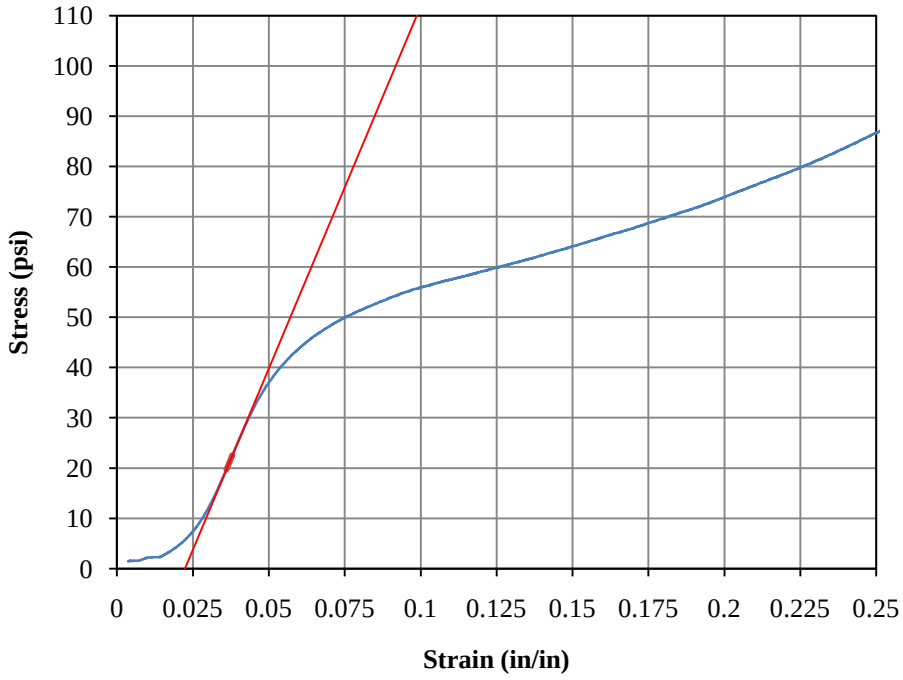

Figure 83. Stress-strain graph. Cube VIII - UC5.

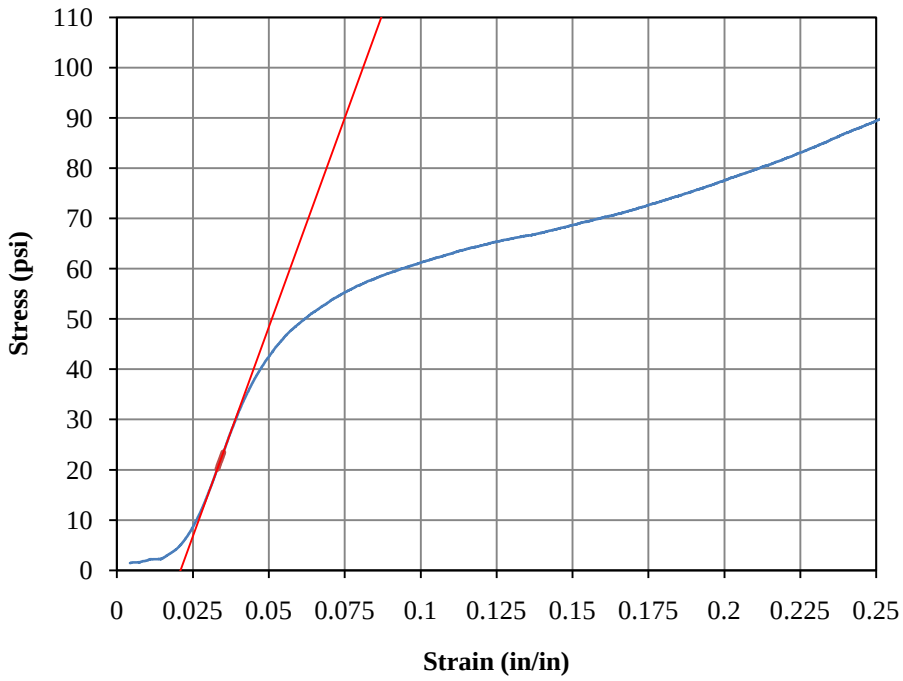

Figure 84. Stress-strain graph. Cube II - UC6.

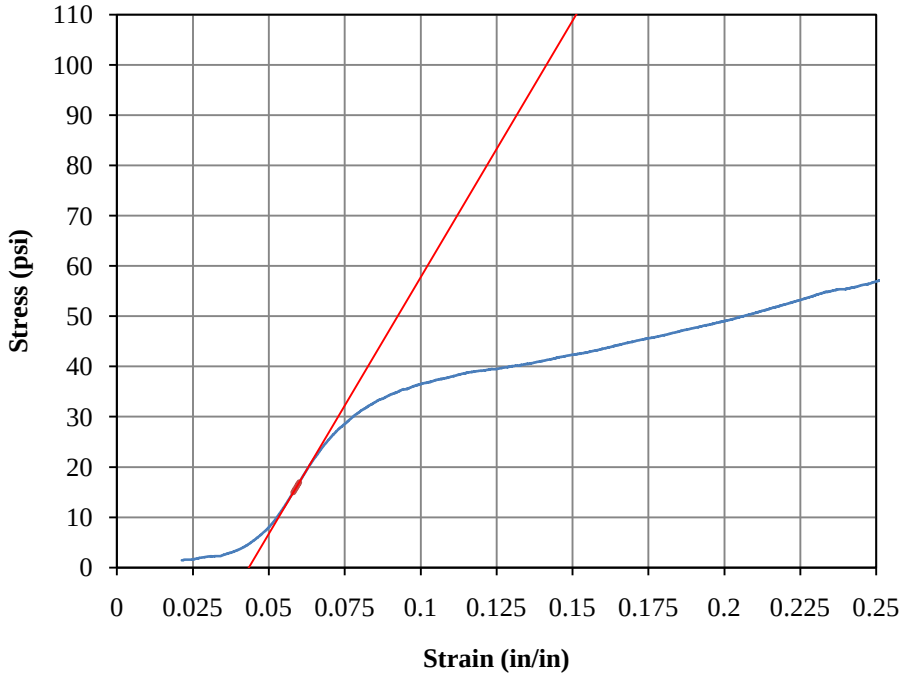

Figure 85. Stress-strain graph. Cube VI - UC6.

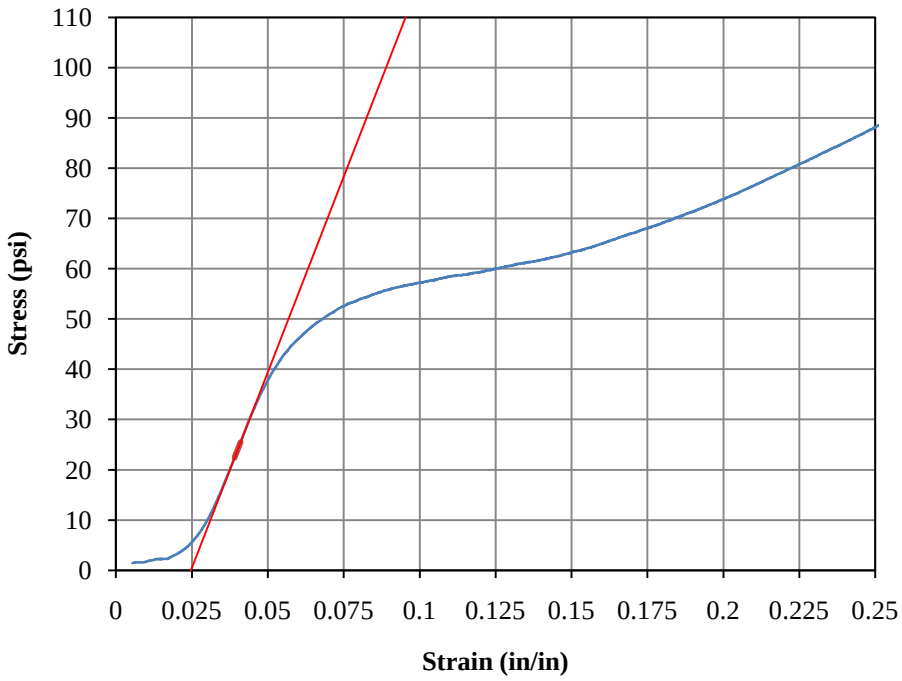

Figure 86. Stress-strain graph. Cube VII - UC6.

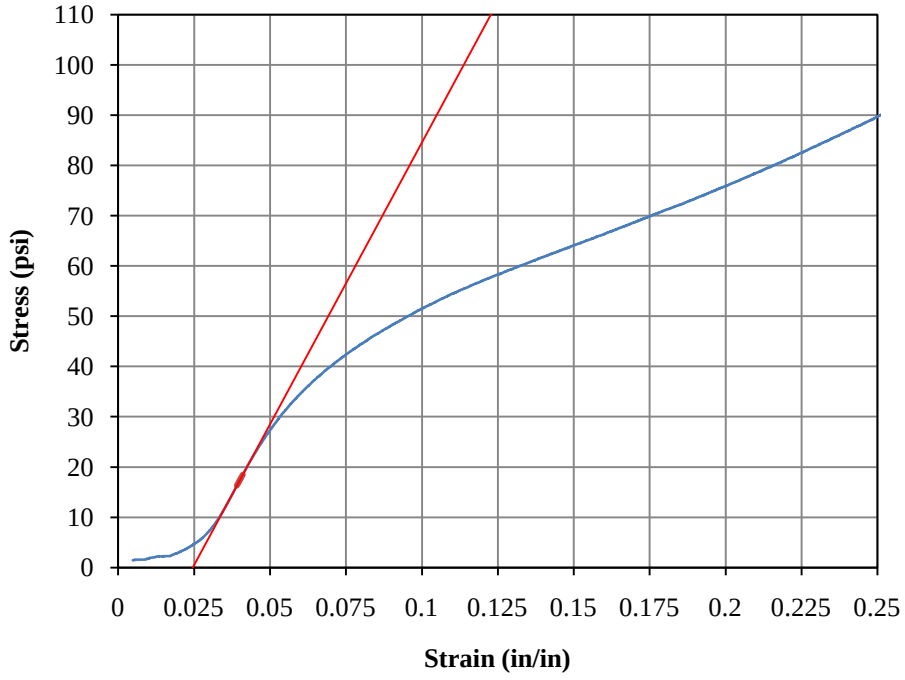

Figure 87. Stress-strain graph. Cube VIII - UC6.

APPENDIX H: Engineering drawings – Straw press

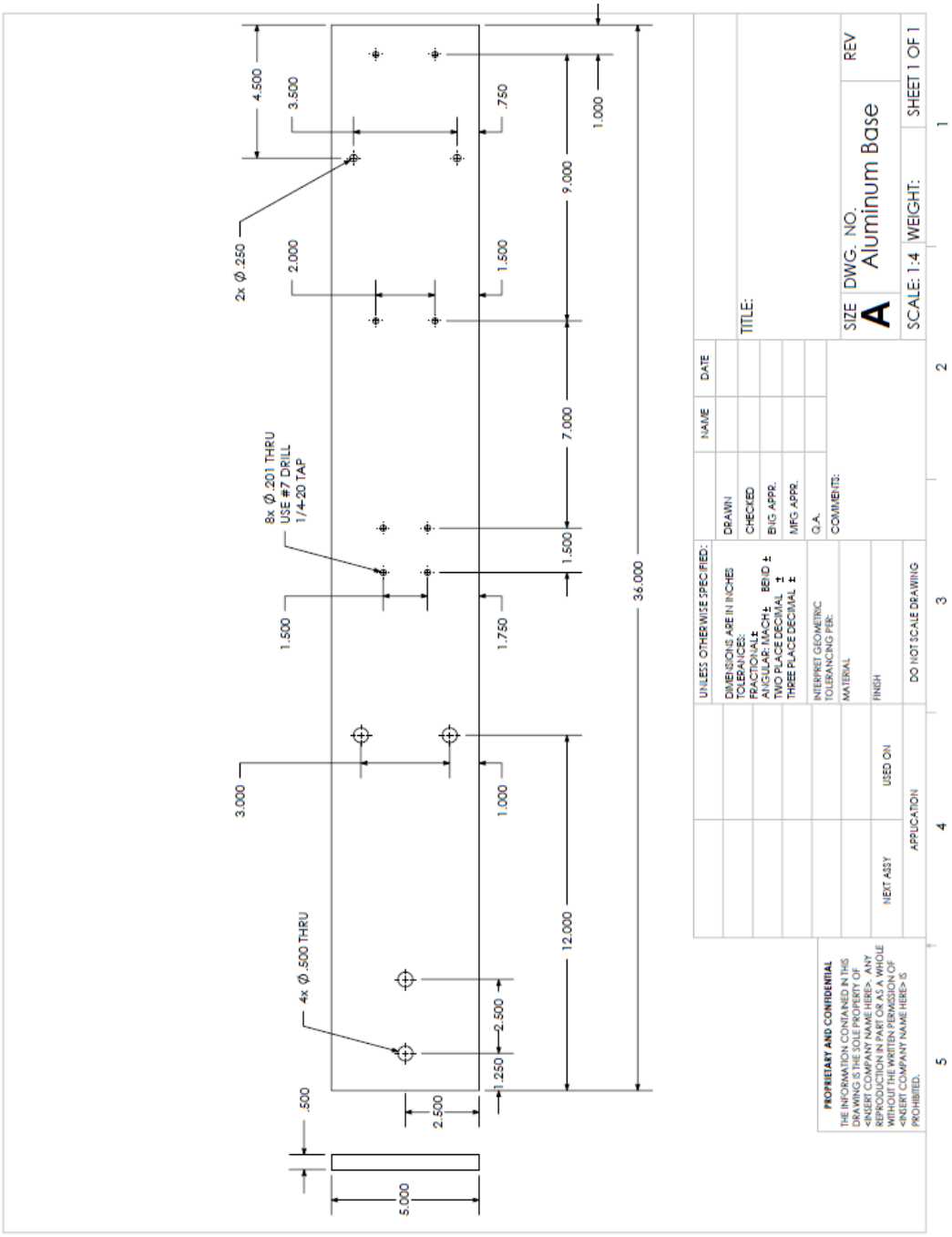

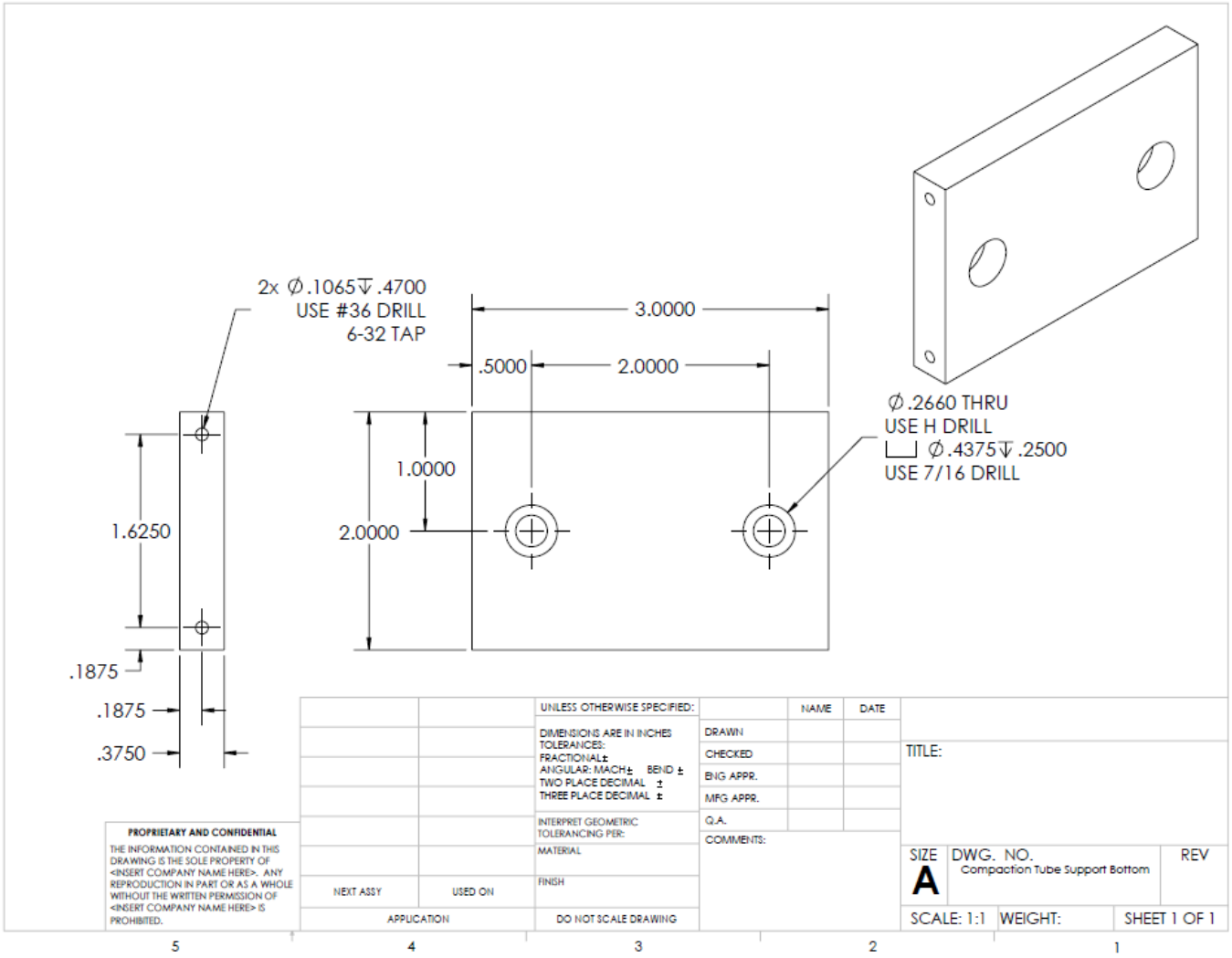
2x Ø.1065↧.4700
USE #36 DRILL
6-32 TAP
3.0000
.5000
2.0000
Ø.2660 THRU
USE H DRILL
⌴ Ø.4375↧.2500
USE 7/16 DRILL
1.0000
2.0000
1.6250
.1875
.1875
.3750
UNLESS OTHERWISE SPECIFIED:
DIMENSIONS ARE IN INCHES
TOLERANCES:
FRACTIONAL ±
ANGULAR: MACH ± BEND ±
TWO PLACE DECIMAL ±
THREE PLACE DECIMAL ±
INTERPRET GEOMETRIC TOLERANCING PER:
MATERIAL
FINISH
DO NOT SCALE DRAWING
NAME
DATE
DRAWN
CHECKED
ENG APPR.
MFG APPR.
Q.A.
COMMENTS:
TITLE:
SIZE A
DWG. NO.
Compaction Tube Support Bottom
REV
SCALE: 1:1
WEIGHT:
SHEET 1 OF 1
NEXT ASSY
USED ON
APPLICATION
PROPRIETARY AND CONFIDENTIAL
THE INFORMATION CONTAINED IN THIS DRAWING IS THE SOLE PROPERTY OF <INSERT COMPANY NAME HERE>. ANY REPRODUCTION IN PART OR AS A WHOLE WITHOUT THE WRITTEN PERMISSION OF <INSERT COMPANY NAME HERE> IS PROHIBITED.
5
4
3
2
1

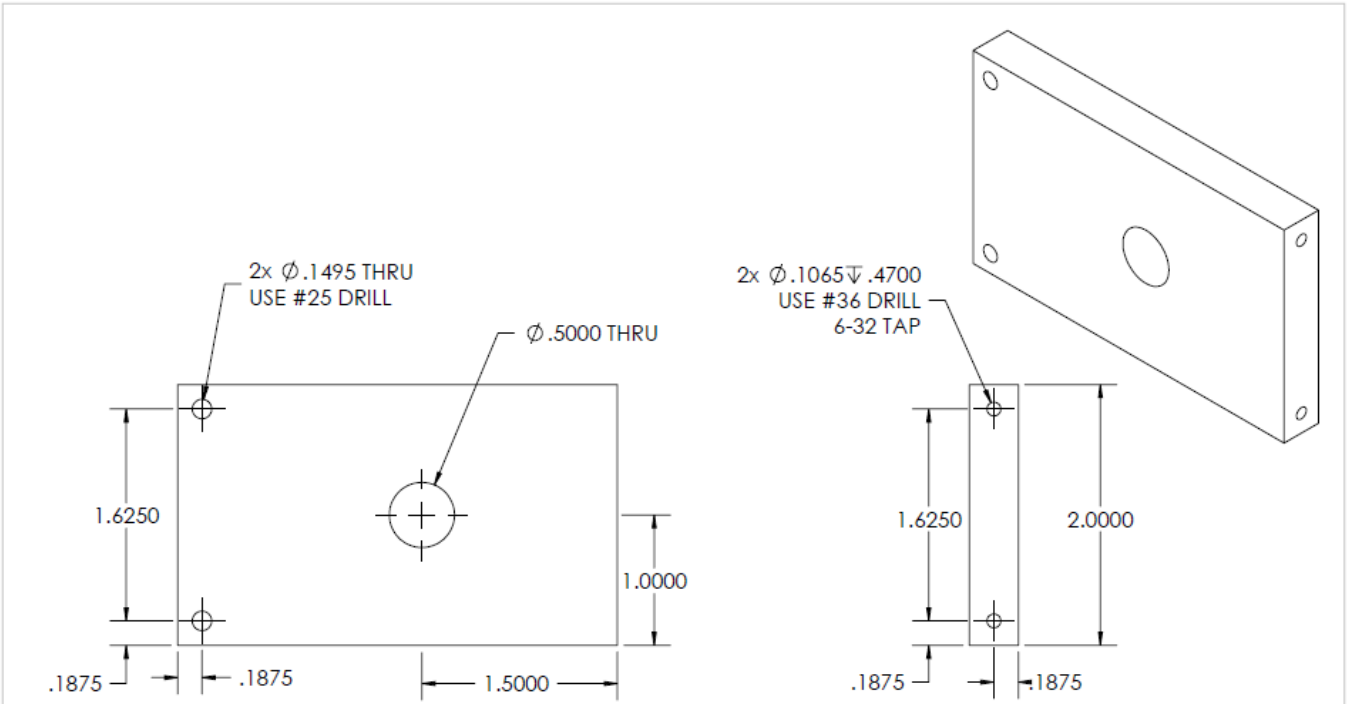

		UNLESS OTHERWISE SPECIFIED:		NAME	DATE
		DIMENSIONS ARE IN INCHES TOLERANCES: FRACTIONAL ± ANGULAR: MACH ± BEND ± TWO PLACE DECIMAL ± THREE PLACE DECIMAL ±	DRAWN		
			CHECKED		
			ENG APPR.		
			MFG APPR.		
		INTERPRET GEOMETRIC TOLERANCING PER:	Q.A.		
		MATERIAL	COMMENTS:		
NEXT ASSY	USED ON	FINISH			
APPLICATION		DO NOT SCALE DRAWING			

PROPRIETARY AND CONFIDENTIAL

THE INFORMATION CONTAINED IN THIS DRAWING IS THE SOLE PROPERTY OF <INSERT COMPANY NAME HERE>. ANY REPRODUCTION IN PART OR AS A WHOLE WITHOUT THE WRITTEN PERMISSION OF <INSERT COMPANY NAME HERE> IS PROHIBITED.

TITLE:

SIZE	DWG. NO.	REV
A	Compaction Tube Support Side with Hole	
SCALE: 1:1	WEIGHT:	SHEET 1 OF 1

5 4 3 2 1

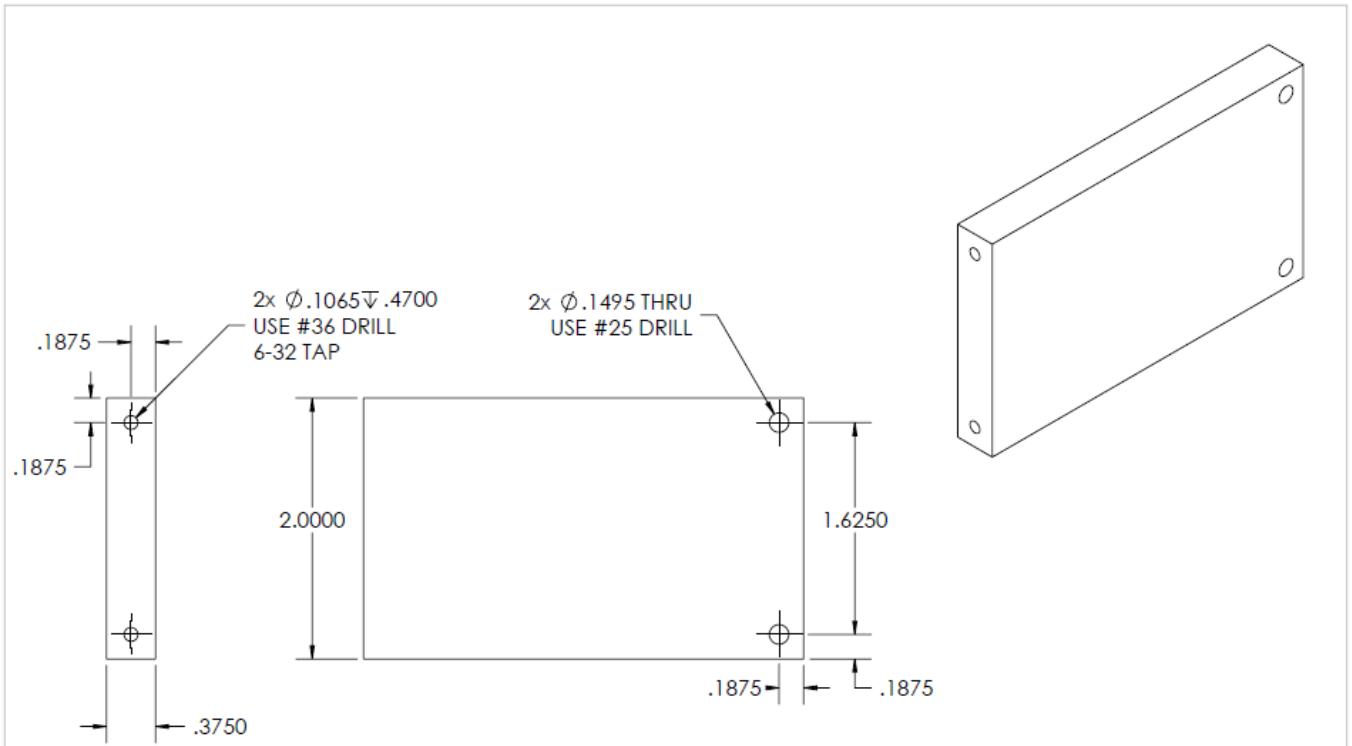

		UNLESS OTHERWISE SPECIFIED:		NAME	DATE
		DIMENSIONS ARE IN INCHES TOLERANCES: FRACTIONAL ± ANGULAR: MACH ± BEND ± TWO PLACE DECIMAL ± THREE PLACE DECIMAL ±	DRAWN		
			CHECKED		
			ENG APPR.		
			MFG APPR.		
		INTERPRET GEOMETRIC TOLERANCING PER:	Q.A.		
		MATERIAL	COMMENTS:		
NEXT ASSY	USED ON	FINISH			
APPLICATION		DO NOT SCALE DRAWING			

PROPRIETARY AND CONFIDENTIAL

THE INFORMATION CONTAINED IN THIS DRAWING IS THE SOLE PROPERTY OF <INSERT COMPANY NAME HERE>. ANY REPRODUCTION IN PART OR AS A WHOLE WITHOUT THE WRITTEN PERMISSION OF <INSERT COMPANY NAME HERE> IS PROHIBITED.

TITLE:

SIZE	DWG. NO.	REV
A	Compaction Tube Support Side	
SCALE: 1:1	WEIGHT:	SHEET 1 OF 1

5 4 3 2 1

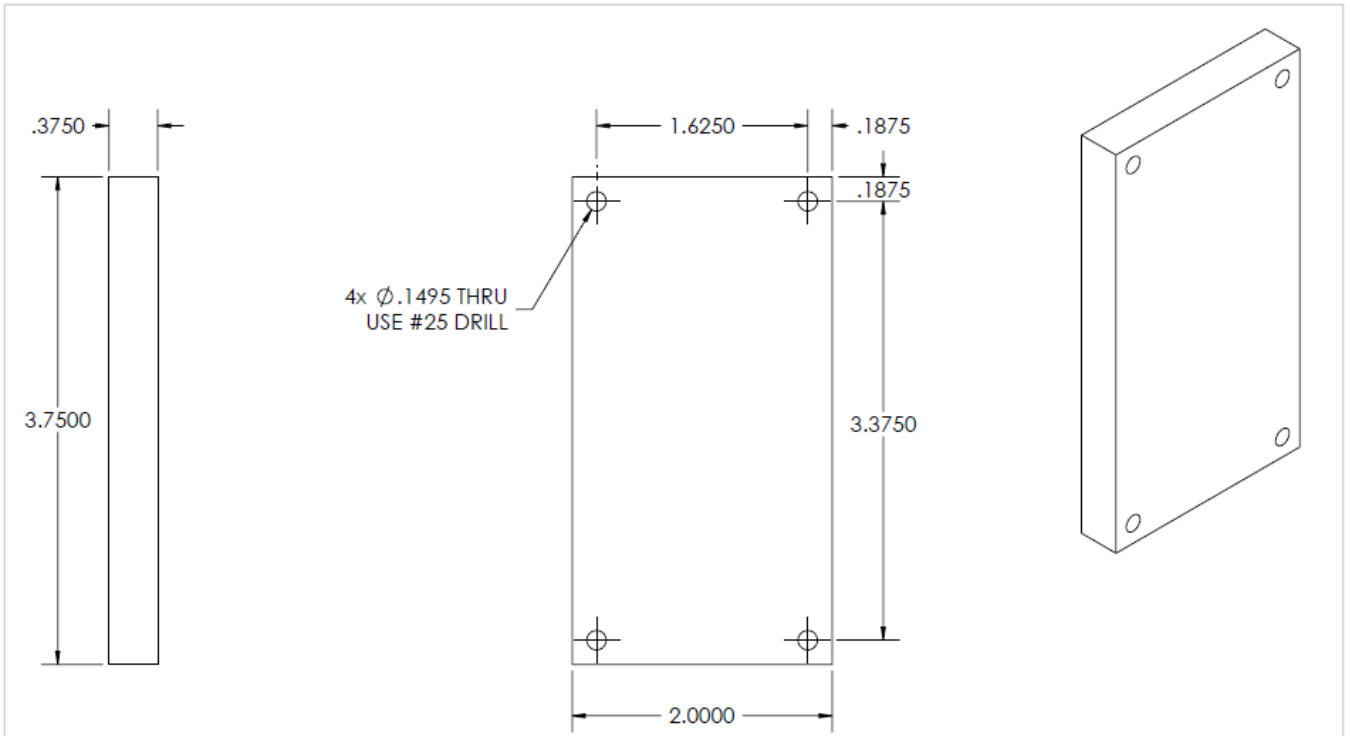

		UNLESS OTHERWISE SPECIFIED:		NAME	DATE
		DIMENSIONS ARE IN INCHES TOLERANCES: FRACTIONAL ± ANGULAR: MACH ± BEND ± TWO PLACE DECIMAL ± THREE PLACE DECIMAL ±	DRAWN		
			CHECKED		
			ENG APPR.		
			MFG APPR.		
		INTERPRET GEOMETRIC TOLERANCING PER:	Q.A.		
		MATERIAL	COMMENTS:		
NEXT ASSY	USED ON	FINISH			
APPLICATION		DO NOT SCALE DRAWING			

TITLE:

SIZE	DWG. NO.	REV
A	Compaction Tube Support Top	
SCALE: 1:1	WEIGHT:	SHEET 1 OF 1

5 4 3 2 1

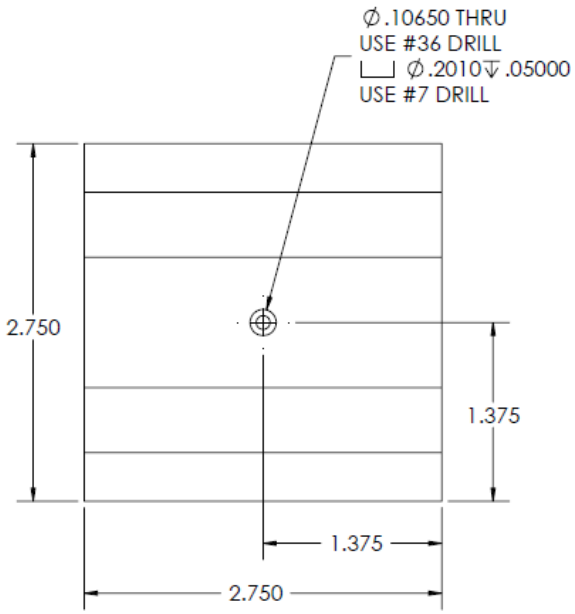

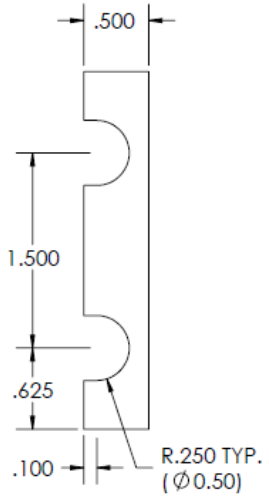

		UNLESS OTHERWISE SPECIFIED:		NAME	DATE
		DIMENSIONS ARE IN INCHES TOLERANCES: FRACTIONAL ± ANGULAR: MACH ± BEND ± TWO PLACE DECIMAL ± THREE PLACE DECIMAL ±	DRAWN		
			CHECKED		
			ENG APPR.		
			MFG APPR.		
		INTERPRET GEOMETRIC TOLERANCING PER:	Q.A.		
		MATERIAL	COMMENTS:		
NEXT ASSY	USED ON	FINISH			
APPLICATION		DO NOT SCALE DRAWING			

TITLE:

SIZE	DWG. NO.	REV
A	Compactor Head	
SCALE: 1:1	WEIGHT:	SHEET 1 OF 1

5 4 3 2 1

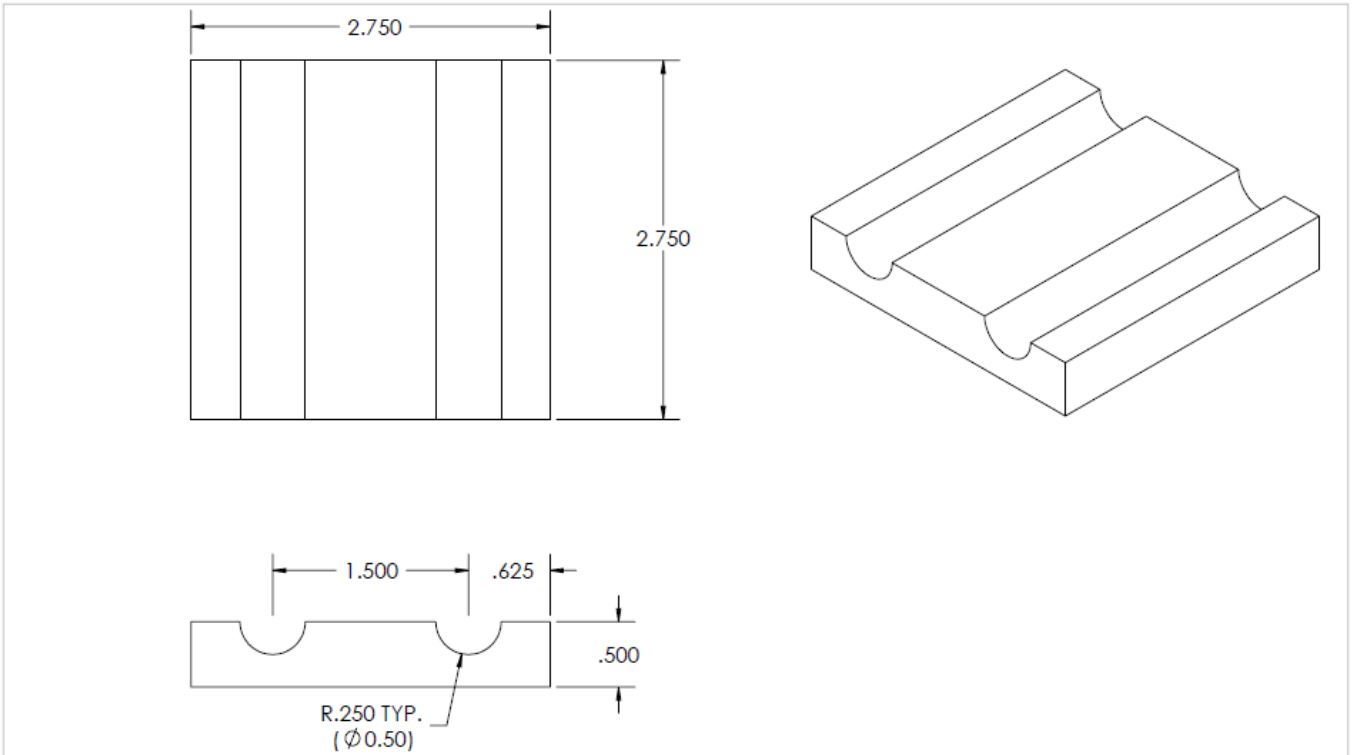

		UNLESS OTHERWISE SPECIFIED:		NAME	DATE
		DIMENSIONS ARE IN INCHES TOLERANCES: FRACTIONAL ± ANGULAR: MACH ± BEND ± TWO PLACE DECIMAL ± THREE PLACE DECIMAL ±	DRAWN		
			CHECKED		
			ENG APPR.		
			MFG APPR.		
		INTERPRET GEOMETRIC TOLERANCING PER:	Q.A.		
		MATERIAL	COMMENTS:		
NEXT ASSY	USED ON	FINISH			
APPLICATION		DO NOT SCALE DRAWING			

PROPRIETARY AND CONFIDENTIAL

THE INFORMATION CONTAINED IN THIS DRAWING IS THE SOLE PROPERTY OF <INSERT COMPANY NAME HERE>. ANY REPRODUCTION IN PART OR AS A WHOLE WITHOUT THE WRITTEN PERMISSION OF <INSERT COMPANY NAME HERE> IS PROHIBITED.

TITLE:

SIZE	DWG. NO.	REV
A	Compressive plate no holes	
SCALE: 1:1	WEIGHT:	SHEET 1 OF 1

5 4 3 2 1

NOTES:
1. DETERMINE WINCH MOUNTING HOLE LOCATIONS
2. REVISE AND EDIT CAD MODEL FOR NEW HOLES
3. MACHINE HOLES

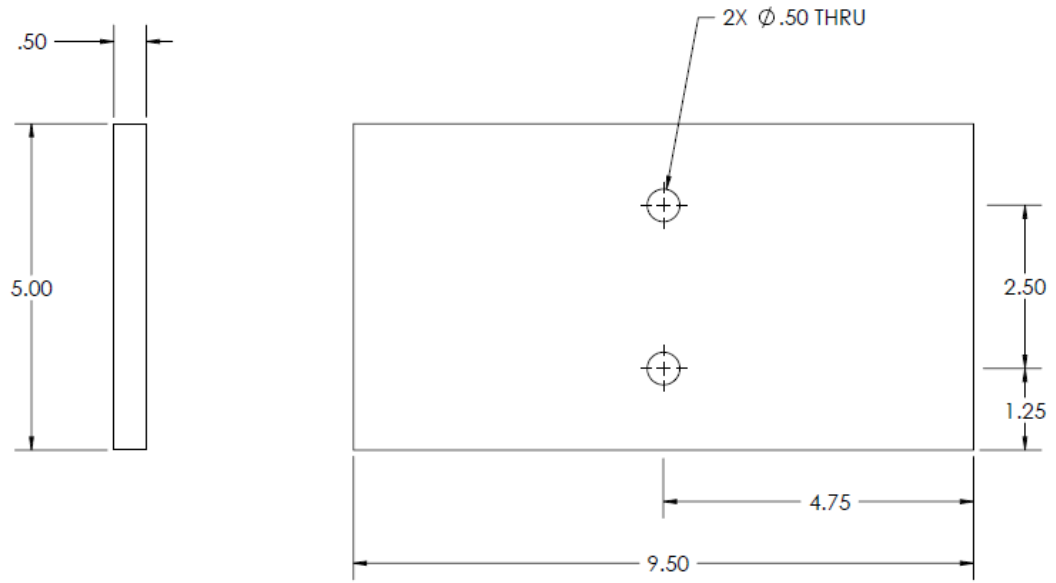

		UNLESS OTHERWISE SPECIFIED:		NAME	DATE
		DIMENSIONS ARE IN INCHES TOLERANCES: FRACTIONAL ± ANGULAR: MACH ± BEND ± TWO PLACE DECIMAL ± THREE PLACE DECIMAL ±	DRAWN		
			CHECKED		
			ENG APPR.		
			MFG APPR.		
		INTERPRET GEOMETRIC TOLERANCING PER:	Q.A.		
		MATERIAL	COMMENTS:		
NEXT ASSY	USED ON	FINISH			
APPLICATION		DO NOT SCALE DRAWING			

TITLE:

SIZE	DWG. NO.	REV
A	Crossbar for Winch	
SCALE: 1:2	WEIGHT:	SHEET 1 OF 1

5 4 3 2 1

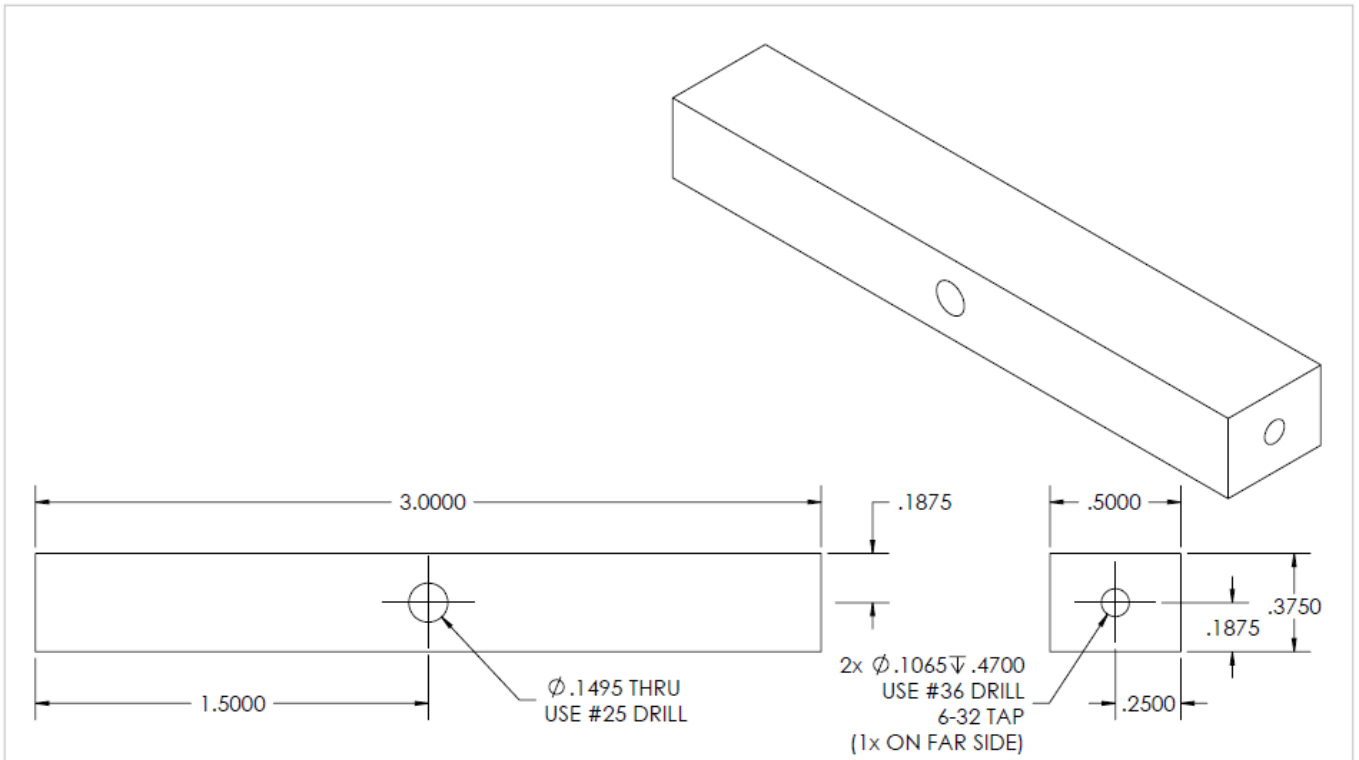
3.0000
.1875
.5000
.3750
.1875
1.5000
Ø.1495 THRU
USE #25 DRILL
2x Ø.1065↧.4700
USE #36 DRILL
6-32 TAP
(1x ON FAR SIDE)
.2500
UNLESS OTHERWISE SPECIFIED:
DIMENSIONS ARE IN INCHES
TOLERANCES:
FRACTIONAL ±
ANGULAR: MACH ± BEND ±
TWO PLACE DECIMAL ±
THREE PLACE DECIMAL ±
INTERPRET GEOMETRIC TOLERANCING PER:
MATERIAL
FINISH
NEXT ASSY
USED ON
APPLICATION
DO NOT SCALE DRAWING
NAME
DATE
DRAWN
CHECKED
ENG APPR.
MFG APPR.
Q.A.
COMMENTS:
TITLE:
SIZE
A
DWG. NO.
Mold Collar Bottom
REV
SCALE: 2:1
WEIGHT:
SHEET 1 OF 1
PROPRIETARY AND CONFIDENTIAL
THE INFORMATION CONTAINED IN THIS DRAWING IS THE SOLE PROPERTY OF <INSERT COMPANY NAME HERE>. ANY REPRODUCTION IN PART OR AS A WHOLE WITHOUT THE WRITTEN PERMISSION OF <INSERT COMPANY NAME HERE> IS PROHIBITED.
5
4
3
2
1

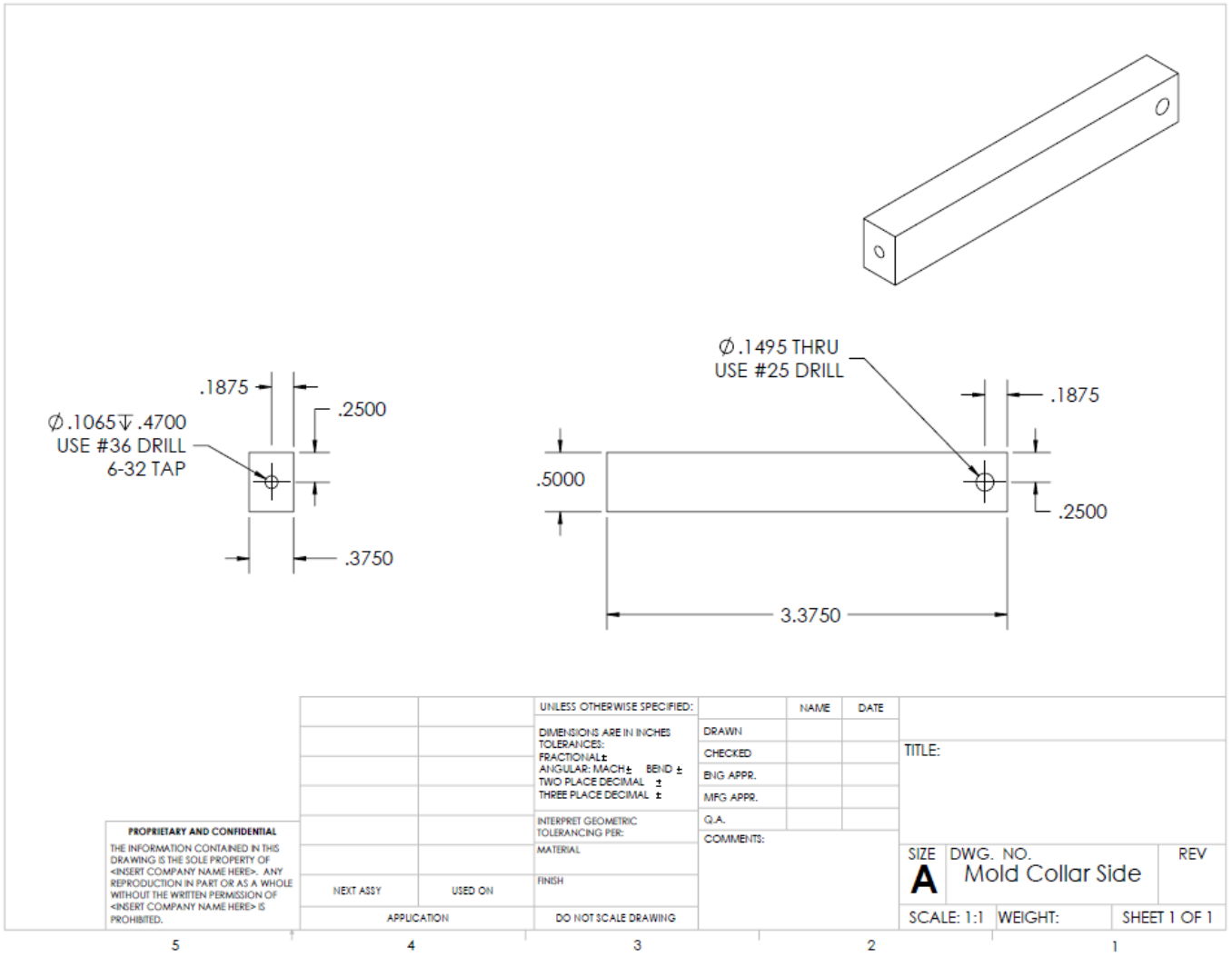
.1875
.2500
∅.1065↧.4700
USE #36 DRILL
6-32 TAP
.3750
∅.1495 THRU
USE #25 DRILL
.1875
.5000
.2500
3.3750
UNLESS OTHERWISE SPECIFIED:
DIMENSIONS ARE IN INCHES
TOLERANCES:
FRACTIONAL ±
ANGULAR: MACH ± BEND ±
TWO PLACE DECIMAL ±
THREE PLACE DECIMAL ±
INTERPRET GEOMETRIC TOLERANCING PER:
MATERIAL
FINISH
DO NOT SCALE DRAWING
NEXT ASSY
USED ON
APPLICATION
NAME
DATE
DRAWN
CHECKED
ENG APPR.
MFG APPR.
Q.A.
COMMENTS:
TITLE:
SIZE
A
DWG. NO.
Mold Collar Side
REV
SCALE: 1:1
WEIGHT:
SHEET 1 OF 1
PROPRIETARY AND CONFIDENTIAL
THE INFORMATION CONTAINED IN THIS DRAWING IS THE SOLE PROPERTY OF <INSERT COMPANY NAME HERE>. ANY REPRODUCTION IN PART OR AS A WHOLE WITHOUT THE WRITTEN PERMISSION OF <INSERT COMPANY NAME HERE> IS PROHIBITED.
5
4
3
2
1

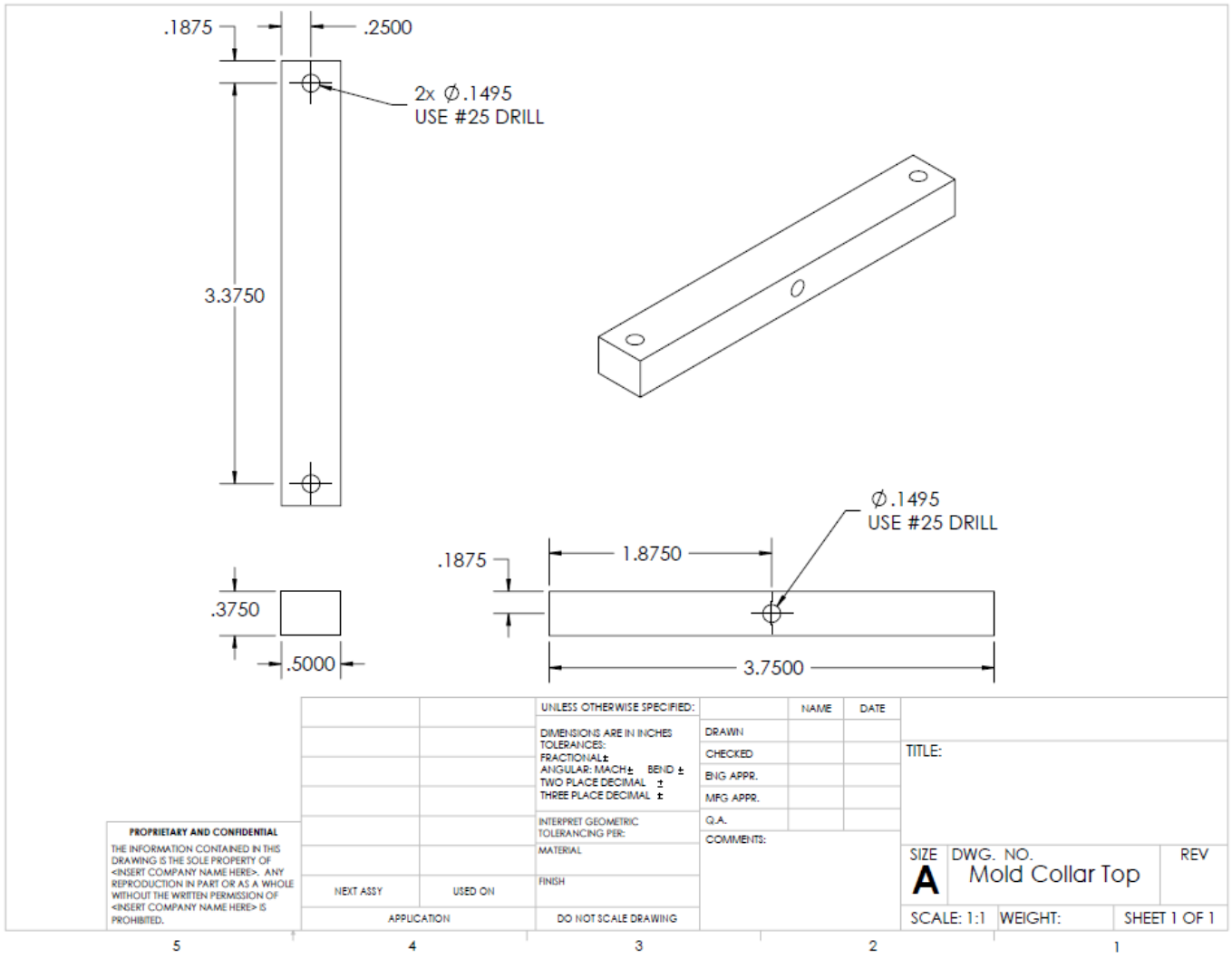
.1875
.2500
2x Ø.1495
USE #25 DRILL
3.3750
Ø.1495
USE #25 DRILL
.1875
1.8750
.3750
.5000
3.7500
UNLESS OTHERWISE SPECIFIED:
DIMENSIONS ARE IN INCHES
TOLERANCES:
FRACTIONAL ±
ANGULAR: MACH ± BEND ±
TWO PLACE DECIMAL ±
THREE PLACE DECIMAL ±
INTERPRET GEOMETRIC TOLERANCING PER:
MATERIAL
FINISH
DO NOT SCALE DRAWING
NAME
DATE
DRAWN
CHECKED
ENG APPR.
MFG APPR.
Q.A.
COMMENTS:
TITLE:
SIZE
A
DWG. NO.
Mold Collar Top
REV
SCALE: 1:1
WEIGHT:
SHEET 1 OF 1
NEXT ASSY
USED ON
APPLICATION
PROPRIETARY AND CONFIDENTIAL
THE INFORMATION CONTAINED IN THIS DRAWING IS THE SOLE PROPERTY OF <INSERT COMPANY NAME HERE>. ANY REPRODUCTION IN PART OR AS A WHOLE WITHOUT THE WRITTEN PERMISSION OF <INSERT COMPANY NAME HERE> IS PROHIBITED.
5
4
3
2
1

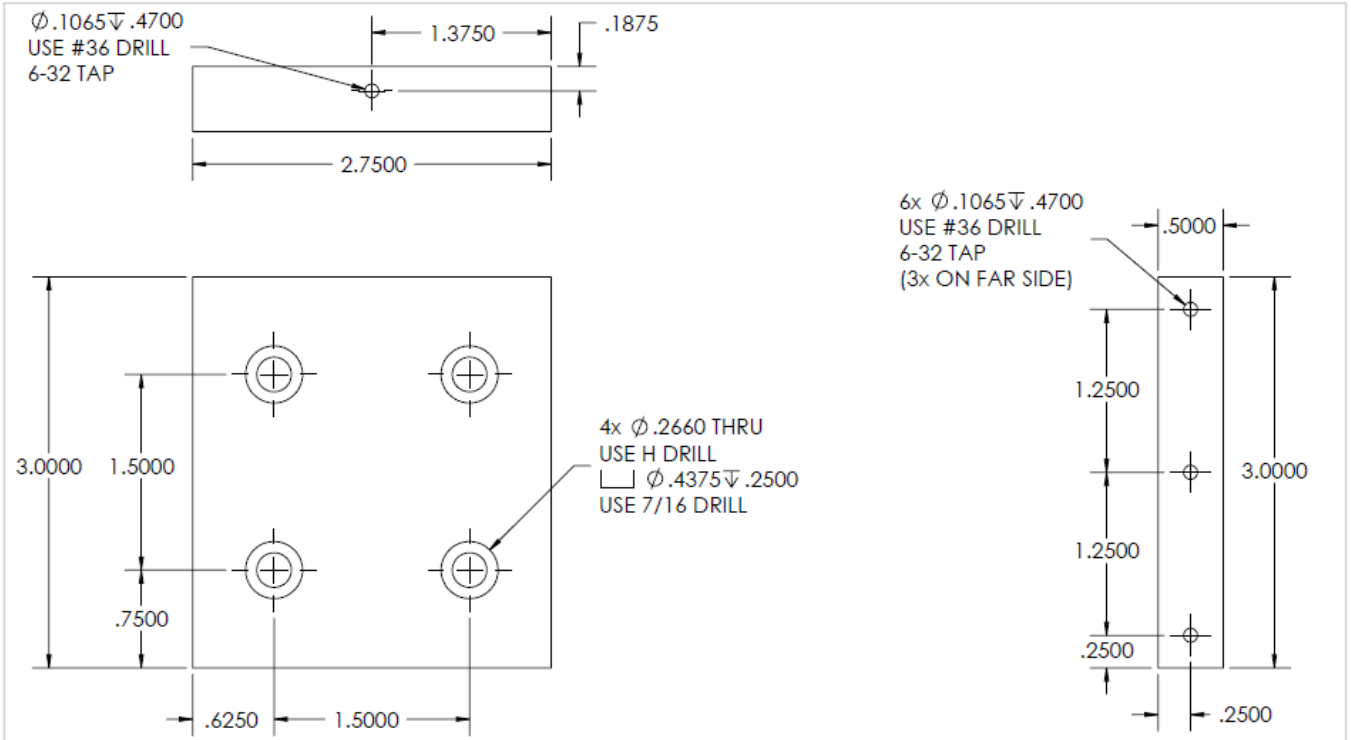
Ø.1065↧.4700
USE #36 DRILL
6-32 TAP
1.3750
.1875
2.7500
6x Ø.1065↧.4700
USE #36 DRILL
6-32 TAP
(3x ON FAR SIDE)
.5000
1.2500
3.0000
1.2500
.2500
.2500
4x Ø.2660 THRU
USE H DRILL
⌴ Ø.4375↧.2500
USE 7/16 DRILL
3.0000
1.5000
.7500
.6250
1.5000
UNLESS OTHERWISE SPECIFIED:
DIMENSIONS ARE IN INCHES
TOLERANCES:
FRACTIONAL ±
ANGULAR: MACH ± BEND ±
TWO PLACE DECIMAL ±
THREE PLACE DECIMAL ±
INTERPRET GEOMETRIC TOLERANCING PER:
MATERIAL
FINISH
DO NOT SCALE DRAWING
NAME
DATE
DRAWN
CHECKED
ENG APPR.
MFG APPR.
Q.A.
COMMENTS:
TITLE:
SIZE
A
DWG. NO.
Mold Guide Base
REV
SCALE: 1:1
WEIGHT:
SHEET 1 OF 1
NEXT ASSY
USED ON
APPLICATION
PROPRIETARY AND CONFIDENTIAL
THE INFORMATION CONTAINED IN THIS DRAWING IS THE SOLE PROPERTY OF <INSERT COMPANY NAME HERE>. ANY REPRODUCTION IN PART OR AS A WHOLE WITHOUT THE WRITTEN PERMISSION OF <INSERT COMPANY NAME HERE> IS PROHIBITED.
5
4
3
2
1

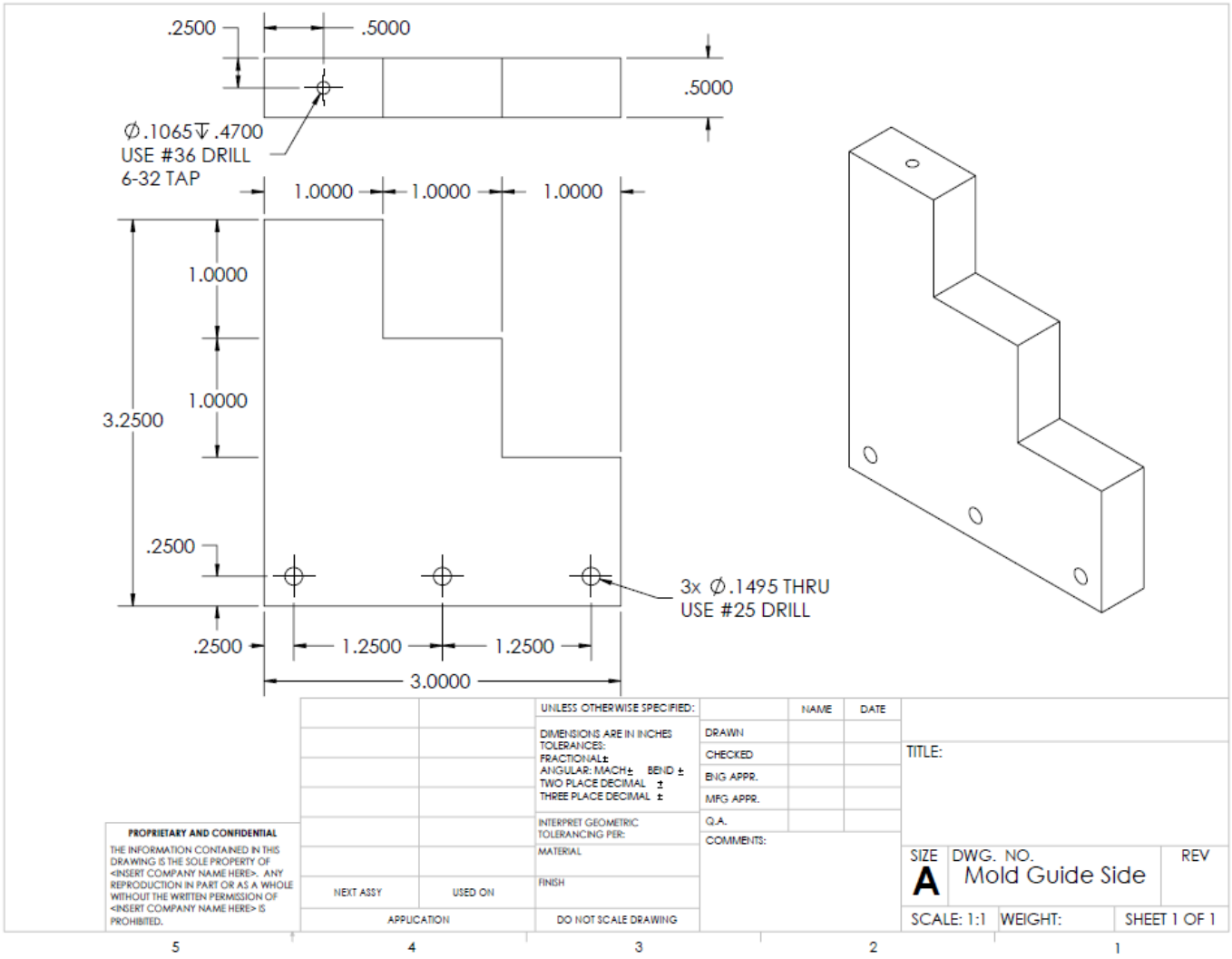
.2500
.5000
.5000
Ø.1065↧.4700
USE #36 DRILL
6-32 TAP
1.0000
1.0000
1.0000
1.0000
1.0000
3.2500
.2500
3x Ø.1495 THRU
USE #25 DRILL
.2500
1.2500
1.2500
3.0000
UNLESS OTHERWISE SPECIFIED:
DIMENSIONS ARE IN INCHES
TOLERANCES:
FRACTIONAL ±
ANGULAR: MACH ± BEND ±
TWO PLACE DECIMAL ±
THREE PLACE DECIMAL ±
INTERPRET GEOMETRIC TOLERANCING PER:
MATERIAL
FINISH
DO NOT SCALE DRAWING
NAME
DATE
DRAWN
CHECKED
ENG APPR.
MFG APPR.
Q.A.
COMMENTS:
TITLE:
SIZE
A
DWG. NO.
Mold Guide Side
REV
SCALE: 1:1
WEIGHT:
SHEET 1 OF 1
NEXT ASSY
USED ON
APPLICATION
PROPRIETARY AND CONFIDENTIAL
THE INFORMATION CONTAINED IN THIS DRAWING IS THE SOLE PROPERTY OF <INSERT COMPANY NAME HERE>. ANY REPRODUCTION IN PART OR AS A WHOLE WITHOUT THE WRITTEN PERMISSION OF <INSERT COMPANY NAME HERE> IS PROHIBITED.
5
4
3
2
1

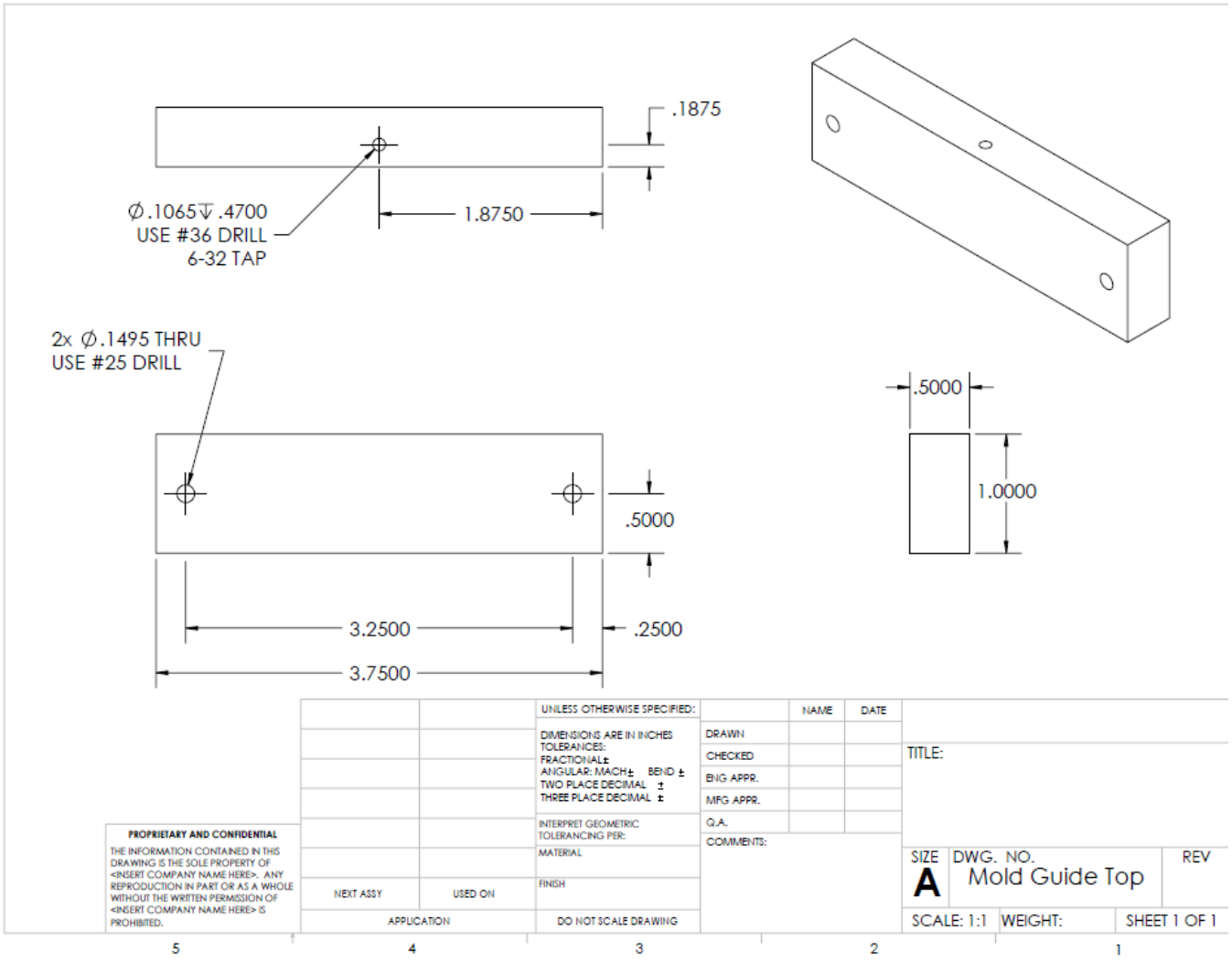
.1875
Ø.1065↧.4700
USE #36 DRILL
6-32 TAP
1.8750
2x Ø.1495 THRU
USE #25 DRILL
.5000
3.2500
.2500
3.7500
.5000
1.0000
UNLESS OTHERWISE SPECIFIED:
DIMENSIONS ARE IN INCHES
TOLERANCES:
FRACTIONAL ±
ANGULAR: MACH ± BEND ±
TWO PLACE DECIMAL ±
THREE PLACE DECIMAL ±
INTERPRET GEOMETRIC TOLERANCING PER:
MATERIAL
FINISH
DO NOT SCALE DRAWING
NAME
DATE
DRAWN
CHECKED
ENG APPR.
MFG APPR.
Q.A.
COMMENTS:
TITLE:
SIZE
A
DWG. NO.
Mold Guide Top
REV
SCALE: 1:1
WEIGHT:
SHEET 1 OF 1
NEXT ASSY
USED ON
APPLICATION
PROPRIETARY AND CONFIDENTIAL
THE INFORMATION CONTAINED IN THIS DRAWING IS THE SOLE PROPERTY OF <INSERT COMPANY NAME HERE>. ANY REPRODUCTION IN PART OR AS A WHOLE WITHOUT THE WRITTEN PERMISSION OF <INSERT COMPANY NAME HERE> IS PROHIBITED.
5
4
3
2
1

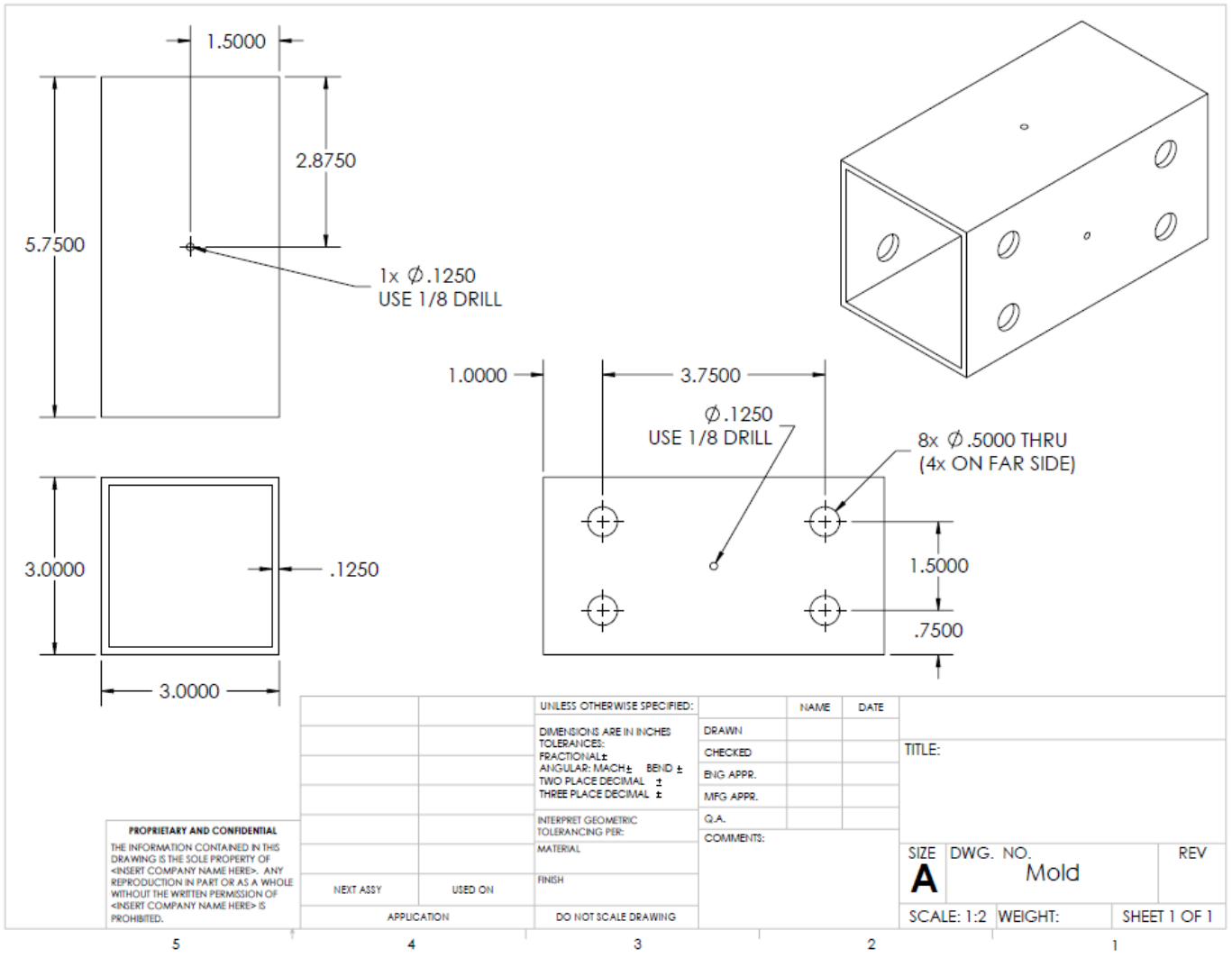
1.5000
2.8750
5.7500
1x ∅.1250
USE 1/8 DRILL
1.0000
3.7500
∅.1250
USE 1/8 DRILL
8x ∅.5000 THRU
(4x ON FAR SIDE)
3.0000
.1250
1.5000
.7500
3.0000
UNLESS OTHERWISE SPECIFIED:
DIMENSIONS ARE IN INCHES
TOLERANCES:
FRACTIONAL ±
ANGULAR: MACH ± BEND ±
TWO PLACE DECIMAL ±
THREE PLACE DECIMAL ±
INTERPRET GEOMETRIC TOLERANCING PER:
MATERIAL
FINISH
DO NOT SCALE DRAWING
NEXT ASSY
USED ON
APPLICATION
NAME
DATE
DRAWN
CHECKED
ENG APPR.
MFG APPR.
Q.A.
COMMENTS:
TITLE:
SIZE
A
DWG. NO.
Mold
REV
SCALE: 1:2
WEIGHT:
SHEET 1 OF 1
PROPRIETARY AND CONFIDENTIAL
THE INFORMATION CONTAINED IN THIS DRAWING IS THE SOLE PROPERTY OF <INSERT COMPANY NAME HERE>. ANY REPRODUCTION IN PART OR AS A WHOLE WITHOUT THE WRITTEN PERMISSION OF <INSERT COMPANY NAME HERE> IS PROHIBITED.
5
4
3
2
1

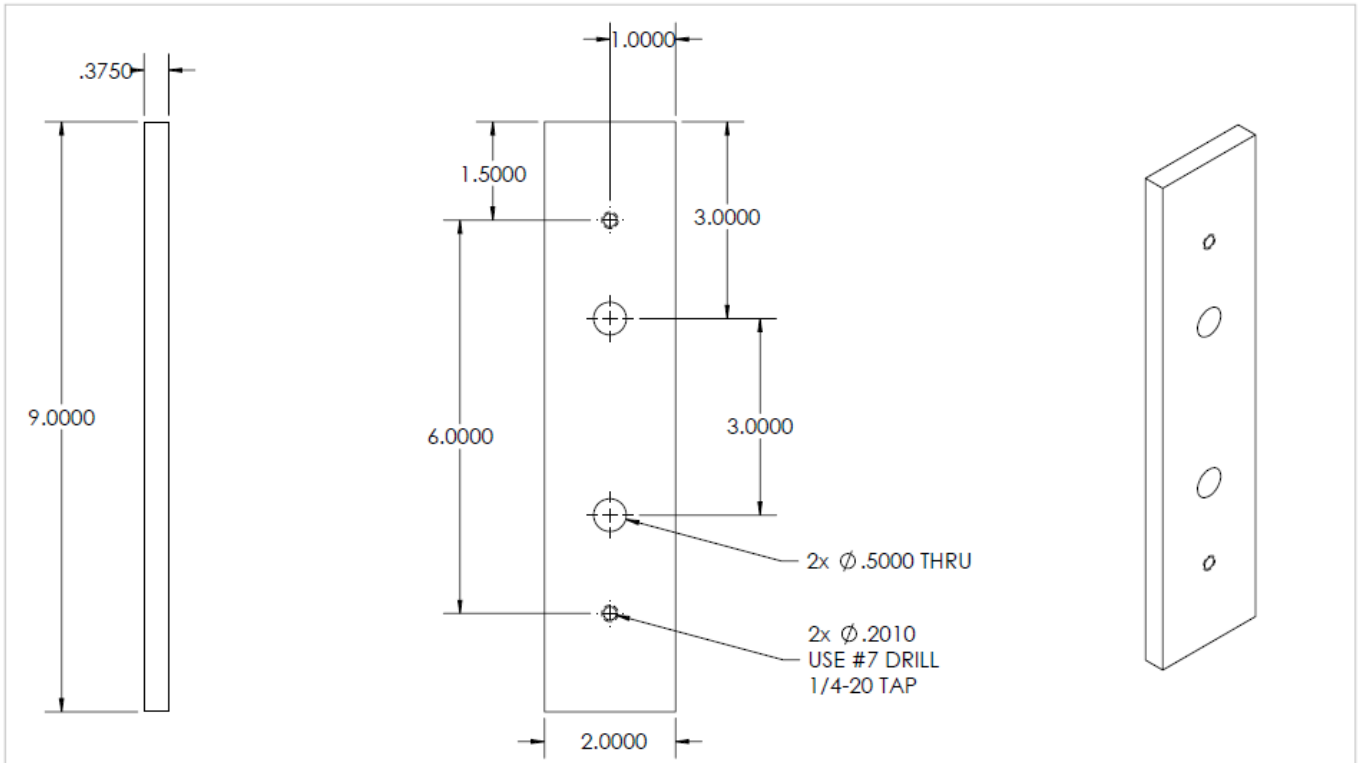

		UNLESS OTHERWISE SPECIFIED:		NAME	DATE
		DIMENSIONS ARE IN INCHES TOLERANCES: FRACTIONAL ± ANGULAR: MACH ± BEND ± TWO PLACE DECIMAL ± THREE PLACE DECIMAL ±	DRAWN		
			CHECKED		
			ENG APPR.		
			MFG APPR.		
		INTERPRET GEOMETRIC TOLERANCING PER:	Q.A.		
		MATERIAL	COMMENTS:		
NEXT ASSY	USED ON	FINISH			
APPLICATION		DO NOT SCALE DRAWING			

TITLE:

SIZE	DWG. NO.	REV
A	Rope Guide Support	
SCALE: 1:2	WEIGHT:	SHEET 1 OF 1

5 4 3 2 1

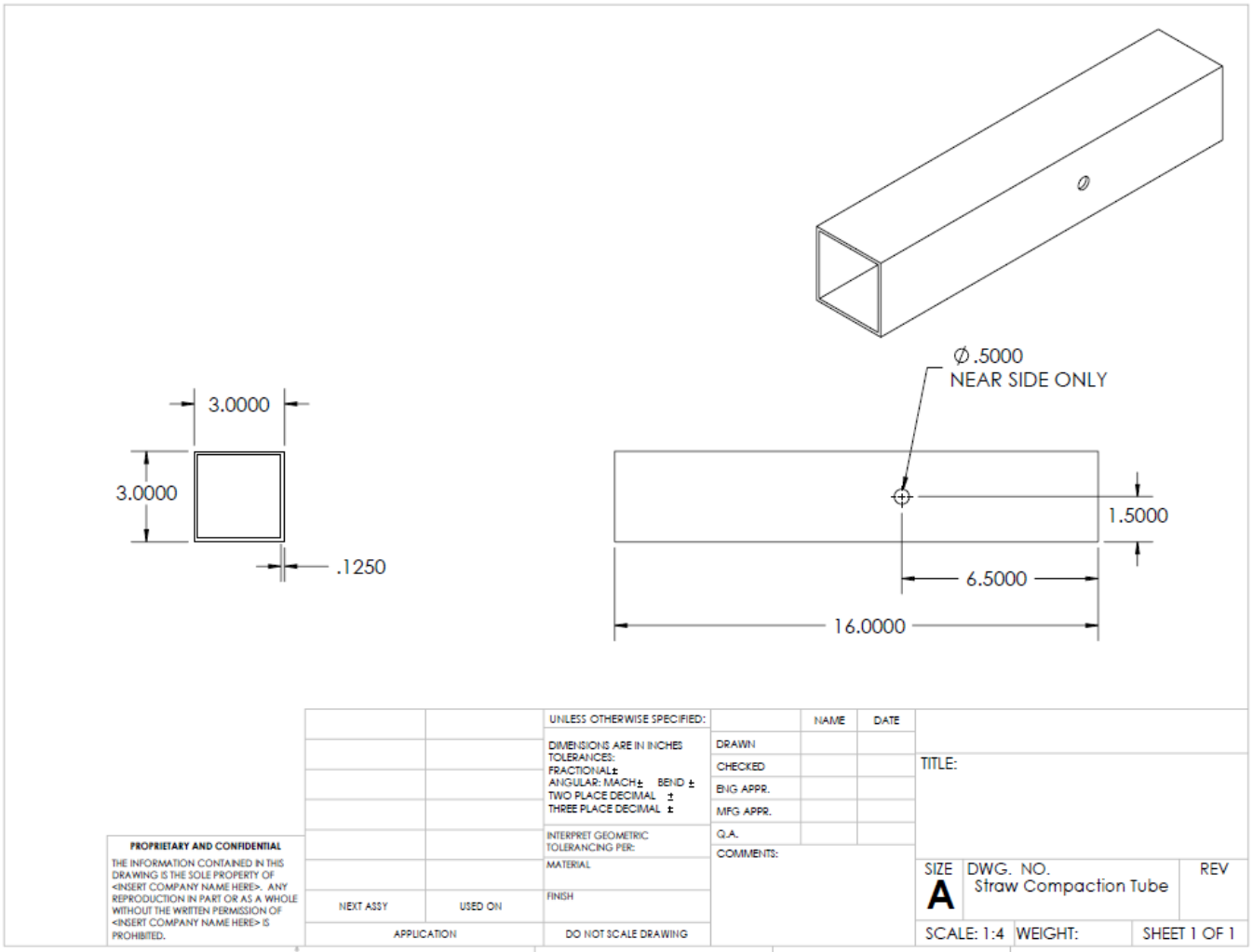

		UNLESS OTHERWISE SPECIFIED:		NAME	DATE
		DIMENSIONS ARE IN INCHES TOLERANCES: FRACTIONAL ± ANGULAR: MACH ± BEND ± TWO PLACE DECIMAL ± THREE PLACE DECIMAL ±	DRAWN		
			CHECKED		
			ENG APPR.		
			MFG APPR.		
		INTERPRET GEOMETRIC TOLERANCING PER:	Q.A.		
		MATERIAL	COMMENTS:		
NEXT ASSY	USED ON	FINISH			
APPLICATION		DO NOT SCALE DRAWING			

PROPRIETARY AND CONFIDENTIAL

THE INFORMATION CONTAINED IN THIS DRAWING IS THE SOLE PROPERTY OF <INSERT COMPANY NAME HERE>. ANY REPRODUCTION IN PART OR AS A WHOLE WITHOUT THE WRITTEN PERMISSION OF <INSERT COMPANY NAME HERE> IS PROHIBITED.

TITLE:

SIZE	DWG. NO.	REV
A	Straw Compaction Tube	
SCALE: 1:4	WEIGHT:	SHEET 1 OF 1

5 4 3 2 1

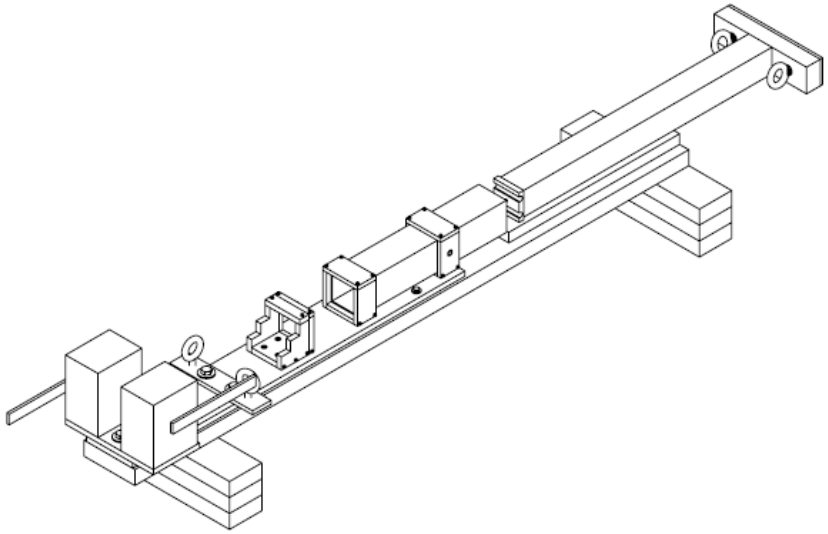

		UNLESS OTHERWISE SPECIFIED:		NAME	DATE
		DIMENSIONS ARE IN INCHES TOLERANCES: FRACTIONAL ± ANGULAR: MACH ± BEND ± TWO PLACE DECIMAL ± THREE PLACE DECIMAL ±	DRAWN		
			CHECKED		
			ENG APPR.		
			MFG APPR.		
		INTERPRET GEOMETRIC TOLERANCING PER:	Q.A.		
		MATERIAL	COMMENTS:		
NEXT ASSY	USED ON	FINISH			
APPLICATION		DO NOT SCALE DRAWING			

PROPRIETARY AND CONFIDENTIAL

THE INFORMATION CONTAINED IN THIS DRAWING IS THE SOLE PROPERTY OF <INSERT COMPANY NAME HERE>. ANY REPRODUCTION IN PART OR AS A WHOLE WITHOUT THE WRITTEN PERMISSION OF <INSERT COMPANY NAME HERE> IS PROHIBITED.

TITLE:

SIZE	DWG. NO.	REV
A	Compression Assembly Mk 2 Complete	
SCALE: 1:10	WEIGHT:	SHEET 1 OF 1

5 4 3 2 1

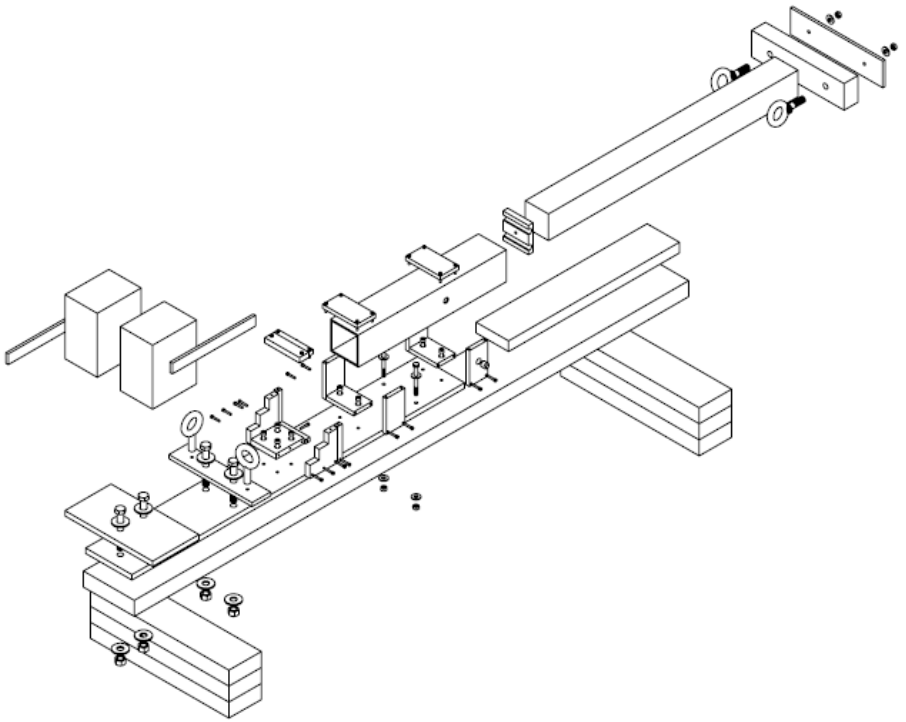

		UNLESS OTHERWISE SPECIFIED:		NAME	DATE
		DIMENSIONS ARE IN INCHES TOLERANCES: FRACTIONAL ± ANGULAR: MACH ± BEND ± TWO PLACE DECIMAL ± THREE PLACE DECIMAL ±	DRAWN		
			CHECKED		
			ENG APPR.		
			MFG APPR.		
		INTERPRET GEOMETRIC TOLERANCING PER:	Q.A.		
		MATERIAL	COMMENTS:		
NEXT ASSY	USED ON	FINISH			
APPLICATION		DO NOT SCALE DRAWING			

PROPRIETARY AND CONFIDENTIAL

THE INFORMATION CONTAINED IN THIS DRAWING IS THE SOLE PROPERTY OF <INSERT COMPANY NAME HERE>. ANY REPRODUCTION IN PART OR AS A WHOLE WITHOUT THE WRITTEN PERMISSION OF <INSERT COMPANY NAME HERE> IS PROHIBITED.

TITLE:

SIZE	DWG. NO.	REV
A	Compression Assembly Mk 2 Exploded	
SCALE: 1:10	WEIGHT:	SHEET 1 OF 1

5 4 3 2 1

APPENDIX I: Engineering drawings – Compression test fixtures

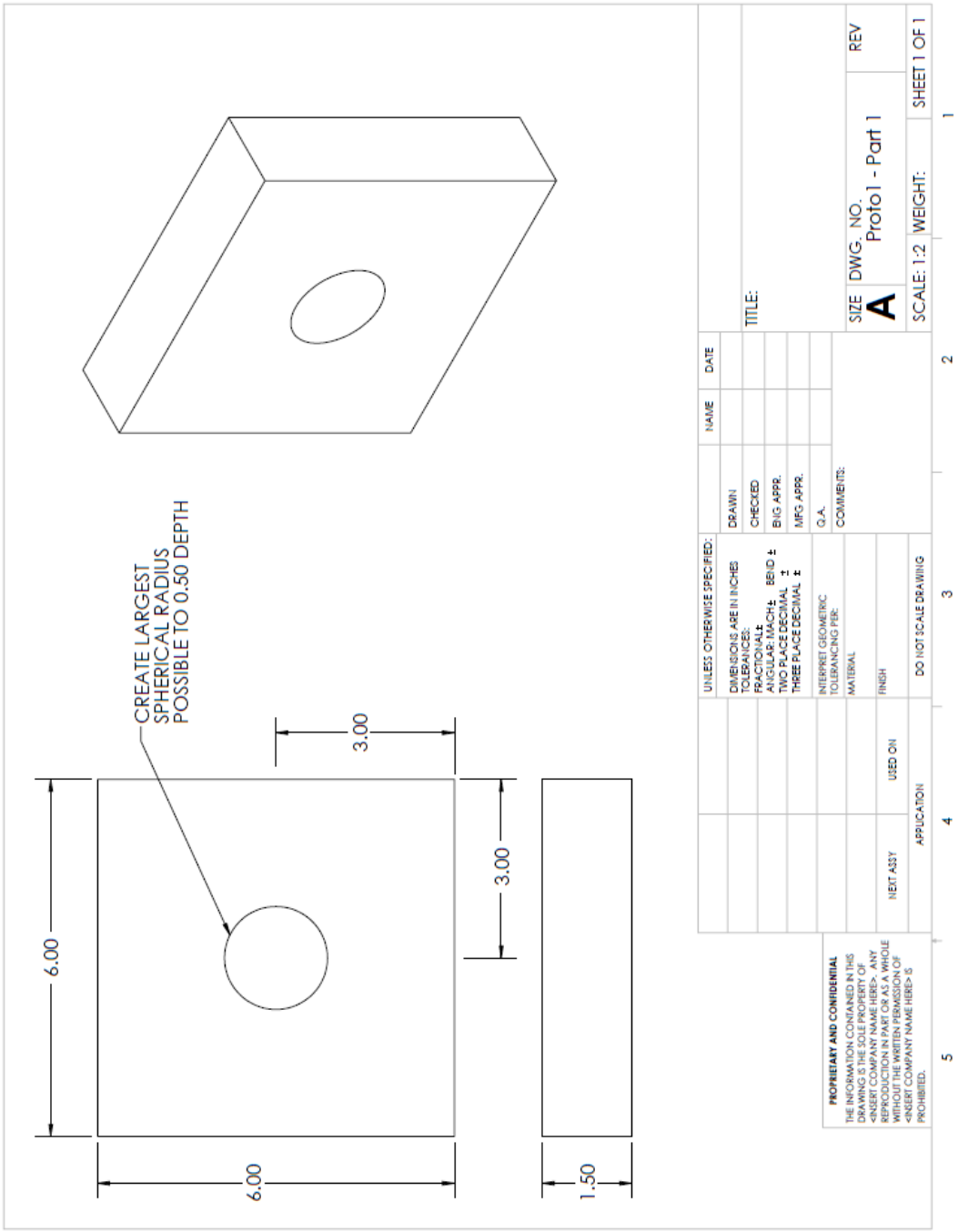

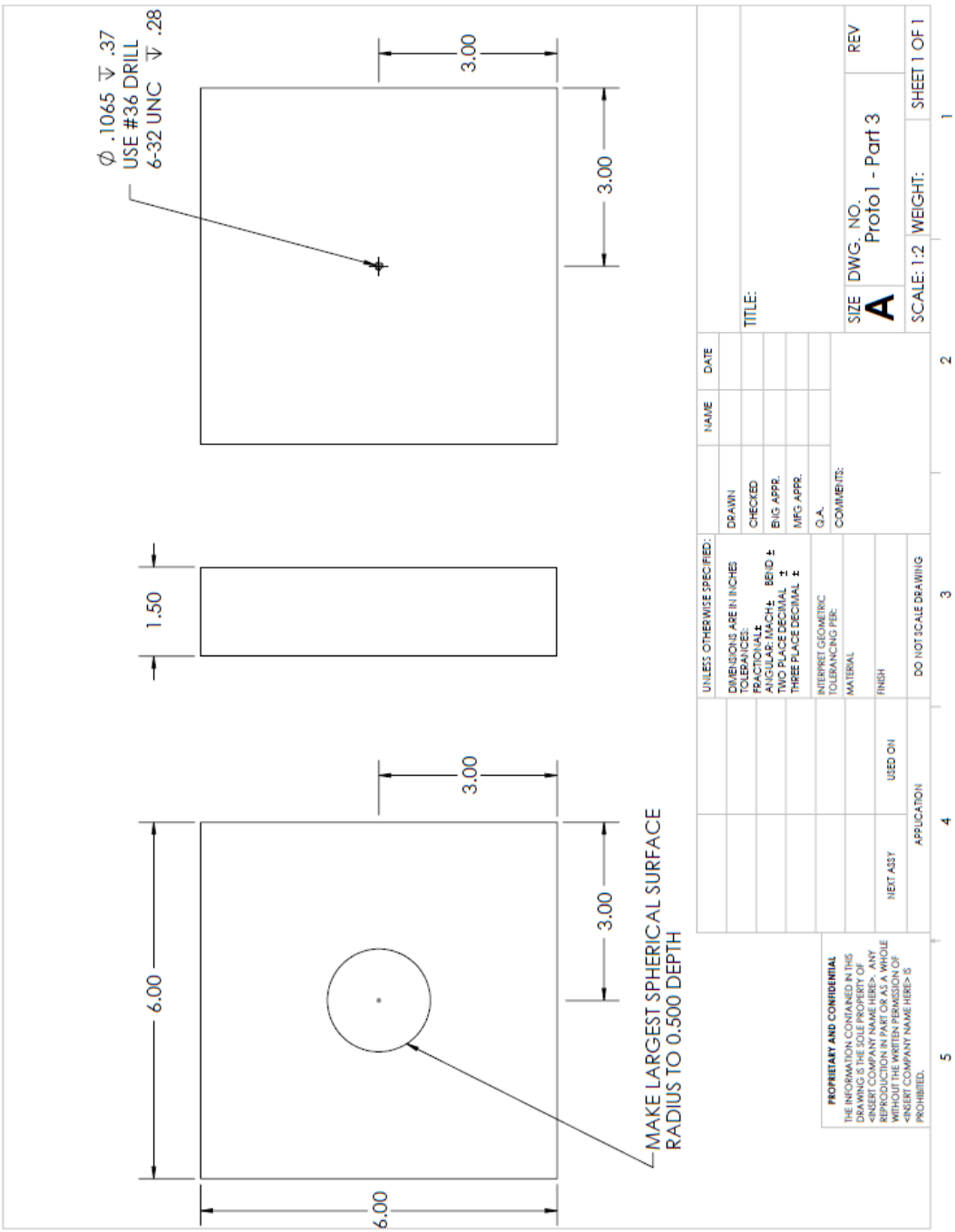

NOTE: Proto 1 – Part 2 was not fabricated. It was purchased from McMasterCarr.com as a 2” diameter ball. The material was bearing-quality aircraft-grade E52100 Alloy Steel. (Part Number 9528K71) The mating spherical surfaces were machined to a 1” radius.

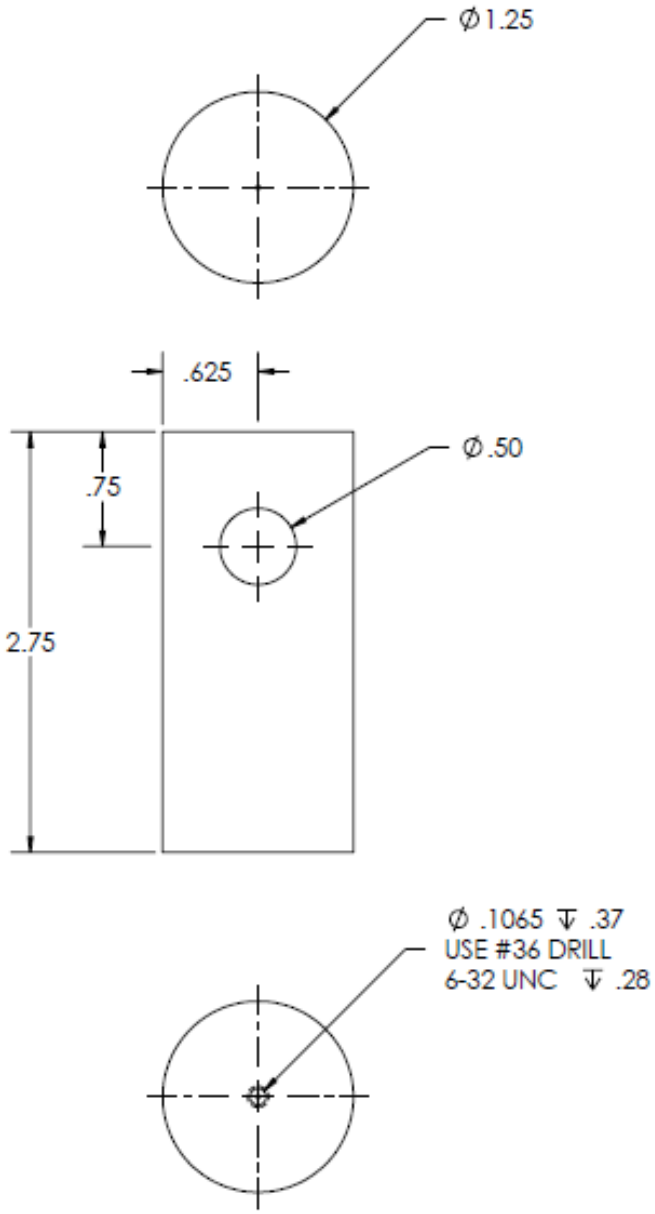

		DIMENSIONS ARE IN INCHES TOLERANCES: FRACTIONAL ± ANGULAR: MACH ± BEND ± TWO PLACE DECIMAL ± THREE PLACE DECIMAL ±		NAME	DATE	
			DRAWN			
			CHECKED			
			ENG APPR.			
			MFG APPR.			
			Q.A.			
		MATERIAL	COMMENTS:			
NEXT ASSY	USED ON	FINISH				
APPLICATION		DO NOT SCALE DRAWING				

SIZE	DWG. NO.	REV.
A	Proto1 - Part 4	
SCALE:1:1	WEIGHT:	SHEET 1 OF 1

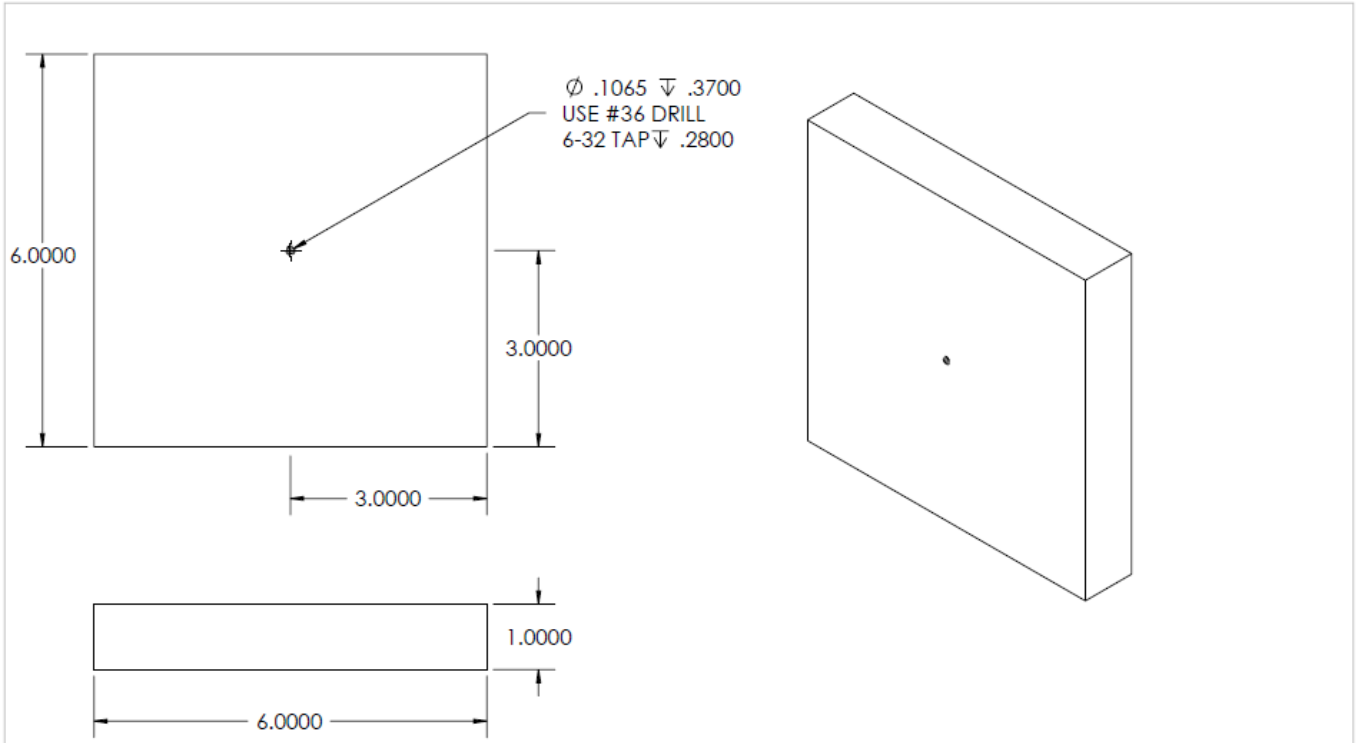

		UNLESS OTHERWISE SPECIFIED:		NAME	DATE
		DIMENSIONS ARE IN INCHES TOLERANCES: FRACTIONAL ± ANGULAR: MACH ± BEND ± TWO PLACE DECIMAL ± THREE PLACE DECIMAL ±	DRAWN		
			CHECKED		
			ENG APPR.		
			MFG APPR.		
		INTERPRET GEOMETRIC TOLERANCING PER:	Q.A.		
		MATERIAL	COMMENTS:		
NEXT ASSY	USED ON	FINISH			
APPLICATION		DO NOT SCALE DRAWING			

PROPRIETARY AND CONFIDENTIAL

THE INFORMATION CONTAINED IN THIS DRAWING IS THE SOLE PROPERTY OF <INSERT COMPANY NAME HERE>. ANY REPRODUCTION IN PART OR AS A WHOLE WITHOUT THE WRITTEN PERMISSION OF <INSERT COMPANY NAME HERE> IS PROHIBITED.

TITLE:

SIZE	DWG. NO.	REV
A	Proto1 - Part 5	
SCALE: 1:2	WEIGHT:	SHEET 1 OF 1

5 4 3 2 1

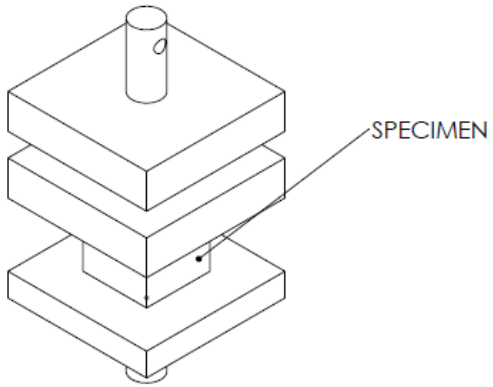

		UNLESS OTHERWISE SPECIFIED:		NAME	DATE
		DIMENSIONS ARE IN INCHES TOLERANCES: FRACTIONAL ± ANGULAR: MACH ± BEND ± TWO PLACE DECIMAL ± THREE PLACE DECIMAL ±	DRAWN		
			CHECKED		
			ENG APPR.		
			MFG APPR.		
		INTERPRET GEOMETRIC TOLERANCING PER:	Q.A.		
		MATERIAL	COMMENTS:		
NEXT ASSY	USED ON	FINISH			
APPLICATION		DO NOT SCALE DRAWING			

PROPRIETARY AND CONFIDENTIAL

THE INFORMATION CONTAINED IN THIS DRAWING IS THE SOLE PROPERTY OF <INSERT COMPANY NAME HERE>. ANY REPRODUCTION IN PART OR AS A WHOLE WITHOUT THE WRITTEN PERMISSION OF <INSERT COMPANY NAME HERE> IS PROHIBITED.

TITLE:

SIZE	DWG. NO.	REV
A	Mechanical Testing Setup Complete	
SCALE: 1:4	WEIGHT:	SHEET 1 OF 1

5 4 3 2 1

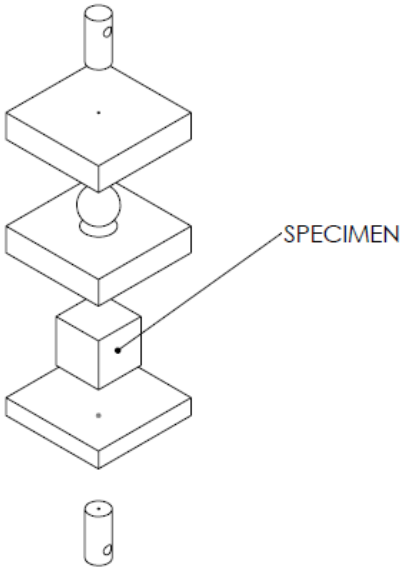

		UNLESS OTHERWISE SPECIFIED:		NAME	DATE
		DIMENSIONS ARE IN INCHES TOLERANCES: FRACTIONAL ± ANGULAR: MACH ± BEND ± TWO PLACE DECIMAL ± THREE PLACE DECIMAL ±	DRAWN		
			CHECKED		
			ENG APPR.		
			MFG APPR.		
		INTERPRET GEOMETRIC TOLERANCING PER:	Q.A.		
		MATERIAL	COMMENTS:		
NEXT ASSY	USED ON	FINISH			
APPLICATION		DO NOT SCALE DRAWING			

TITLE:

SIZE	DWG. NO.	REV
A	Mechanical Testing Setup Exploded	
SCALE: 1:6	WEIGHT:	SHEET 1 OF 1

5 4 3 2 1